2013

USING COMPOSITE FUELS AS A SUBSTITUTE FOR STANDARD FUELS FOR COMBUSTION

Adam Duszkiewicz
University of Rhode Island, adamdusky@my.uri.edu

USING COMPOSITE FUELS AS A SUBSTITUTE FOR STANDARD FUELS FOR COMBUSTION

BY

ADAM DUSZKIEWICZ

A THESIS SUBMITTED IN PARTIAL FULFILLMENT OF THE REQUIREMENTS FOR THE DEGREE OF

MASTER OF SCIENCE

IN

CHEMICAL ENGINEERING

UNIVERSITY OF RHODE ISLAND

2013

USING COMPOSITE FUELS AS A SUBSTITUTE FOR STANDARD FUELS FOR COMBUSTION

BY

ADAM DUSZKIEWICZ

APPROVED:

Thesis Committee:

Major Professor Harold Knickle

Donald Gray

Leon Thiem

David Taggart

Nasser H. Zawia
DEAN OF THE GRADUATE SCHOOL

UNIVERSITY OF RHODE ISLAND
2013

ABSTRACT

This study will examine the practicality of using composite solid-liquid fuel technology and it they can by improved through emulsification. The practicality of this technology was determined based on whether a composite fuel could be modeled that had acceptable combustion properties. These properties were determined through experimentation, literature analysis and modeling. Experiments determining settling velocity were conducted on coal-soybean oil and wood-soybean oil composite mixtures. Settling velocities were determined varying mass concentrations, temperatures and average solid particulate size. Then 20% mass concentration of water was added to the same mixtures and the experiments were repeated. It was found that lower temperatures, smaller average particle sizes and emulsifying all aided in slowing settling velocity, with emulsification being the largest factor. Next, documented viscosity experiments involving composite fuels found in literature were examined. Factors affecting viscosity were noted and viscosity modeling equations were determined. It was found that that the greater the solid amount and the less the liquid amount in a given composite mixture, the smaller the viscosity. Also water was found to lower viscosity if the liquid fuel it was emulsified had a much higher viscosity and raise viscosity if the fuel was similar in viscosity. Composite combustion modeling found that composite fuels, whether emulsified or not, would provide similar combustion properties, such as combustion time and heat of combustion compared to popular liquid and solid fuels used today.

ACKNOWLEDGMENTS

I would to begin by thanking my major professor, Dr. Harold Knickle. His patience, motivation, inspiration, support and immense knowledge were absolutely paramount to the completion of this project. More importantly, I would like to thank him for teaching me to not guess, but to think and investigate. It is with through this advice that I have truly learned the most.

I would also like to thank my thesis committee of Dr. Donald Grey, Dr. Leon Thiem and defense chair Dr. David Taggart. Throughout the writing process they provided sound advice, suggestions and support. During my defense their insightful comments and thought provoking questions further projected my learning and work to greater heights.

Thank you to the entire Chemical Engineering academic Department. Through courses and other interactions, it has aided in the final product of this thesis as well as my overall development as a chemical engineer.

Lastly I would like to thank Sheryl Girard and Brenda Moyer of the Chemical Engineering Department. Without them constantly keeping me in line and helping out in various other ways, I surely would have never completed my degree. Thank you for making my time at Crawford Hall that much more enjoyable.

TABLE OF CONTENTS

LIST OF TABLES

TABLE PAGE

LIST OF FIGURES

FIGURE PAGE

CHAPTER 1 – INTRODUCTION

1.1 Overview

The global population is ever increasing. Previously un-developed countries are now advancing technologically and are requiring more energy per person than was necessary in the past. There are alternatives to fossil fuels such as nuclear power, ethanol and hydro-electricity. If it was decided that these alternatives had to shoulder a much larger energy burden then they currently do, which is about 15%, this conversion would take an immense amount of time and resources. There are countless research projects being conducted all over the world to try and find new renewable energy sources that can, in the near future, provide the raw amount of energy required to shoulder a greater portion the global energy burden. None have yet made the necessary strides to be a fossil fuel contender due to how economical, energy dense, easy to harvest, easy to use and ingrained into current technology fossil fuel is.

Current studies predict that there are enough fossil fuel resources within the U.S. to last at least another 90 years [1]. Regardless of how much fossil fuel is still available to be burned, there are numerous undeniable advantages to be had in the creation of composite fuel (solid-liquid fuel) technology. One advantage is the opportunity to turn used oil and other hydrocarbon based wastes into combustible fuel sources. Current technology does not allow for efficient use of these wastes resulting in their collection and storage. This is known to happen in the oil refinery industry. Specifically when oil tankers are emptied of their oil contents, there is always a large amount of highly dense and viscous unusable oil that remains. As there is no use for this grade of fuel, it is expensively cleaned out of the tankers and then stored in

barrels. If there were a process that could take this incredibly viscous fuel byproduct, and harness the energy it still has, a viable 'new' energy source could be acquired. By the same principle, if a process could use other hydrocarbon solid based wastes, such as crumb rubber from tires, even more 'new' sources of fuel could be obtained. The most common process used to make these normally useless waste products into fuels, is by combining them with a small amount of common fuel oil such as gasoline or diesel. This mixture is commonly called, a composite fuel mixture, where the composite represents a solid or extremely viscous part of the mixture and the remainder is the common fuel oil

Another useful composite that could be made is a biomass-fuel oil mixture. Harnessing biomasses would allow the extension of local fossil fuel stores by using local biomass resources in conjunction with fossil fuels. Most regions in the world have a different abundance of some type of biomass that could be harvested and combined with fuel oil. Not only would this increase the life of fossil fuels, but it could also be a cheaper source of fuel. Just as the idea that coal-oil is cheaper than pure oil because coal is cheaper than oil, the same is true for most biomass sources. They are usually quite easy and relatively cheap to harvest, creating a more economic fuel source. Then there is the fact that current fuel oils all have some amount of sulfur in them. Therefore when they are combusted, that sulfur, which is not used in the combustion reaction, is released to the environment having negative effects. Biomasses, for intensive purposes, do not have sulfur, so any biomass-oil mixture would inherently be cleaner burning then any current fuel oil.

A huge incentive for the use of composite fuel oils is the idea that switching from pure fuel oil to solid/biosolid-fuel oil, if done properly, might not require a complete revamp of current industrial technology. This would clearly be a huge money and time saver for any industrial complex that wished to make the switch. With that in mine an important goal is to produce a combustible composite fuel that that can be used in power plants saving integration time and costs [2]. It is clear that despite having an ample supply of fossil fuel for years to come, a short term obtainable solution would prove very beneficial to society.

This thesis will be looking at modeling simple composite mixtures in an attempt to accurately calculate various properties important to combustion based on variable certain controllable parameters such as: composite mixture composition and concentrations, particle sizes of the solid fuels and furnace temperature. The solid fuels that will be looked at will consist of coal, representing a common sulfurous solid fuel and wood, representing a biomass solid fuel. The liquid fuels being used in the models will be, diesel, representing a commonly used sulfurous fuel oil and soybean oil, a biomass liquid fuel. The hope is to find out if it is possible to create a composite fuel mixture that has current fuel oil like rheological and combustion properties. The main properties of importance being, viscosity, combustion time and heat of combustion. As long as these three properties are close to what is being used currently, a fuel transition is not out of the question.

Another aspect being examined in regards to the composite fuel, is the advantages to emulsifying the composite mixtures with water. Emulsions are known to reduce settling amount and settling velocity in mixtures, which could enhanced the

composite fuels ability to remain well mixed. If the composite fuel mixture, consisting of solids and liquid were to separate too much, it would be disastrous. Because of these concerns, a series of experiments will be conducted to try and determining the validity of creating a composite fuel that would consist of solid fuel-liquid fuel-water. The effects water has on combustion will also be taken into account in the modeling section.

As not a lot of previous work has been conducted in the composite fuel field, the following method will be used to create a model for composite fuel combustion. First the separate pieces of composite combustion will be modeled, including, pure fuel combustion, emulsion fuel combustion and solid fuel combustion. Then a composite physical model will be presented combining all aspects of these three models. After this model equations will be formulated based off of previous modeling segments and the composite physical model. The end composite model will be linear.

Through said experimentation and modeling, this thesis will seek to address the possibility of using composite fuel mixtures in the near future.

1.2 References

[1] <http://dailycaller.com/2011/03/10/new-report-says-u-s-has-largest-fossil-fuel-reserves-in-world/> June 12 2012

[2] Steenari, B-M, and O. Lindqvist. Fly ash characteristics in co-combustion of wood with coal, oil or peat. Fuel, 78; 1999, 479-488, Print.

[3] Jared, John Marano, and Ronald Munson. Carbon Capture and Storage. Chemical Engineering Process.; Aug 2011. 33-54, Print.

CHAPTER 2 - MATERIALS

2.1 Introduction

The fuel materials of importance that are being explored in this thesis are coal, oil, wood and solid biomaterials. This chapter will introduce and define the properties of each substance used in this thesis, whether used in an experiment or in a model.

2.2 Coal

"Coal is a combustible carbonaceous rock that is formed from accumulated vegetable matter that has been altered by decay and various amounts of heat and pressure over millions of years." [1] Coal is normally categorized by "rank" which indicates the degree of alteration the coal has undergone during its formation, as is seen in table 1. Some values of increasing rank are as follows: brown coal (lignite), sub-bituminous coal, bituminous coal and anthracite. Coal varies from location to location, but in all cases it is mostly comprised of ring molecules comprised of six carbons [1]. Also included in the composition of coal is oxygen, nitrogen, hydrogen and to a lesser extent sulfur. Anywhere up to 10% of the total mass of coal has no fuel value.

As coal is heated with oxygen it softens and undergoes devolatilization. The volatiles that are released undergo homogenous combustion, and the leftover mass of coal is now referred to as char. Char can undergo heterogeneous combustion. The quantity of the volatiles released from the coal is a function of the final heating temperature of the coal as well as the type of coal. The residual mass after all forms of combustion is known as ash [2].

Simplified coal combustion reactions can take the following forms:

$C(s)+O_2(g) \rightarrow CO_2(g)$

$C(s)+CO_2(g) \rightarrow 2CO(g)$

Table 1: Coal Physical Properties [3]

Rank	Block Formula	Density (g/cc)	Volatile Matter (%)	Fixed Carbon (dmmf) *(%)	Calorific Value (Btu/lb)	Moisture (%)
Peat	$C_{100}H_{116}O_{39}$	0.4	50-70	25-30	4,000-5,000	70-95
Lignite	$C_{100}H_{90}O_{25}NS$	1.2	40-70	40-60	6,300-8,300	30-40
Subbituminous	$C_{100}H_{80}O_{15}NS$	1.3	46-52	45-60	8,300-11,500	10-30
hv-Bituminous	$C_{100}H_{80}O_{10}NS$	-	31-46	45-65	11,500-15,000	1-10
mv-Bituminous	$C_{100}H_{70}O_6NS$	1.4	22-31	69-78	15,000-15,500	2
lv-Bituminous	$C_{100}H_{60}O_5NS$	-	14-22	78-86	15,500-16,000	2
Anthracite	$C_{100}H_{40}O_3NS$	1.7	2-14	86-98	14,200-15,200	0-5

*dry, mineral matter free

2.3 Oil

Practical fuel oils consist of multiple components with different chemical structures. Even fuels such as gasoline are mixtures of hydrocarbons, having different molecular weights which lead to different heats of combustion and effectively result in different energy efficiencies. Fuel oil comes in many different grades. The American Society for Testing and Materials currently defines six grades of fuel oil. As the grade increases the viscosity, carbon chain length and boiling point increases.

Number 1 fuel oil or volatile distillate oil, is the kerosene refinery cut that boils off right after the heavy naphtha cut used for gasoline. Number 2 fuel oil is used as distillate home heating oil. Trucks and some cars use similar diesel fuel with a cetane number limit describing the ignition quality of the fuel. Both are typically obtained from the light gas oil cut. Gas oil refers to the process of distillation where crude oil is heated, becomes a gas and then condenses. Number 3 fuel oil is the distillate oil for burners requiring low-viscosity fuel. Number 4 fuel oil is commercial heating oil for burner installations not equipped with preheaters. It may be obtained from the heavy gas oil cut. Number 5 fuel oil is residual-type industrial heating oil requiring preheating to between 170 and 220 degrees Fahrenheit for proper atomization at the burners. This fuel is sometimes known as Bunker B. It may be obtained from the heavy gas oil cut, or it may be a blend of residual oil with enough number 2 oil to adjust viscosity until it can be pumped without preheating. Number 6 fuel oil is a high-viscosity residual oil requiring preheating to between 220 to 260 degrees Fahrenheit. [4]

For all grades of oil, combustion takes place when the liquid oil is heated to the point of vaporization. In almost all cases the liquid fuel oil is sprayed into the combustion chamber through jets that atomize the fuel into very small droplets, allowing for faster vaporization time and therefore faster combustion time.

The following, tables 2 and 3, are general values for the major grades of fuel oils. Two of these values, specifically heating value and viscosity, are some of the most important traits of a combustible fuel that need to be duplicated in the creation of a composite fuel mixture if it is to be a viable competitor of existing fuel sources.

Table 2: Fuel Properties (excluding viscosity) [5]

Grade No.	API Gravity	Density (lb/gal)	Higher Heating Value (Btu/gal)
1	38-45	6.950-6.675	137,000-132,9000
2	30-38	7.296-6.960	141,800-137,000
4	20-28	7.787-7.396	148,100-143,100
5L	17-22	7.940-7.686	150,000-146,600
5H	14-18	8.080-7.890	152,000-149,400
6	8-15	8.448-8.053	155,900-151,300

Table 3: Fuel viscosities at varying temperatures [6]

	(^{o}F)	(^{o}C)	CentiStokes (cSt)	Seconds Saybolt Universal (SSU)
Fuel oil 1	70	21.1	2.39-4.28	34-40
	100	37.8	-2.69	32-35
Fuel oil 2	70	21.1	3.0-7.4	36-50
	100	37.8	2.11-4.28	33-40
Fuel oil 3	70	21.1	2.69-5.84	35-45
	100	37.8	2.06-3.97	32.8-39
Fuel oil 5A	70	21.1	7.4-26.4	50-125
	100	37.8	4.91-13.7	42-72
Fuel oil 5B	70	21.1	26.4-	125-
	100	37.8	13.6-67.1	72-310
Fuel oil 6	122	50	97.4-660	450-3M
	160	71.1	37.5-172	175-780

2.4 Wood

Wood is a key organic solid to study when considering general biomass combustion. This is due to its wide availability and basic chemical composition being similar to other organic solids. Cellulose and lignin are the main components found in wood. Cellulose is comprised of many glucose molecules $(C_6H_{10}O_5)_x$. Lignin is usually one of the following: $C_9H_{10}O_2, C_{10}H_{12}O_3,$ or $C_{11}H_{14}O_4$. A simplified combustion reaction of wood can be represented by:

$$C_6H_{12}O_6 + 6O_2 = 6CO_2 + 6H_2O$$

with wood disappearing and carbon dioxide being produced along with water vapor. Any portion of the wood that is not combustible would remain behind as inert ash. Common woods are made up of approximately 50% carbon, 6% hydrogen and 44% oxygen on an ash free basis. Hardwoods have lower carbon and higher oxygen contents then softwoods. The combustion process of wood starts off with the wood heating up to approximately 212 ^{o}F (100 ^{o}C) which results in the evaporation of any moisture. At 575 ^{o}F (300 ^{o}C) the wood solids start to break down converting to fuel gases. From 575 ^{o}F to 1100 ^{o}F (300 - 600 ^{o}C) the most abundant source of energy in the wood is released when fuel vapors containing 40% to 60% of the energy combust. After the fuel vapors are consumed, what remains of the wood is charcoal, which burns at temperatures higher than 1100 ^{o}F. [6]

Different types of wood and their respective densities and heat values are presented in table 4.

Table 4: Wood Combustion Properties [6]

Wood Species	Density of Dry Wood (lb/ft^3)	Weight of Cord (lb/cord)	Recoverable Heat Value of Cord (Dry Wood) (millions Btu/cord	Heat Value of Cord (Green Wood) (millions Btu/cord	Units needed to produce 1 Million (cord/Btu's)
Red Oak	44.2	3760	24	16.8	0.060
Red Maple	34.4	2920	18.7	13.1	0.076
Hickory	50.9	4330	27.7	19.4	0.052
Hackberry	38.2	3250	19.5	13.7	0.073
Paper Birch	37.4	3180	20.3	14.2	0.070
Yellow Birch	43.4	3690	23.6	16.5	0.061
Cherry	36.7	3120	20	14	0.071

Beech	44.2	3760	24	16.8	0.060
Jack Pine	31.4	267	17.1	12.0	0.084
White Pine	26.3	2240	14.3	10.0	0.100

2.5 Solid Biomaterials

Solid biomaterials consist of the following: wood, sawdust, grass trimmings, domestic refuse, charcoal, agricultural waste, nonfood energy crops, peat, rubber, dried manure, rubber and many other carbon based entities. One of the advantages of a solid biomass fuel is that it is often a byproduct, residue or waste-product of other processes, such as farming, animal husbandry and forestry. In theory, this means fuel and food production do not compete for resources, although this is not always the case. As there are many different types of solid biomaterials and these biomaterials differ even compared to each other, it is difficult to present information on their physical and combustion properties.

One of the more common biosolids presently being used in research are tires. Tires are the most interesting of the above mentioned fuel sources due to a multitude of reasons. To date there has been no recycled use for tires that generates nearly as much energy as is required to create them or even successfully disposes of them faster than they are created. Compared to other commonly used solid fuels, the heating value of tires is 25-50% higher than coal and 100-200% higher than wood [7]. Currently the most common fuel related use of tires is a technology called Tire-Derived Fuel, which is when specially shredded tires are mixed with other fuels such as coal or wood and burned in a kiln. There are some studies being done on combining ground rubber tires with heavy fuel oil through a hyrdrocavitation reactor

process [8]. The results were a fuel paste that could be easily combusted. The hope is that with future research similar to hydrocaviation technology, a fuel with a high heating value could be made using relatively unused materials such as used tires and #6 fuel oil. The following are some combustion values found for crumb rubber as well as tire composition. These should be taken as general values due to the unavoidable variability in tire creation.

Table 5: Average chemical composition of rubber chips [9]

pH	Lower Heating Value (KJ/Kg)	Mineral Oil (mg/Kg)	Total cyanide (mg/Kg)	Chloride (mg/Kg)	Chromium VI (mg/Kg)	Mercury (mg/Kg)	Lead (mg/Kg)	Copper (mg/Kg)	Total Hydrocarbons (mg/Kg)
7,9	36.2	46.6	n.d.	31.00	n.d.	n.d.	n.d.	10.2	91.2

Table 6: The chemical composition of tires [7]

Carbon	Hydrogen	Zinc oxide	Sulfur	Iron	Additives	Oxygen	Nitrogen	Stearic acid
70 .0-75.0	6.0-7.0	1.2 - 2.0	1.3 - 1.7	13.0 - 15.0	3.5 - 5.0	4	0.005	0.003

Table 7: The chemical composition of tires continued [7]

Halogens	Copper compounds	Cadmium	Chromium	Nickel	Lead
0.001	200ppm	10ppm	90ppm	80ppm	50ppm

Another good potential biomass is peat. Peat is an accumulation of partially decayed vegetation. While peat was used for thousands of years as a fuel source, it eventually died out in popularity like most other early fuels due to fuel oil. The recent energy shortages, especially in electricity, have renewed peat to being a potential fuel source. "Peat's vary greatly in character partly depending on the state of decomposition of their plant. Weakly decomposed peat is poorly suited to

combustion, and therefore peat should be at least moderately decomposed for use as a fuel." [10] Below, are tables 8, 9 and 10 show some combustion relevant information about peat gathered from the literature.

Table 8: The most important elements in peat according to degree of decomposition [10]

	Slightly decomposed	Moderately decomposed	Highly decomposed peat
Carbon	48-501	53-54	58-60
Hydrogen	5.5-6.5	5.0-6.0	5.0-5.5
Nitrogen	0.5-1	1.0-2.0	1.0-3.0
Oxygen	38-42	35-40	30-35

Table 9: General chemical and fuel properties of a range of solid fuels [10]

		Coal	Lignite	Peat	Wood
Chemical composition					
Carbon (C)	weight %	76-87	65-75	50-60	48-55
Hydrogen (H)	weight %	3.5-5.0	4.5-5.5	5-7	6-7
Oxygen (O)	weight %	3-11	20-30	30-40	38-43
Nitrogen (N)	weight %	0.8-1.2	1-2	0.5-2.5	<0.6
Sulfur (S)	weight %	1-3	1-3	0.1-0.4	0.02-0.06
Fuel properties					
Volatile matter	weight %	10-50	50-60	60-70	75-85
Ash	weight %	4-10	6-10	2.0-15.0	0.1-2.0
Melting point of ash	°C	1100-1300	1100-1300	1100-1300	1350-1450
Bulk density	kg/m3	728-880	650-780	300-400	320-420
Effective calorific value of dry substance	MJ/kg1	28-33	20-24	20-23	17-20

"Three types of commercial peat are commonly distinguished: milled peat having a moisture content of 40-50 percent, air-dried sod peat with a moisture content of 30-40 percent and artificially dried compressed peat briquettes with a moisture

content of 10-20 percent. Milled peat is commonly produced by large scale mechanized peat extractions, whereas the other two are produced on a smaller scale by manual, semi-mechanical or mechanical methods, either in dry or in wet conditions." [10]

Table 10: Combustion properties of peat [10]

	Milled	Sod	Briquettes
Effective calorific value of dry matter (MJ/kg-mean)	18-22	18-22	18-22
Effective calorific value at operating moisture content (MJ/kg-mean)	7-12	11-14	17-18
Volatile substances (% dry matter-mean)	65-70	65-70	65-70
Bulk density at operating moisture content (kg/m3)	300-400	300-400	700-800
Operating moisture content (%)	40-55	30-40	10-20

2.6 Water

Due to the general knowledge of water, time will not be taken breaking down the chemical composition and common traits of water. It is not a fuel, and in this thesis is only being considered for its emulsion creating capabilities. Tables 11 and 12 show emulsion relevant properties of water. One important trait not noted in these tables is that oil is hydrophobic.

Table 11: Density and viscosity of water at varying temperatures [6]

Temperature ^{o}C	Density (kg/m)	Viscosity (cSt)
0	916.8	1.787
5	1000	1.519
10	999.8	1.307
20	998.3	1.004
30	995.7	0.801
40	992.3	0.658
50	988	0.553
60	983	0.475
70	978	0.413

80	972	0.365
90	965	0.326
100	958	0.29

Table 12: Other combustion relevant water properties [6]

Boiling temperature (^{o}C)	Latent heat of evaporation (kJ/kg)	Specific heat water (kJ/kg*K)	Specific heat water vapor (kJ/kg*K)
100	2,270	4.187	1.996

2.7 Soybean oil

Soybean oil will be used in the settling experiments throughout this thesis in both the experimental and modeling sections. Soybean oil is mostly "unsaturated fatty acids in soybean oil triglycerides are the poly-unsaturates, alpha-linolenic acid (C-18:3), 7-10%, and linoleic acid (C-18:2), 51%; and the mono-unsaturate, oleic acid (C-18:1), 23%. It also contains the saturated fatty acids, stearic acid, (C-18:0), 4%, and palmitic acid, (c-16:0), 10%".[11] As average soybean oil properties from a combustion stand point are difficult to find in the literature, an intensive process was used to calculate them which will be seen in the modeling section of the thesis and will not be presented here.

2.8 Vapor Pressure

As vapor pressure is directly related to volatility and volatility is an important variable in combustion, the vapor pressure of the various liquid fuels to be modeled will be represented in the following figure. Diesel will be represented by an average of the vapor pressure of two similar hydrocarbons, hexadecane and dodecane.

Soybean oil vapor pressure was calculated using a method from [12]. These vapor pressure are presented in figures 1, 2 and 3.

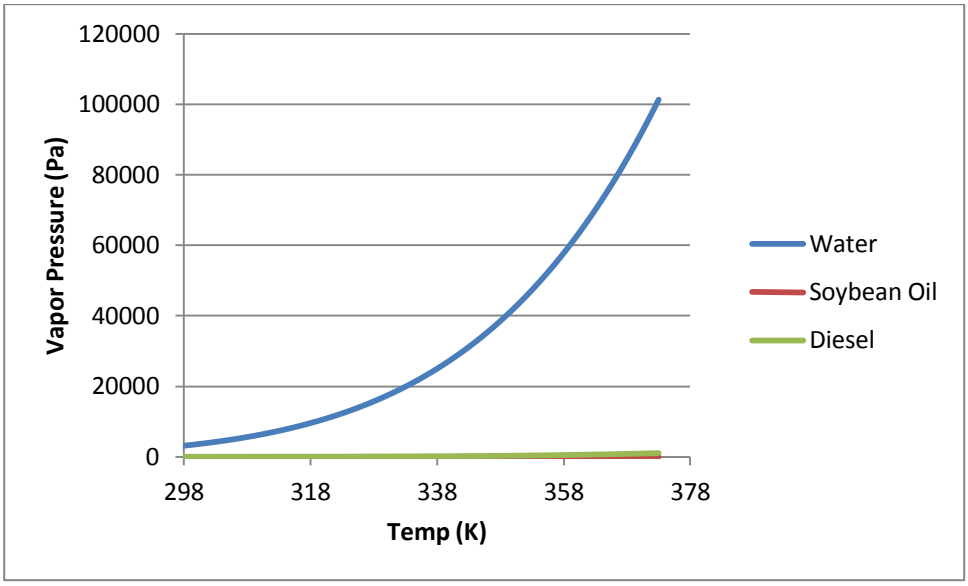

Figure 1: Vapor pressure graph consisting of water, diesel and soybean oil

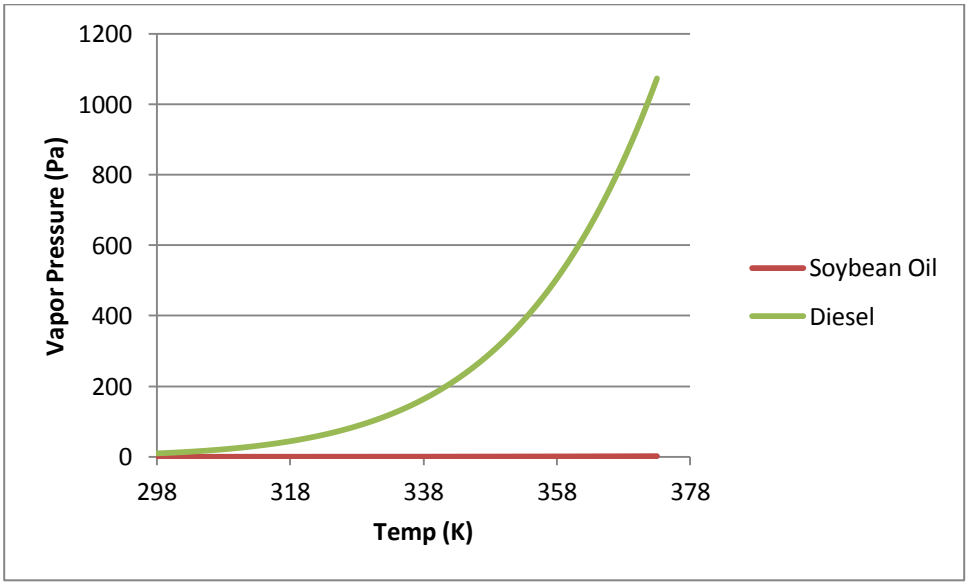

Figure 2: Vapor pressure graph consisting of diesel and soybean oil

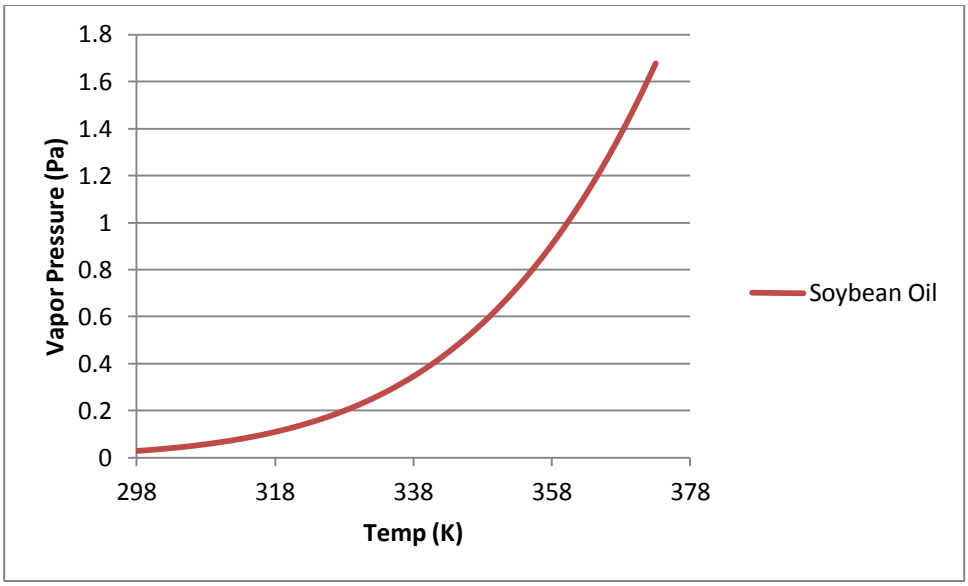

Figure 3: Vapor pressure graph for soybean oil

2.8 Summary

Again this section served as an introduction to the materials from a combustion stand point that will be used to in later experiments and models. The physical properties of the composite fuels will depend on their derivative fuels and therefore detailed physical information as well as a general understanding of these simple fuels is necessary. In future sections more physical properties may be shown that are pertinent to the topic.

2.9 References

[1] "Educations Fact Sheets." *Aie.org.au*. N.p., n.d. Web. 30 Nov. 2011. <http://www.aie.org.au/AIE/Energy_Info/Educational_Fact_sheets/AIE/Energy_Info/Educations_Fact_sheets.aspx?hkey=06810f4b-06be-4647-af90-c7a9dafbfa4f>.

[2] Smoot, Leon Douglas. *Fundamentals of coal combustion: for clean and efficient use*. Vol. 20. Elsevier Science Ltd, 1993.

[3] Singer, Stanley. "Pulverized coal combustion-recent developments." (1984): 42-83

[4] *Diesel Fuel, All Types*; MSDS No. 9909 [Online]; Hess Corporation: Woodbridge, NJ,
August 13, 2012, http://www.hess.com/ehs/msds/9909dieselfuelalltypes.pdf (accessed December 12 2011)

[5] Turns, Stephen R. *An introduction to combustion*. Vol. 3. New York: McGraw-Hill, 2012

[6] "Engineering ToolBox." *Engineering ToolBox*. N.p., n.d. Web. 5 Apr. 2013.

[7] Lechtenberg, Dirk. "Tyres as an Alternative Fuel." *CemFuels.com*. MVW Lechtenberg & Partner, 03 Mar. 2011. Web. 14 Dec. 2011. <http://www.cemfuels.com/articles/318-tyres-as-an-alternative-fuel>.

[8] AIChE Spring meeting May 2012, *Innovative Hydrocavitation Technology*, Knickle

[9] "Tire Chips." *Europeanrecycle.com*. N.p., n.d. Web. 28 Dec. 2012. <http://www.europeanrecycle.com/subpagine.asp?id=71>

[10] "9. ENERGY USE OFPEAT." *Fao.org*. N.p., n.d. Web. 29 Dec. 2011. <http://www.fao.org/docrep/x5872e/x5872e0b.htm>

[11] Ivanov, Dušica S.; Lević, Jovanka D.; Sredanović, Slavica A. (2010). "Fatty acid composition of various soybean products". *Journal of the Institute for Food Technology in Novi Sad* **37** (2): 65–70. Retrieved 21 June 2013.

CHAPTER 3 - SETTLING EXPERIMENTS USING SOYBEAN OIL, WOOD AND WATER

3.1 Introduction

In order for a composite fuel, any fuel source containing a mixture of both solids and liquids, to be able to function in a combustion environment, it needs to maintain as close to a homogenous mixture as possible. The goal of the next two chapters is to see if composite fuels will can be made to exists as extremely well mixed heterogeneous mixtures with homogenous properties and how long they can stay in that form. For composite fuels, the main concern is the fuel losing its stability due to the process known as settling, where the different phases of a mixture separate. While settling can occur in liquid-liquid mixtures, it is particularly devastating in a composite fuel mixture. The main problem caused by settling is buildup of the solid in pipes and ineffective atomization from the fuel spray guns effectively halting all combustion. However new designs of spray guns may alleviate this problem.

Before composite fuel technology can make any kind of forward progress, a solution for settling must be found. A method to slow or stop settling is keeping the mixture moving with enough velocity to remain mixed. Obvious problems with this method of settling control are as follows. By having a minimum flow rate that must be met at all times certain restrictions are put on the process, such as pipe diameter maximums, which can make expansion or maintenance/upgrading a more tedious task then necessary. A better solution is to create an emulsion by addition of water and energy to the solid-liquid fuel composite mixture. When emulsified with water, the liquid fuel-solid mixtures will see an increase in mixture density and a decrease in

mixture viscosity. According to Stokes Law of settling shown below, these changes in the mixture properties will slow settling velocity.

$$v_s = \frac{2}{9}\frac{(\rho_p - \rho_f)}{\mu} g \frac{4}{3}\pi R^3$$

In this equation v_s is settling velocity, $\rho_p \rho_f \; gR^3$

To test this theory, a settling experiment was performed where the settling rates of oil-solid non-emulsion mixtures were compared with those of oil-solid-water emulsions. Specifically, two separate mixture makeups were tested: soybean oil with wood particles and soybean oil with coal particles. In both cases the emulsions were created with water. Particle sizes, mixture concentrations and mixture temperatures were also varied to find their effect on settling velocity.

3.2 Procedure

A fine toothed saw was used to cut a block of wood until enough saw dust was collected to fill a 30 ml cup. The diameter of multiple wood particles was estimated. Various weights and volumes of substances were recorded. One 30 ml cup of oil was mixed with one 30 ml cup of saw dust in a 100 ml beaker and the weight of the contents was determined. A qualitative observation of the mixture viscosity was made. Then a new 30 ml cup of oil was added to the contents in the beaker. Again a qualitative observation of the viscosity was made. The separation front was measured for the second mixture at 26 ^{o}C. The second mixture was then heated to about 66 ^{o}C and the settling front was again measured.

15 g of water was then added to the second mixture and the resulting mixture was shaken and well mixed to make an emulsion. The settling front of this emulsion

mixture was observed and a qualitative test of the viscosity of this mixture with temperature was observed. This entire procedure was then repeated using larger wood particles of around 1 mm diameters on average.

3.3 Data

All data was separated into two trials. The trials differ in the size of the wood particles used. Trial 1 represents wood particles diameters of ~ 0.00001 m while Trial 2 used wood particle diameters of ~ 0.001 m

The individual measurements comprising the mixtures used in the experiments are tabulated below in tables 13 and 14.

Table 13: Mass of individual wood and soybean oil in Trial 1

Object	Weight (g)
Empty 30 ml Cup	1.3
Wood Particles	5.5
Soybean oil amount in 1st 30 ml cup	24.7
Soybean oil amount in 2nd 30 ml cup	25.2
Water (30 ml cup)	31

Table 14: Mass of individual wood and soybean oil in Trial 2

Object	Weight (g)
Empty 30 ml Cup	1.3
Wood Particles	3.3
Soybean oil amount in 1st 30 ml cup	25.7
Soybean oil amount in 2nd 30 ml cup	26.2

Table 15 lists the mixture weights used in trial 1.

Table 15: Various Weights of combined wood/soybean oil mixtures in a beaker

	Mixture 1 (g)	Mixture 2 (g)	Mixture 3 (g)
Soybean Oil	24	49.5	49.5

Wood Particles	5.4	5.4	5.4
Water	-	-	15
Total	29.4	54.9	69.9
Total (with beaker)	79	104.5	119.5
Empty Beaker	49.6	49.6	49.6

Table 16 lists the mixture weights used in trial 2.

Table 16: Various Weights of combined wood/soybean oil mixtures in a beaker

	Mixture 1 (g)	Mixture 2 (g)	Mixture 3 (g)
Soybean Oil	25.2	50.9	50.9
Wood Particles	3.3	3.3	3.3
Water	-	-	15
Total	28.5	54.2	69.2
Total (with beaker)	78.1	103.8	118.8
Empty Beaker	49.6	49.6	49.6

The trial 1 settling fronts for the second mixture at both temperatures were recorded and tabulated below in tables 17 and 18. This is followed by a recording of the settling front for the water emulsion mixture at both temperatures in tables 19 and 20.

Table 17: Settling clear front for Mixture 1 at 26 °C

Minutes	Separation Front Top Layer Mostly Oil (mm)	Bottom Layer Heterogeneous Top Front (mm)
0	0	36.0
15	10.0	26.0
45	15.0	21.0
infinite	17.5	19.5

Table 18: Settling clear front for Mixture 1 at 66 °C

Minutes	Separation Front Top Layer Mostly	Bottom Layer Heterogeneous Top Front

	Oil (mm)	(mm)
0	0	36.0
7.5	0.70	29.0
13.5	12.0	24.0
17.5	15.0	21.0
24.5	18.0	18.0
infinite	19.5	17.5

Table 19: Settling Clear front for Mixture 2 at 26 °C

Minutes	Separation Front Top Layer Mostly Oil/Water (mm)	Bottom Layer Heterogeneous Top Front (mm)
0	0.0	42.0
15	0.0	42.0
45	0.0	42.0
480	1.0	41.0
1440	2.0	40.0

Table 20: Settling Clear front for Mixture 2 at 66 C

Minutes	Separation Front Top Layer Mostly Oil/Water (mm)	Bottom Layer Heterogeneous Top Front (mm)
0	0.0	42.0
15	1.0	42.0
45	3.0	42.0
90	4.5	37.5

The following is a qualitative particle distribution of the wood particles used throughout trial 1.

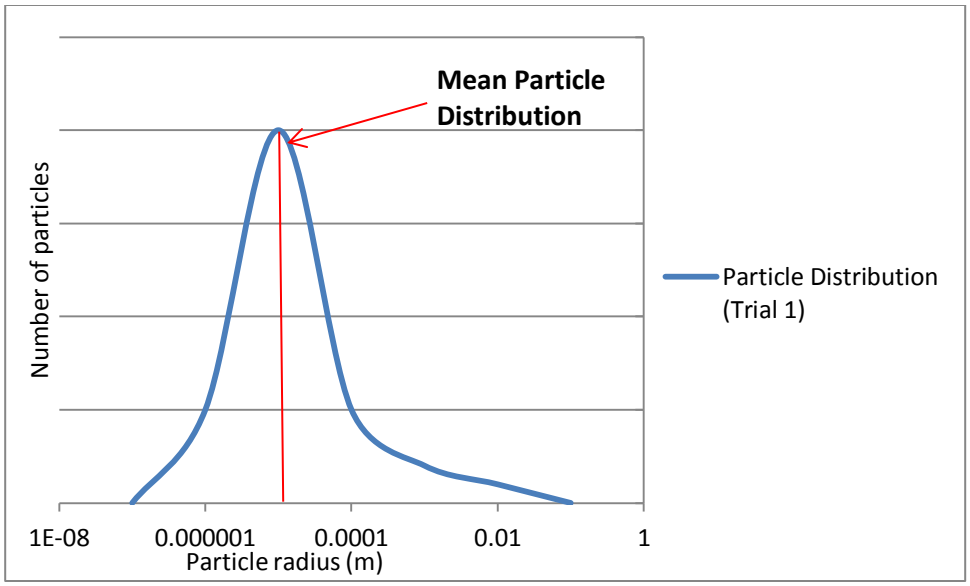

Figure 4: Qualitative particle distribution of wood particles used in Trial 1

The trial 2 settling fronts for the second mixture at both temperatures were recorded and tabulated below in tables 21 and 22. This is followed by a recording of the settling front for the water emulsion mixture at both temperatures in tables 23 and 24.

Table 21: Settling clear front for Mixture 1 at 24 °C

Minutes	Separation Front Top Layer Mostly Oil (mm)	Bottom Layer Heterogeneous Top Front (mm)
0	0.0	35.0
8	7.0	28.0
15	15.0	20.0
25	19.0	16.0
40	20.0	15.0
infinite	20.0	15.0

Table 22: Settling clear front for Mixture 1 at 60 °C

Minutes	Separation Front Top Layer Mostly Oil (mm)	Bottom Layer Heterogeneous Top Front (mm)
0	0.0	35.0

5	10.0	25.0
10	16.0	19.0
15	20.0	15.0
20	20.5	14.5
30	22.0	13.0
infinite	22.0	13.0

Table 23: Settling Clear front for Mixture 2 at 24 ^{o}C

Minutes	Separation Front Top Layer Mostly Oil/Water (mm)	Bottom Layer Heterogeneous Top Front (mm)
0	0.0	41.0
6	14.0	27.0
15	16.0	25.0
30	17.0	24.0
65	18.0	23.0
120	18.0	23.0
infinite	18.0	23.0

Table 24: Settling Clear front for Mixture 2 at 60 C

Minutes	Separation Front Top Layer Mostly Oil/Water (mm)	Bottom Layer Heterogeneous Top Front (mm)
0	3.0	41.0
5	10.0	31.0
15	15.0	36.0
30	20.0	21.0
infinite	20.0	21.0

The following is a qualitative particle distribution of the wood particles used throughout Trial 2.

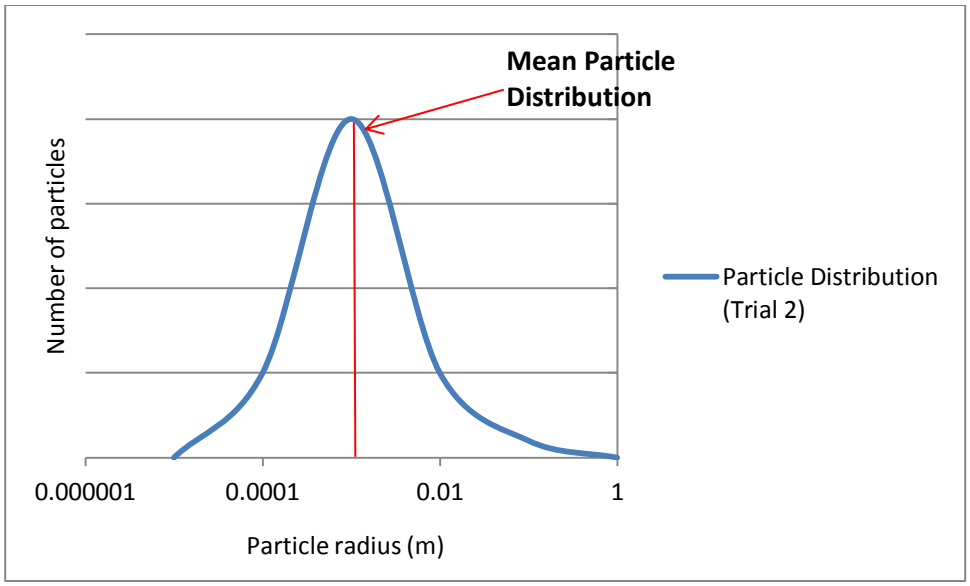

Figure 5: Qualitative particle distribution of wood particles used in Trial 2

3.4 Sample Calculations

Below are the mixture independent calculations for this experiment.

$$Total\ volume\ of\ cup = \frac{Mass\ of\ Water\ in\ cup}{Density\ of\ water} = \frac{29.8g}{.996600g/cm^3} = 29.9\ cm^3$$

$$Volume\ of\ Wood\ in\ cup = \frac{Mass\ of\ wood\ in\ cup}{Density\ of\ wood} = \frac{5.50\ g}{0.480\ g/cm^3} = 11.5\ cm^3$$

$$Density\ of\ soybean\ oil = \frac{Mass\ of\ soybean\ oil\ in\ cup}{Volume\ of\ soybean\ oil\ in\ cup} = \frac{25.9\ g\ oil}{29.9\ cm^3}$$

$$= \frac{.87\ g\ oil}{cm^3}$$

$$Wood\ fraction = \frac{11.5\ cm^3}{29.9\ cm^3} = .38$$

$$\boldsymbol{Void\ Fraction = 1 - .38 = .62}$$

Next are the calculations made for the mass percent of each mixture used throughout the experiment. Only one trial calculation will be shown as the process will not change from trial to trial.

$$Mixture\ 1 = 24.0\ g\ oil + 5.40\ g\ wood = \ 29.4\ g\ mixture$$

$$\frac{24.7\ g\ oil}{29.4\ g\ mixture} = \ \mathbf{84\%\ oil}$$

$$\frac{5.40\ g\ wood}{29.4\ g\ mixture} = \mathbf{16\%\ wood}$$

$$Mixture\ 2 = 49.5\ g\ oil + 5.40\ g\ wood = 54.9\ g\ mixture$$

$$\frac{49.5\ g\ oil}{54.9\ g\ mixture} = \ \mathbf{90\%\ oil}$$

$$\frac{5.40\ g\ wood}{54.9\ g\ mixture} = \ \mathbf{10\%\ wood}$$

It should be noted that mixture 3 has water added to it in order to create an emulsion.

$$Mixture\ 3 = 49.5\ g\ oil + 5.40\ g\ wood + 15\ g\ water = 69.9\ g\ mixture$$

$$\frac{49.5\ g\ oil}{69.9\ g\ mixture} = \ \mathbf{70.8\%\ oil}$$

$$\frac{5.40\ g\ wood}{69.9\ g\ mixture} = \ \mathbf{7.7\%\ wood}$$

$$\frac{15\ g\ water}{69.9\ g\ mixture} = \ \mathbf{21.5\%\ water}$$

The same calculations were performed in order to find the volume fractions.

$$Mix\ 1 = 24.0\ g\ oil * \left(\frac{cm^3}{0.860\ g\ oil}\right) + 5.40\ g\ wood * \left(\frac{cm^3}{.480g}\right)$$

$$= \ 39.2\ cm^3\ mixture$$

$$Mix\ 1 = 27.9\ cm^3 oil + 11.3\ cm^3\ wood = \ 39.2\ cm^3\ mixture$$

$$\frac{27.9\ cm^3 oil}{39.2\ cm^3\ mixture} = \ \mathbf{71\%\ oil}$$

$$\frac{11.3\ cm^3\ wood}{39.2\ cm^3\ mixture} = \ \mathbf{29\%\ wood}$$

$$Mix\ 2 = 49.5\ g\ oil * \left(\frac{cm^3}{0.860\ g\ oil}\right) + 5.40\ g\ wood * \left(\frac{cm^3}{.48g}\right)$$

$$= 68.9\ cm^3\ mixture$$

$$Mix\ 2 = 57.6\ cm^3 oil + 11.3\ cm^3\ wood = 68.9\ cm^3\ mixture$$

$$\frac{57.6\ cm^3 oil}{68.9\ cm^3\ mixture} = \mathbf{84\%\ oil}$$

$$\frac{11.3\ cm^3\ wood}{68.9\ cm^3\ mixture} = \mathbf{16\%\ wood}$$

$$Mix\ 3 = 49.5\ g\ oil * \left(\frac{cm^3}{0.860\ g\ oil}\right) + 5.40\ g\ wood * \left(\frac{cm^3}{.48\ g\ wood}\right) + 15\ g\ water$$

$$* \left(\frac{1\ cm^3}{.997\ g\ water}\right) = 83.9\ cm^3\ mixture$$

After adding water the emulsion properties were as follows.

$$Mix\ 3 = 57.6\ cm^3 oil + 11.3\ cm^3\ wood\ + 15.01\ cm^3\ water = 83.9\ cm^3\ mixture$$

$$\frac{57.6\ cm^3 oil}{83.9\ cm^3\ mixture} = \mathbf{68.6\%\ oil}$$

$$\frac{11.3\ cm^3\ wood}{83.9\ cm^3\ mixture} = \mathbf{13.5\%\ wood}$$

$$\frac{15.01\ cm^3\ water}{83.9\ cm^3\ mixture} = \mathbf{17.9\%\ water}$$

3.5 Results

The results are separated into two trials. The trials differ in the size of the wood particles used. Trial 1 represents wood particle diameters of ~0.00001 m while trial 2 used wood particle diameters of around ~0.001 m

3.5.1 Settling

The following series of figures represents all trial 1 settling front results. There will be a figure for each mixture at each temperature. In each figure the data points are graphed alongside a model equation that describes each settling front. Each graph is illustrating the settling front from the top oil rich phase. Figure 6 shows the settling front of mixture 1 for trial 1 at 26 ^{o}C.

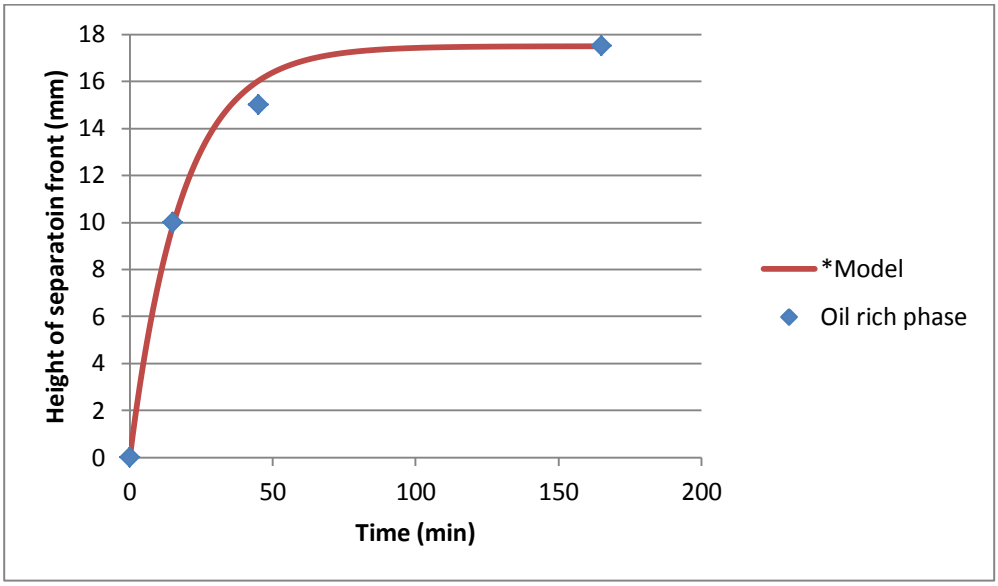

Figure 6: Settling clear front for the mixture data from table 17 at 26 ^{o}C
$*height = 17.5(1 - EXP(-0.055 * time))$ This is the model equation found from the data. It is a power curve representing the increase in the top oil rich phase of the mixture as time increases.

Figure 7 shows the settling front of mixture 1 for trial 1 at 66 ^{o}C.

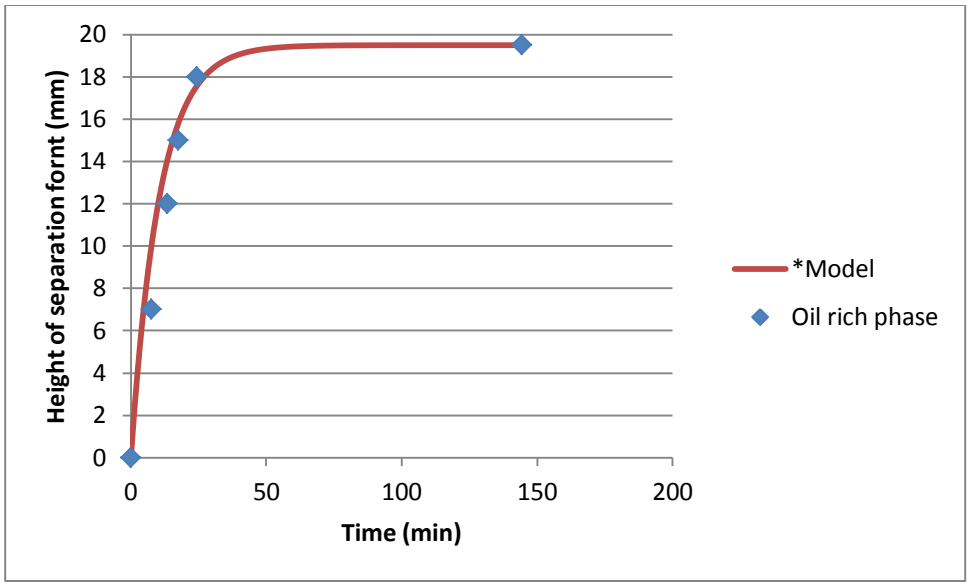

Figure 7: Settling clear front for the mixture data from table 18 at 66 °C
$*height = 19.5(1 - EXP(-0.095 * time))$ **This is the model equation found from the data. It is a power curve representing the increase in the top oil rich phase of the mixture as time increases.**

Figure 8 shows the settling front of mixture 2 for trial 1 at 26 °C.

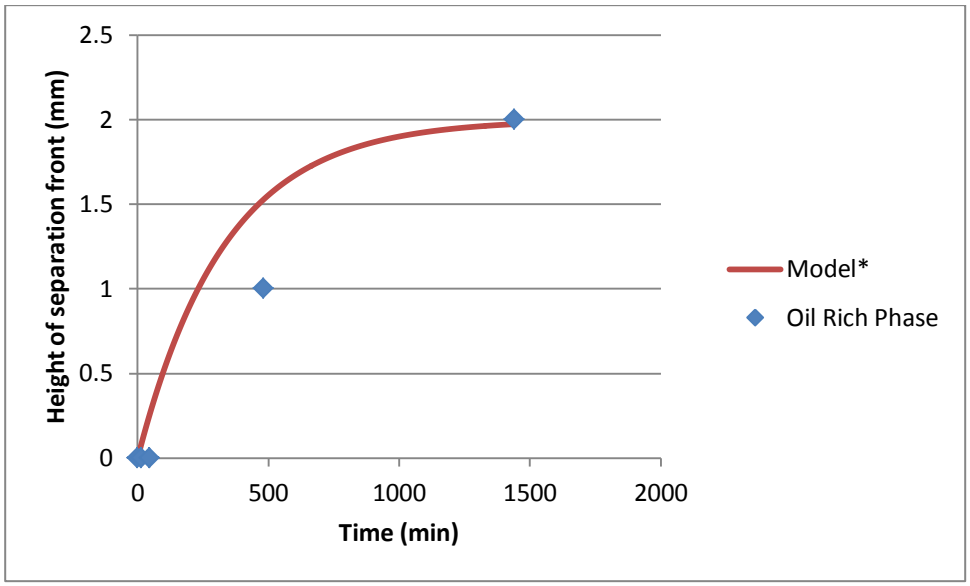

Figure 8: Settling clear front for the emulsion data from table 19 at 26 °C
$*height = 2(1 - EXP(-0.003 * time))$ **This is the model equation found from the data. It is a power curve representing the increase in the top oil rich phase of the mixture as time increases.**

Figure 9 shows the settling front of mixture 2 for trial 1 at 66 °C.

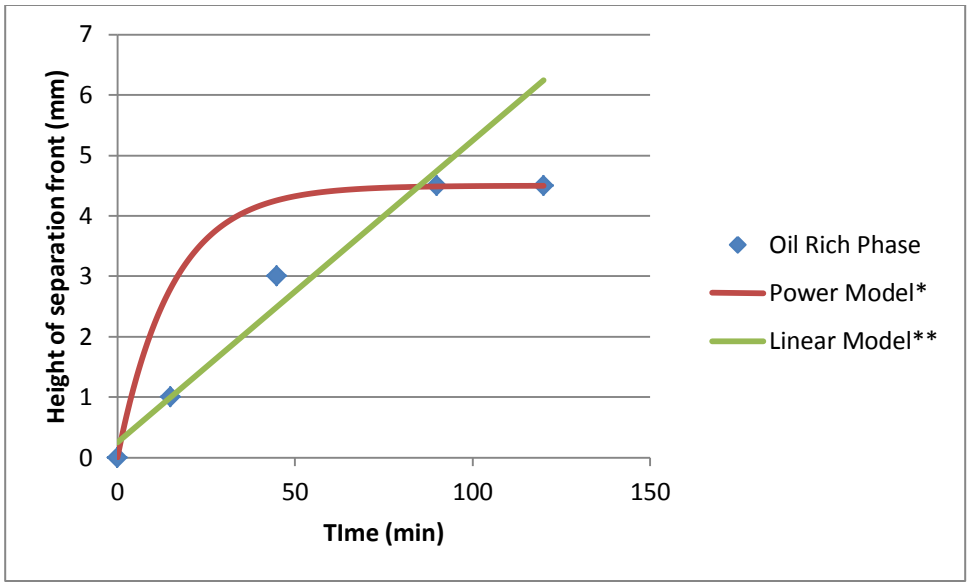

Figure 9: Settling clear front for the emulsion data from table 20 at 66 °C
***height* = 4.5(1 − *EXP*(−0.065 ∗ *time*))** **This is a model equation found from the data. It is a power curve representing the increase in the top oil rich phase of the mixture as time increases.**
****height* = 4.5 ∗ (1 − (−0.0111 ∗ *AG*3 + 0.9443))** **This is another model equation found from the data. It is a linear curve representing the increase in the top oil rich phase of the mixture as time increases.**

Figure 10 shows the settling front of mixture 1 for trial 2 at 24 °C.

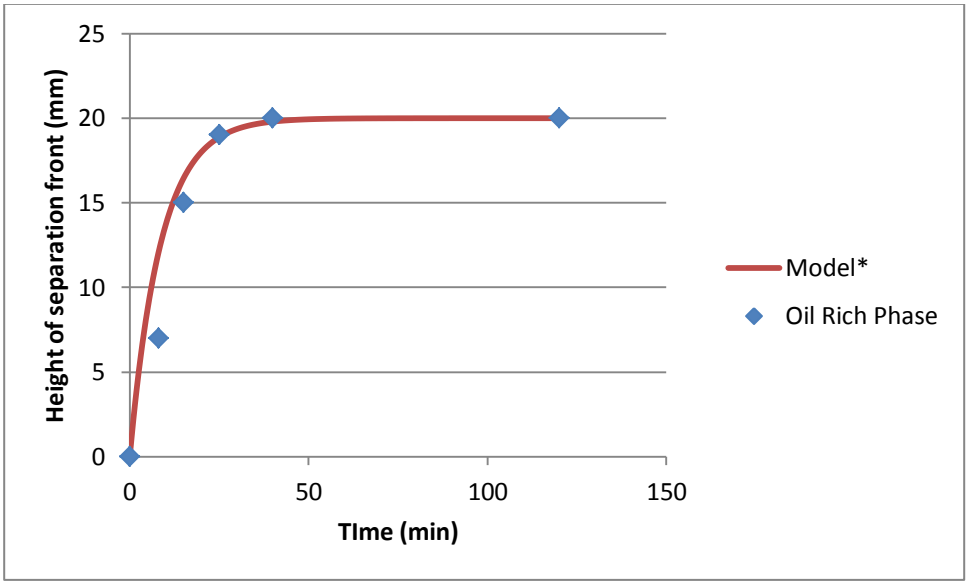

Figure 10: Settling clear front for the mixture data from table 21 at 66 °C
***height* = 20(1 − *EXP*(−0.115 ∗ *time*))** **This is the model equation found from the data. It is a power curve representing the increase in the top oil rich phase of the mixture as time increases.**

Figure 11 shows the settling front of mixture 1 for trial 2 at 60 ^{o}C.

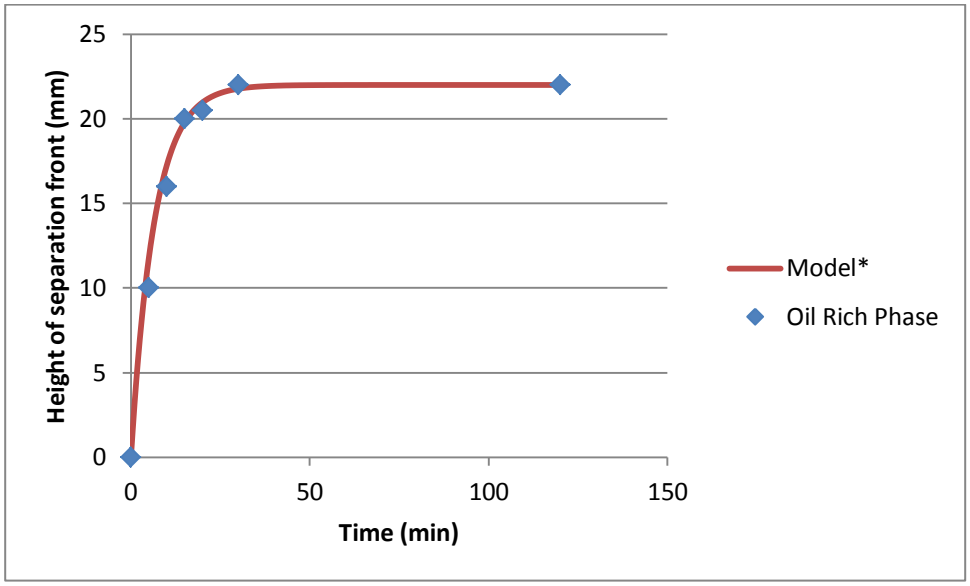

Figure 11: Settling clear front for the mixture data from table 22 at 60 ^{o}C
***$height = 22(1 - EXP(-0.153 * time))$* This is the model equation found from the data. It is a power curve representing the increase in the top oil rich phase of the mixture as time increases.**

Figure 12 shows the settling front of mixture 2 for trial 2 at 24 ^{o}C.

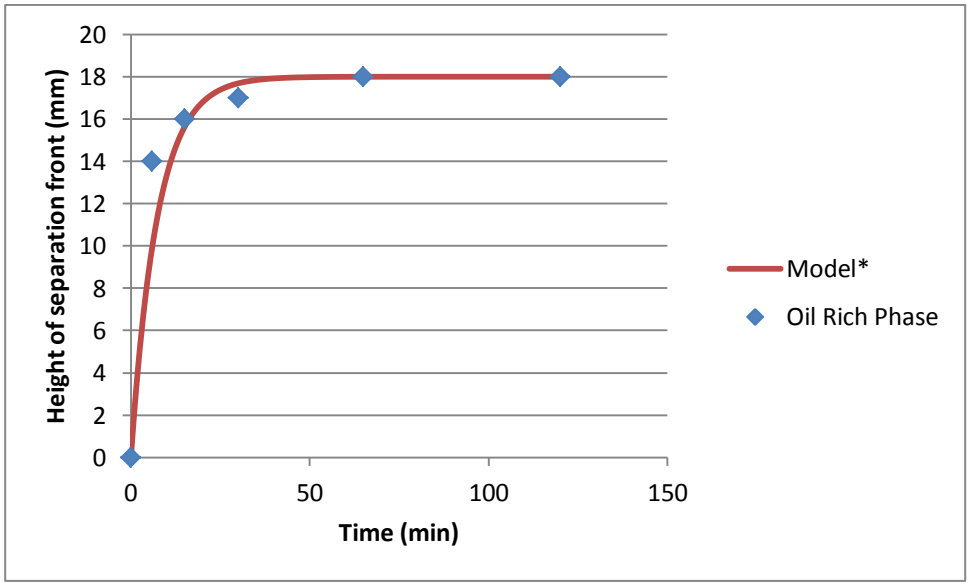

Figure 12: Settling clear front for the emulsion data from table 23 at 24 ^{o}C
***$height = 18(1 - EXP(-0.135 * time))$* This is the model equation found from the data. It is a power curve representing the increase in the top oil rich phase of the mixture as time increases.**

Figure 13 shows the settling front of mixture 2 for trial 1 at 60 ^{o}C.

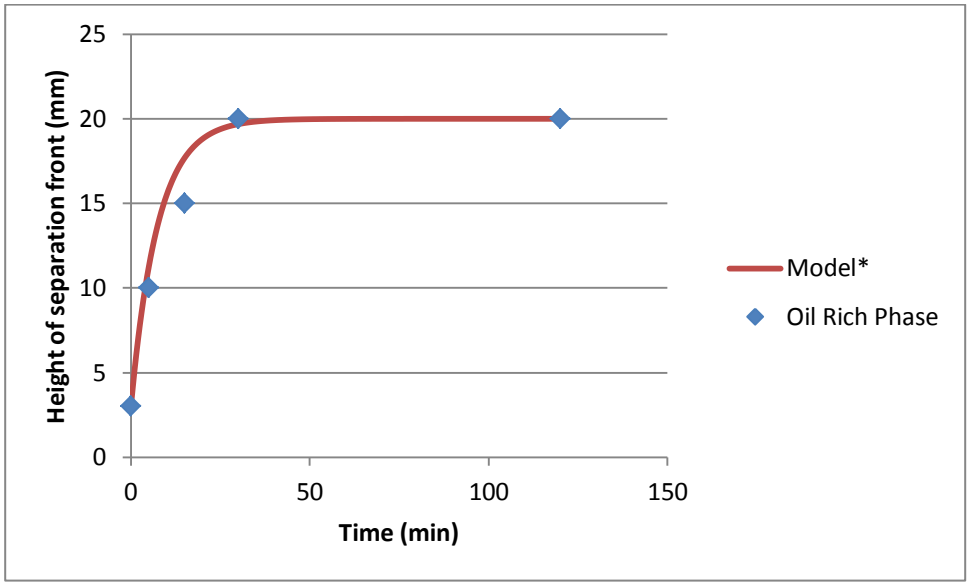

Figure 13: Settling clear front for the emulsion data from table 24 at 60^{o}C
***height* $= 20(1 - EXP(-0.133 * time))$ This is the model equation found from the data. It is a power curve representing the increase in the top oil rich phase of the mixture as time increases.**

Figures 14 and 15 are graphical representations of the normalized separation front height of the top oil rich phase of all mixture and emulsions. The heights are normalized in that 1 is no settling while 0 is a completely settled mixture. This was done to allow all data to be represented on one graph.

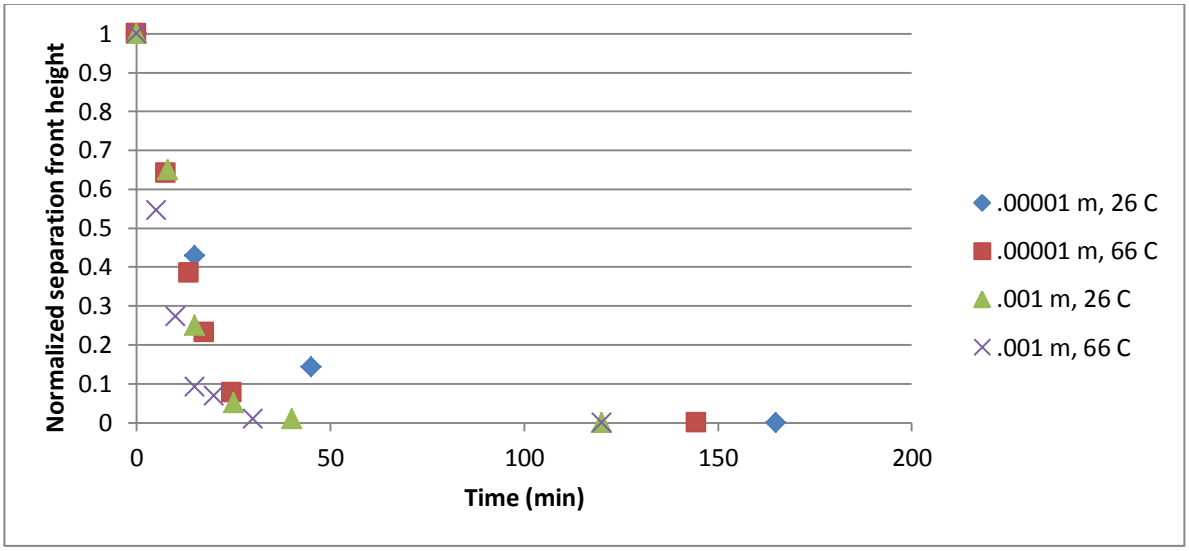

Figure 14: Normalized separation front of each non-emulsion mixture for both trials

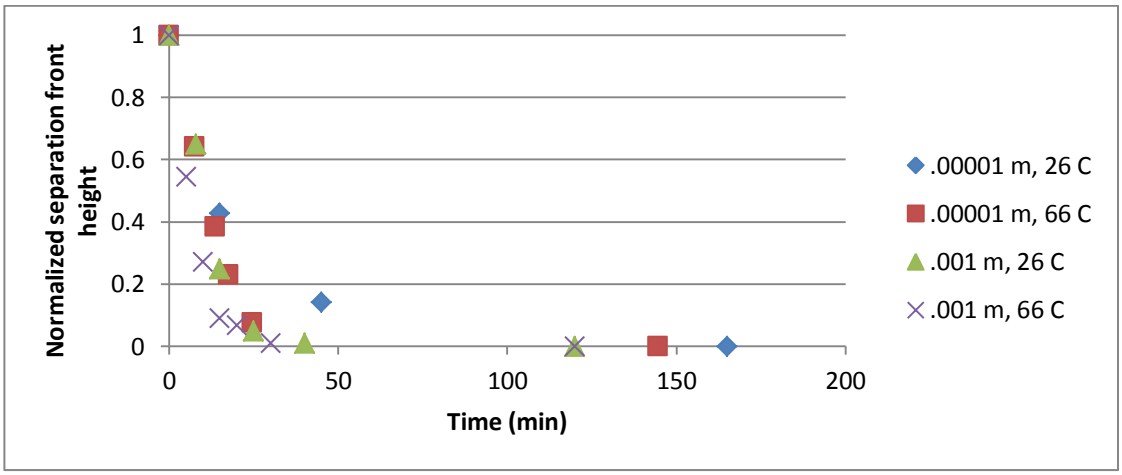

Figure 15: Normalized separation front of each emulsion for both trials

The final figure is a comparison of the emulsion and non-emulsion with the smallest wood particle diameters.

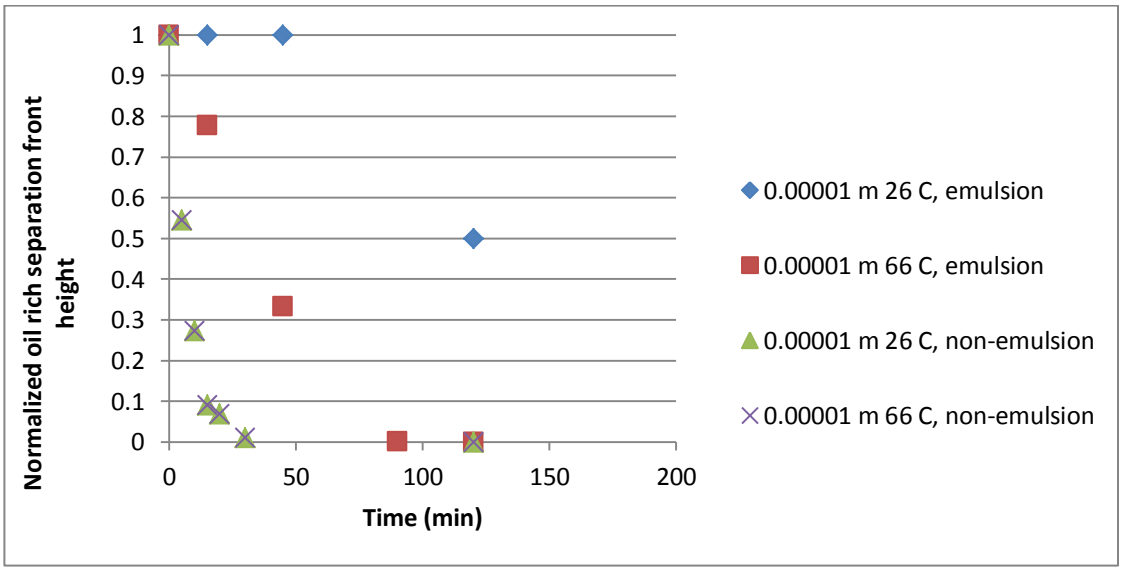

Figure 16: Comparison of trial 1 and 2 emulsion and non-emulsion normalized separation fronts for 0.00001 mm wood particle diameter range

3.5.2 Mixture Composition

Table 25 is a collection of all mass fraction and volume fractions calculated used in trial 1.

Table 25: Mass and Volume Fractions of the mixtures in Trial 1

	Mass Fraction Mixture 1	Volume Fraction Mixture 1	Mass Fraction Mixture 2	Volume Fraction Mixture 2	Mass Fraction Mixture 3	Volume Fraction Mixture 3
Oil	84	71	90	86	70.8	68.6
Wood	16	29	10	14	7.7	13.5
Water	-	-	-	-	21.5	17.9
Total	100	100	100	100	100	100

Table 26 is a collection of all mass fraction and volume fractions calculated used in trial 2.

Table 26: Mass and Volume Fractions of the mixtures in Trial 2

	Mass Fraction Mixture 1	Volume Fraction Mixture 1	Mass Fraction Mixture 2	Volume Fraction Mixture 2	Mass Fraction Mixture 3	Volume Fraction Mixture 3
Oil	88.4	80.9	93.9	89.6	70.8	73.0
Wood	11.6	19.1	6.1	10.4	7.7	8.5
Water	-	-	-	-	21.5	18.5
Total	100	100	100	100	100	100

3.5 Discussion

For trial 1, the oil-wood particle mixture at 26 ^{o}C separated to its maximum separation front of almost 50% oil rich top phase, 50% well mixed wood and oil bottom phase. This result was reached in 2 hours at 26 ^{o}C. When the temperature of the mixture was increased to 66 ^{o}C the resulting maximum separation front was closer to 55-45% in favor of the oil rich phase and this maximum separation front was reached in 45 minutes.

When 21.5% of the mixture mass was made up of water, the settling velocity became dramatically slower as well as the maximum settling front becoming close to 1% top oil rich phase, 99% well mixed mixture of water, wood and oil. Though the mixture did remain mixed, it was slightly more wood rich further towards the bottom of the mixture.

The initial mixture was far too viscous to be used in practical applications. The second mixture achieved a lower and potentially useable viscosity. The fact that the non-emulsion mixture separated in under 2 hours, while not exactly fast, could be a problem depending on the process. When heated, the non-emulsion mixture separated faster as well as reaching a slightly higher final separation front. The faster separation velocity can be attributed to the much lower viscosity soybean has at higher temperatures. The slightly higher separation front is likely due to the greater level of dense packing of the wood particles due to the heat effects on the oil. It is important to note that the settling velocity speeds up dramatically because it is possible that some oil-solid fuel mixtures will be pre-heated for flow reasons. Upon examining the heated mixture, it was found that the top oil rich layer had a very low viscosity while the wood particle rich bottom layer had a higher viscosity.

When enough water was added to the mixture to have it make up 21.5% of the mixture mass, the separation velocity and maximum separation front decreased dramatically. Even heating of the new emulsion barely caused an increase in the separation front. The viscosity of the mixture after water was added was noticeably lower than before water was added. It is clear that the addition of water to create an emulsion allowed the mixture to remain as close to homogenous as possible.

Due to the emulsions having much more favorable properties than the non-emulsion mixtures, it was concluded that water can successfully create emulsions, with oil and wood, which see an increase in mixture stability. Another important discovery was that smaller solid particles led to increased mixture stability when compared to larger solid particles. This is convenient as smaller particles will fire easier in fuel spray guns. The settling observed was not considered to be hindered settling due to the concentration of solids in the emulsions being low. Also a general form for a model equation that can predict the settling of an emulsion was obtained.

3.6 Conclusions

Even when a composite fuel is emulsified with minimal energy and no surfactant, a satisfactory change in settling is observed. It was found that smaller solid fuel particle size aided in slowing settling times. Higher mixture temperature was seen to quicken settling times.

CHAPTER 4 - SETTLING FRONT EXPERIMENTS AND MODELING CONTINUED, USING SOYBEAN OIL, COAL AND WATER

4.1 Introduction

This chapter is an extension of the wood settling chapter, except now coal will be examined as the solid.

4.2 Procedure

Anthracite coal was grounded into fine particles. The coal particles were then sifted out using various U.S. scale mesh sifting units. Various weights and volumes of substances and containers used were recorded. A 30 ml cup of oil was mixed with a 30 ml cup of saw dust in a 125 ml beaker. A qualitative observation of the mixture viscosity was observed. Then a new 30 ml cup of oil was added to the contents in the flask. Again a qualitative observation of the viscosity was made. The separation front was measured for the second mixtures at room temperature. The second mixture was then heated to ~70 ^{o}C and the settling front was again measured.

To create an emulsion, 20 g of water was then added to the second mixture and the resulting mixture was well mixed. The settling front of this emulsion mixture was observed and a qualitative test of the viscosity of this mixture with temperature was observed. This entire procedure was then repeated using varying sizes of coal particles.

4.3 Data

The data is separated into 4 trials. Each trial differs by the size range of the coal particles used. The coal particles sizes used in this experiment vary as follows:

Table 27: Coal particle size range by trial

Trial #	Mesh* (U.S.)	Particle Size range (mm)
1	16 onto 30	0.599-1.20
2	30 onto 50	0.297-0.599
3	60 onto 80	0.178-0.251
4	80 onto 120	0.128-0.178

***The first number listed in each row of this column indicates the smallest mesh # that trial of coal particles sifted through. The second number is the mesh # that the particles were resting on top of and collected from.**

The following tables list soybean oil, coal and water weights used for each mixture of each trial. Table 28 lists the mixture weights used in trial 1.

Table 28: Various Weights of combined coal/soybean oil mixtures for trial 1

	Mixture 1 (g)	Mixture 2 (g)	Mixture 3 (g)
Soybean Oil	26.7	53.5	53.5
Coal Particles	25.1	25.1	25.1
Water	-	-	20
Total	51.8	78.6	98.6
Total (Flask)	116.5	143.3	163.3
Empty Flask	64.7	64.7	64.7

Table 29 lists the mixture weights used in trial 2.

Table 29: Various weights of combined coal/soybean oil mixtures for trial 2

	Mixture 1 (g)	Mixture 2 (g)	Mixture 3 (g)
Soybean Oil	26.3	53.5	53.5
Coal Particles	26.2	26.2	26.2
Water	-	-	20
Total	52.5	79.7	99.7
Total (with beaker)	117.2	144.4	164.4
Empty Beaker	64.7	64.7	64.7

Table 30 lists the mixture weights used in trial 3.

Table 30: Various Weights of combined coal/soybean oil mixtures for trial 3

	Mixture 1 (g)	Mixture 2 (g)	Mixture 3 (g)

Soybean Oil	26.3	52.6	52.6
Coal Particles	24.5	24.5	24.5
Water	-	-	20
Total	50.8	77.1	97.1
Total (with beaker)	115.5	141.8	161.8
Empty Beaker	64.7	64.7	64.7

Table 31 lists the mixture weights used in trial 4.

Table 31: Various Weights of combined coal/soybean oil mixtures for trial 4

	Mixture 1 (g)	Mixture 2 (g)	Mixture 3 (g)
Soybean Oil	28.50	57.08	57.08
Coal Particles	26.06	26.06	26.06
Water	-	-	20
Total	54.56	83.14	103.14
Total (with beaker)	119.26	145.32	165.32
Empty Beaker	64.7	64.7	64.7

The trial 1 settling fronts for the second mixture at both temperatures were recorded and tabulated below in tables 32 and 33. This is followed by a recording of the settling front for the water emulsion mixture at both temperatures in tables 34 and 35.

Table 32: Settling clear front for mixture 1 at 26 ^{o}C, trial 1

Minutes	**Separation Front Top Layer Mostly Oil/Water (ml)**	**Bottom Layer Heterogeneous Top Front (ml)**
0	0.0	77
.5	36.25	40.75
2	40.0	37
5	40.0	37
10	40.0	37
15	40.0	37
25	40.0	37
35	40.0	37

infinite	40.0	37

Table 33: Settling clear front for mixture 1 at 76 C, Trial 1

Minutes	Separation Front Top Layer Mostly Oil/Water (ml)	Bottom Layer Heterogeneous Top Front (ml)
0	0.0	77
.5	36.25	40.75
2	40.0	37
5	40.0	37
10	40.0	37
15	40.0	37
25	40.0	37
35	40.0	37
infinite	40.0	37

Table 34: Settling clear front for mixture 2 at 23 C Trial 1

Minutes	Separation Front Top Layer Mostly Oil/Water (ml)	Bottom Layer Heterogeneous Top Front (ml)
0	0	97
1	33.97	63.03
4.5	33.97	63.03
8	33.97	63.03
11	36.47	63.53
15	36.47	63.53
25	36.47	63.53
35	36.47	63.53
infinite	36.47	63.53

Table 35: Settling clear front for mixture 2 at 76 ^{o}C Trial 1

Minutes	Separation Front Top Layer Mostly Oil/Water (ml)	Bottom Layer Heterogeneous Top Front (ml)
0	0	97

.5	33.97	63.03
2	36.47	63.53
4.5	36.47	63.53
8	38.97	58.03
15	38.97	58.03
25	42.72	54.28
35	42.72	54.28
infinite	42.72	54.28

The trial 2 settling fronts for the second mixture at both temperatures were recorded and tabulated below in tables 36 and 37. This is followed by a recording of the settling front for the water emulsion mixture at both temperatures in tables 38 and 39.

Table 36: Settling clear front for mixture 1 at 26 ^{o}C, Trial 2

Minutes	**Separation Front Top Layer Mostly Oil (ml)**	**Bottom Layer Heterogeneous Top Front (ml)**
0	0.0	78
.5	38.75	39.25
2	40.0	38
5	40.0	38
10	40.0	38
15	40.0	38
25	40.0	38
35	40.0	38
infinite	40.0	38

Table 37: Settling clear front for mixture 1 at 66 ^{o}C Trial 2

Minutes	**Separation Front Top Layer Mostly Oil (ml)**	**Bottom Layer Heterogeneous Top Front (ml)**
0	0	78
.5	41.25	36.75
2	42.5	36.50

5	42.5	36.50
10	42.5	36.50
15	42.5	36.50
25	42.5	36.50
35	42.5	36.50
infinite	42.5	36.50

Table 38: Settling clear front for mixture 2 at 26 ^{o}C, Trial 2

Minutes	Separation Front Top Layer Mostly Oil (ml)	Bottom Layer Heterogeneous Top Front (ml)
0	0	98
1.5	7.16	90.84
2	10.74	87.26
3	13.43	84.57
4	16.11	81.89
5	16.11	81.89
8	17.9	80.1
15	25.98	72.06
23	30.48	67.52
30	33.48	64.52
infinite	33.48	64.52

Table 39: Settling clear front for mixture 2 at 76 ^{o}C, Trial 2

Minutes	Separation Front Top Layer Mostly Oil (ml)	Bottom Layer Heterogeneous Top Front (ml)
0	0	98
1	12.53	85.47
2.5	21.48	76.52
6	33.48	64.52
10	38.98	59.02
15	41.48	56.52
25	41.48	56.52
infinite	43.98	54.02

The trial 3 settling fronts for the second mixture at both temperatures were recorded and tabulated below in tables 40 and 41. This is followed by a recording of the settling front for the water emulsion mixture at both temperatures in tables 42 and 43.

Table 40: Settling clear front for mixture 1 at 31 ^{o}C, trial 3

Minutes	Separation Front Top Layer Mostly Oil (ml)	Bottom Layer Heterogeneous Top Front (ml)
0	0	73
0.25	10	63
0.83	20	53
1.16	30	43
2	36	37
8	36	37
11	37	36
32	37	36
55	38	35
120	38	35

Table 41: Settling clear front for mixture 1 at 77 ^{o}C, trial 3

Minutes	Separation Front Top Layer Mostly Oil (ml)	Bottom Layer Heterogeneous Top Front (ml)
0	0	93
0.666667	8	85
2	13	80
5	18	75
9.66667	23	70
18.5	28	65
27	33	60
60	38	55
120	38	55

Table 42: Settling clear front for mixture 2 at 30 ^{o}C trial 3

Minutes	Separation Front Top Layer Mostly Oil (ml)	Bottom Layer Heterogeneous Top Front (ml)
0	0	93
.67	8	85
2	13	80
5	18	75
9.5	23	70
18.5	28	65
27	33	60
60	38	55
120	38	55

Table 43: Settling clear front for mixture 2 at 67 ^{o}C, trial 3

Minutes	Separation Front Top Layer Mostly Oil (ml)	Bottom Layer Heterogeneous Top Front (ml)
0	0	80
1	17	63
3	25	55
5.5	30	50
11	33	47
17	35	45
33	35	45
60	36	44
80	37	43
120	37	43

The trial 4 settling fronts for the second mixture at both temperatures were recorded and tabulated below in tables 44 and 45. This is followed by a recording of the settling front for the water emulsion mixture at both temperatures in tables 46 and 47.

Table 44: Settling clear front for mixture 1 at 31 °C, trial 4

Minutes	Separation Front Top Layer Mostly Oil (ml)	Bottom Layer Heterogeneous Top Front (ml)
0	0	82
12	5	77
23	8	74
32	11	71
40	12	70
52	14	68
64	17	65
79	20	62
91	22	60
110	25	57
125	28	54
140	30	52
155	31	51
165	32	50
186	34	48
480	34	48

Table 45: Settling clear front for mixture 1 at 67 °C, trial 4

Minutes	Separation Front Top Layer Mostly Oil (ml)	Bottom Layer Heterogeneous Top Front (ml)
1	0	80
4	2	78
9	5	75
14.5	9	71
22	11.5	68.5
31	17	63
36	20	60
43	25	55
52	29	51
57	30	50
67	32	48
78	33.5	46.5
87	34	46
102	35	45

125	37	43
143	38	42
175	39	41

Table 46: Settling clear front for mixture 2 at 30 ^{o}C trial 3

Minutes	Separation Front Top Layer Mostly Oil (ml)	Bottom Layer Heterogeneous Top Front (ml)
0	0	91
3	0.5	90.5
11	3.5	87.5
20	5.5	85.5
48	8	83
66	10	81
81	11	80
126	11	80
145	11	80
175	13	78
232	16.5	74.5
255	19	72
300	21	70
345	22	69
380	22.5	68.5
427	23	68
500	24	67

Table 47: Settling clear front for mixture 2 at 67 ^{o}C, trial 3

Minutes	Separation Front Top Layer Mostly Oil (ml)	Bottom Layer Heterogeneous Top Front (ml)
0	0	91
2	0.5	90.5
7	3.5	87.5
14	5.5	85.5
21	7	84
40	10	81
62	13	78

90	15	76
128	16	75
148	18	73
231	21	70
257	24	67
286	26	65
320	27	64
365	28	63
433	29	62
500	29	62

4.4 Sample Calculations

The calculations performed for this experiment exactly the same as done previously for wood. They will not be repeated as they will only have different numerical values.

4.5 Results

The following section shows the settling front for each trial as well as a model equation that can be used to predict that specific settling front.

4.5.1 Settling

The following series of figures represents all trial 1 settling front results. There will be a figure for each mixture at each temperature. In each figure the data points are graphed alongside a model equation that describes each settling front. Each graph is illustrating the settling front from the top oil rich phase.

For mixture 1 at room and elevated temperature, the maximum settling point was reached so fast that a model representing the settling with respect to time could not be formed.

Figure 17 shows mixture 2 for trial 1 at room temperature

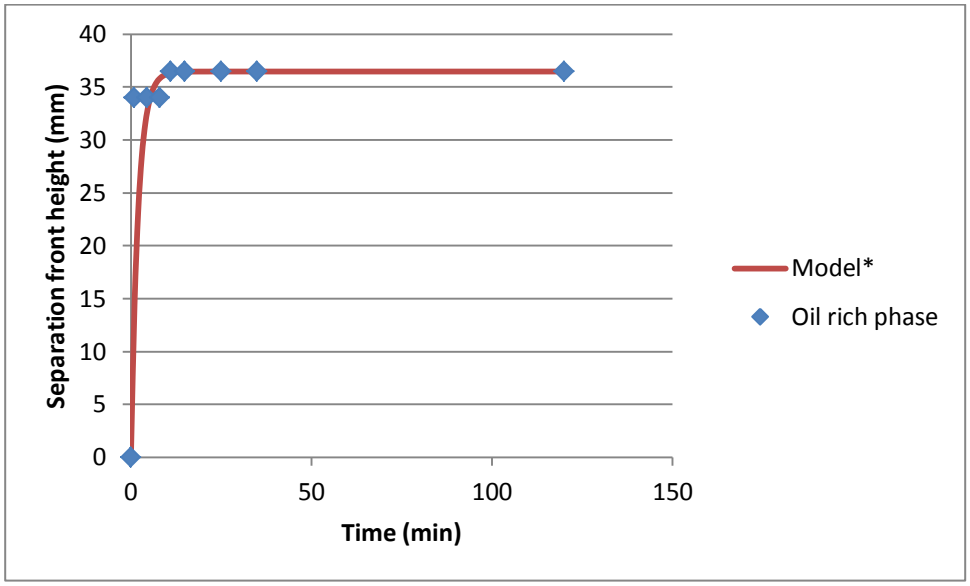

Figure 17: Settling clear front for the mixture data from table 34 at 23 °C
***$height = 36.47 * (1 - EXP(-0.503 * t))$* This is the model equation found from the data. It is a power curve representing the increase in the top oil rich phase of the mixture as time increases.**

Figure 18 shows mixture 2 for trial 1 at elevated temperature

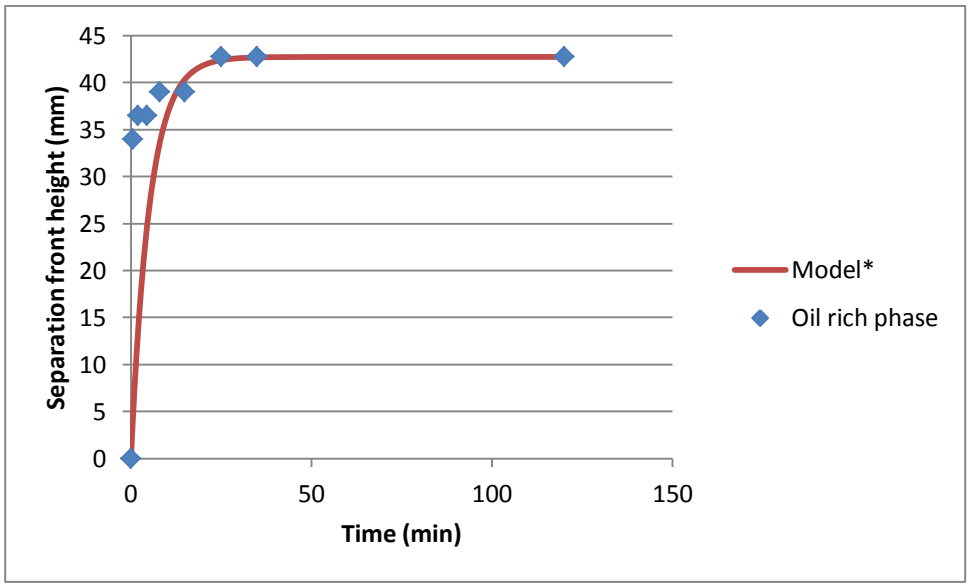

Figure 18: Settling clear front for the mixture data from table 35 at 76 °C
***$height = 42.72 * (1 - EXP(-0.193 * t))$* This is the model equation found from the data. It is a power curve representing the increase in the top oil rich phase of the mixture as time increases.**

For mixture 1 at room and elevated temperature of trial 2, the maximum settling point was reached so fast that a model representing the settling with respect to time could not be formed.

Figure 19 shows mixture 2 for trial 2 at room temperature

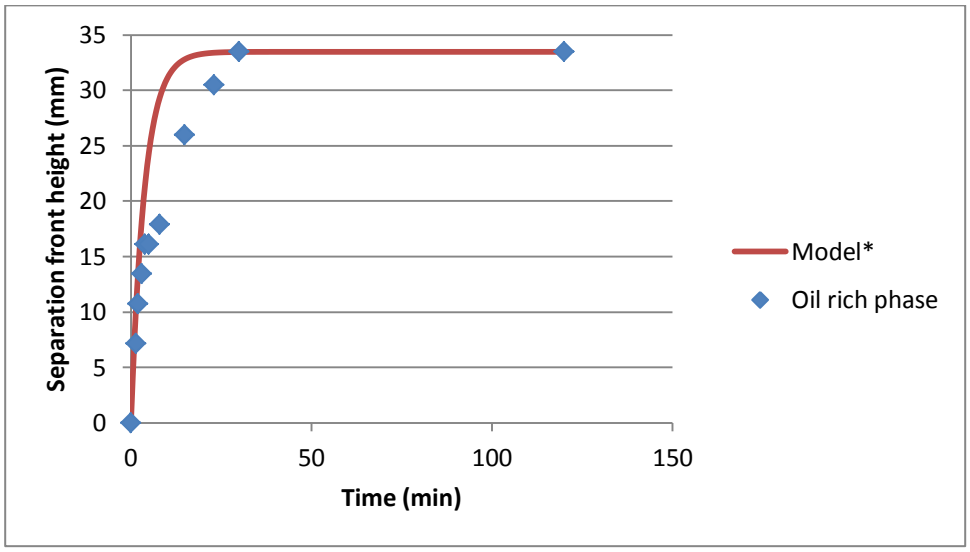

Figure 19: Settling clear front for the mixture data from table 38 at 26 ^{o}C
***33.48 $*$ (1 $-$ EXP(−0.262 $*$ t)) This is the model equation found from the data. It is a power curve representing the increase in the top oil rich phase of the mixture as time increases.**

Figure 20 shows mixture 2 for trial 2 at elevated temperature

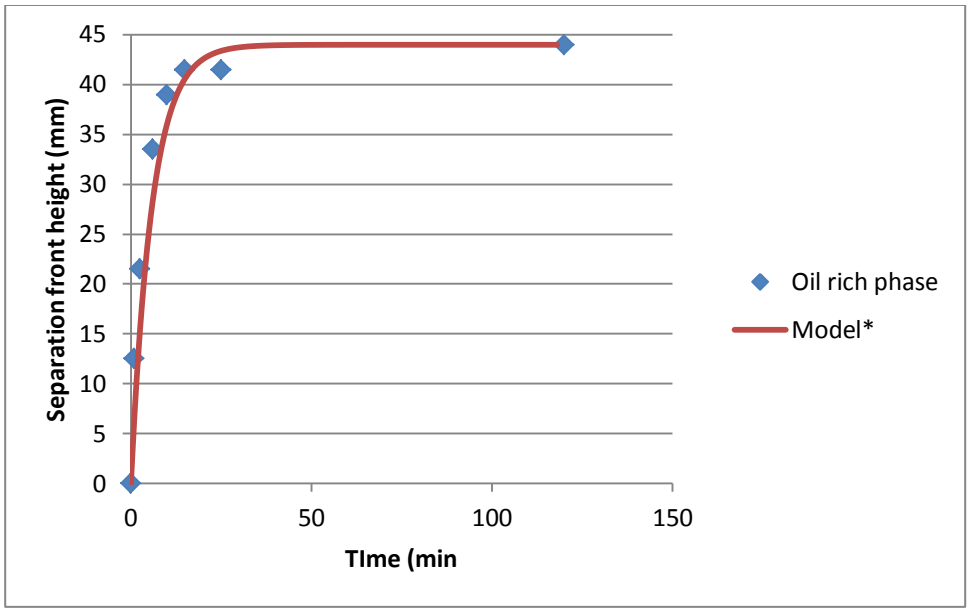

Figure 20: Settling clear front for the mixture data from table 39 at 76 °C
***$height = 43.98 * (1 - EXP(-0.171 * t))$* This is the model equation found from the data. It is a power curve representing the increase in the top oil rich phase of the mixture as time increases.**

Figure 21 shows mixture 1 for trial 3 at room temperature

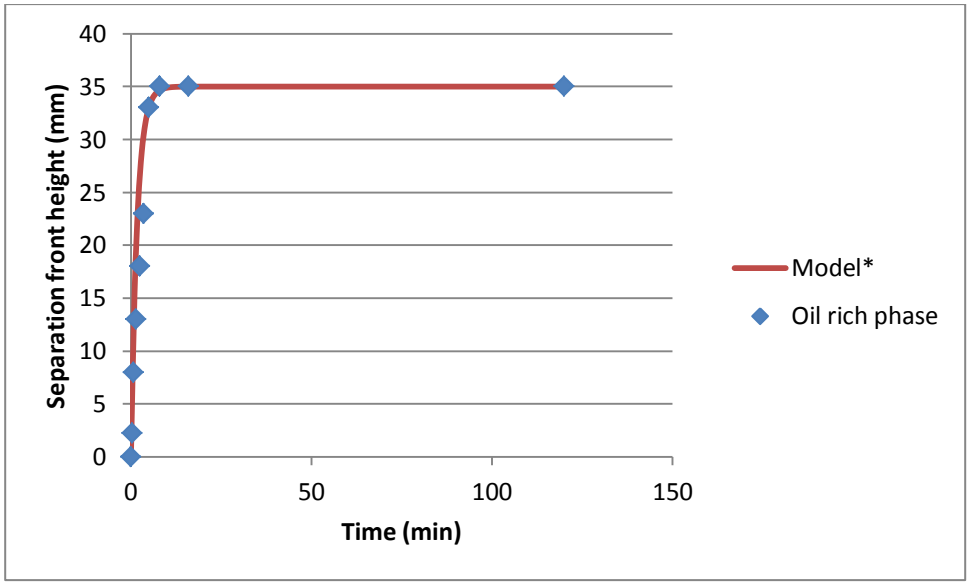

Figure 21: Settling clear front for the mixture data from table 40 at 31 °C
***$height = 35 * (1 - EXP(-0.578 * t))$*This is the model equation found from the data. It is a power curve representing the increase in the top oil rich phase of the mixture as time increases.**

Figure 22 shows mixture 1 for trial 3 at elevated temperature

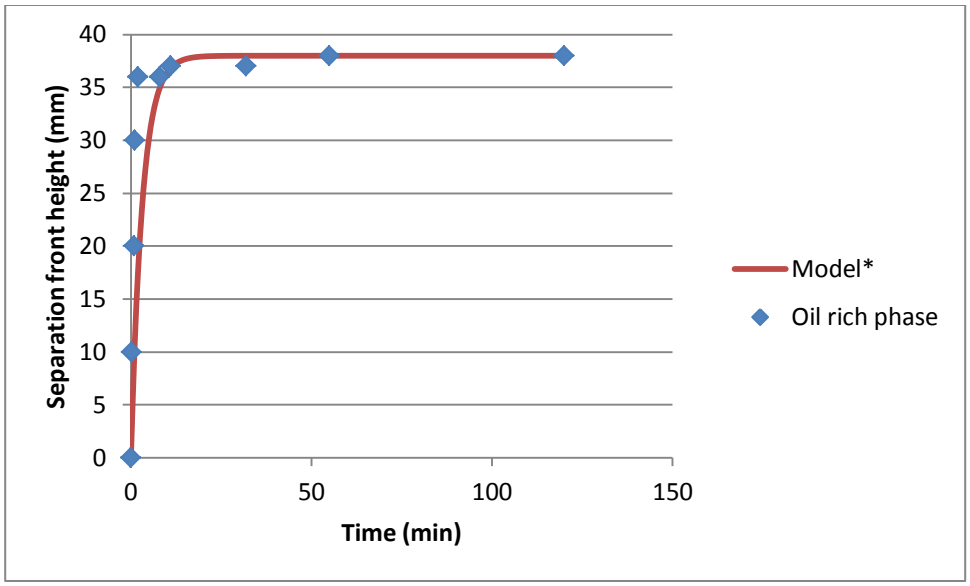

Figure 22: Settling clear front for the mixture data from table 41 at 77 °C
***height* = 38 ∗ (1 − *EXP*(−0.316 ∗ *M*4))This is the model equation found from the data. It is a power curve representing the increase in the top oil rich phase of the mixture as time increases.**

Figure 23 shows mixture 2 for trial 3 at room temperature

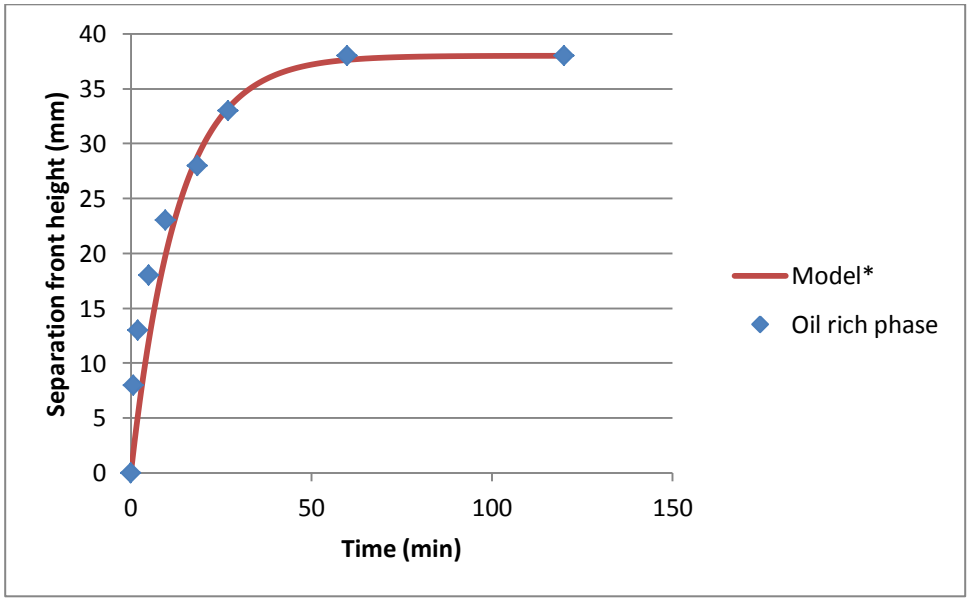

Figure 23: Settling clear front for the mixture data from table 42 at 30 °C
***height* = 38 ∗ (1 − *EXP*(−0.077 ∗ *t*))This is the model equation found from the data. It is a power curve representing the increase in the top oil rich phase of the mixture as time increases.**

Figure 24 shows mixture 2 for trial 3 at elevated temperature

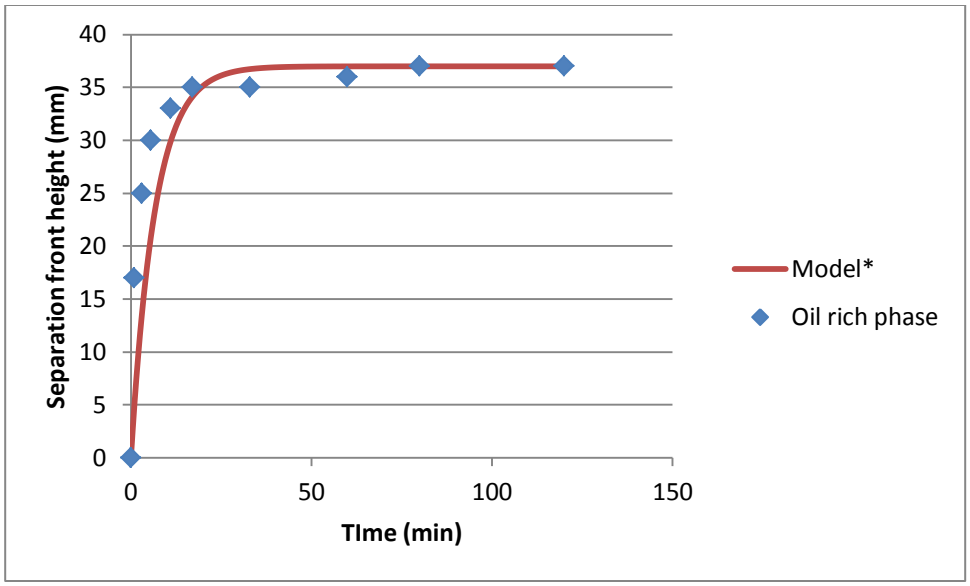

Figure 24: Settling clear front for the mixture data from table 43 at 67 °C
***height* = 37 ∗ (1 − *EXP*(−0.15 ∗ *t*)) This is the model equation found from the data. It is a power curve representing the increase in the top oil rich phase of the mixture as time increases.**

Figure 25 shows mixture 1 for trial 4 at room temperature

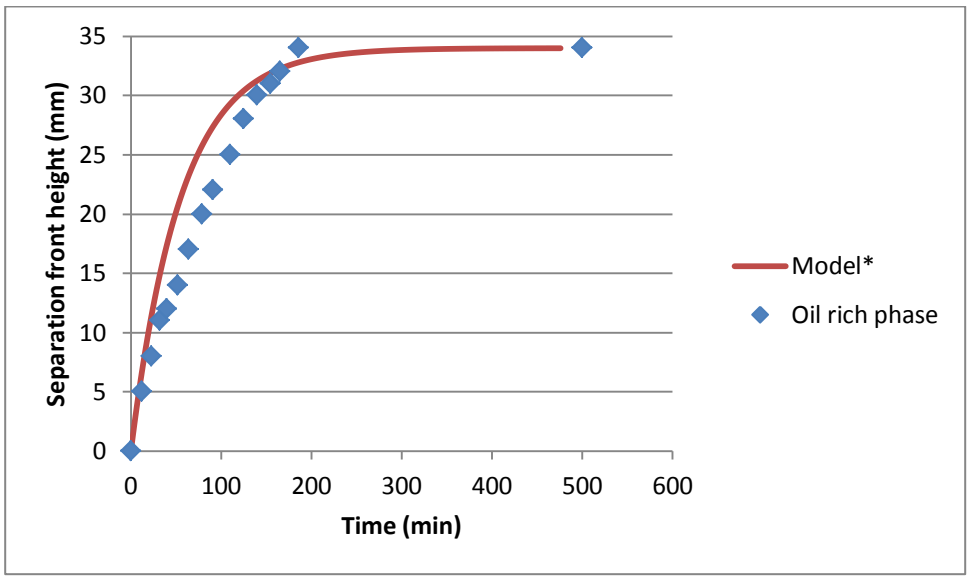

Figure 25: Settling clear front for the mixture data from table 44 at 31 °C
***height* = 34 ∗ (1 − *EXP*(−0.018 ∗ *t*)) This is the model equation found from the data. It is a power curve representing the increase in the top oil rich phase of the mixture as time increases.**

Figure 26 shows mixture 1 for trial 4 at elevated temperature

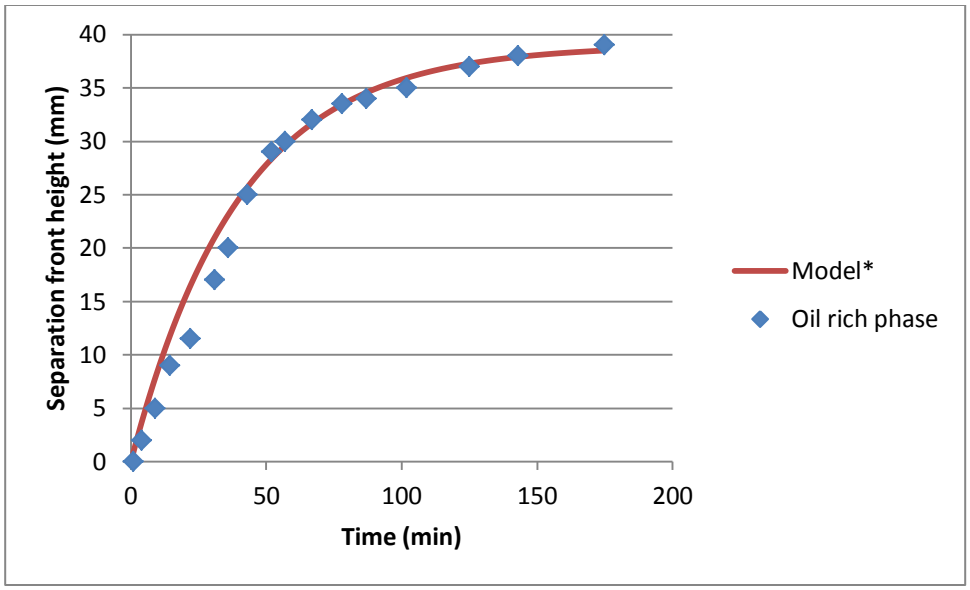

Figure 26: Settling clear front for the mixture data from table 45 at 67 °C
***height* = 39 ∗ (1 − *EXP*(−0.025 ∗ *t*)) This is the model equation found from the data. It is a power curve representing the increase in the top oil rich phase of the mixture as time increases.**

Figure 27 shows mixture 2 for trial 4 at room temperature

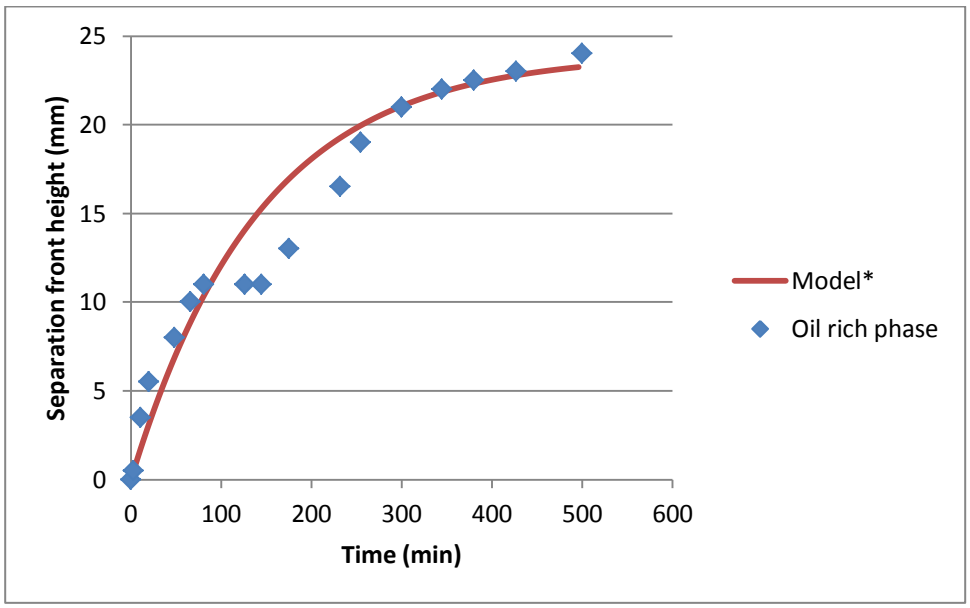

Figure 27: Settling clear front for the mixture data from table 46 at 30 °C
***height* = 24 ∗ (1 − *EXP*(−0.007 ∗ *t*)) This is the model equation found from the data. It is a power curve representing the increase in the top oil rich phase of the mixture as time increases.**

Figure 28 shows mixture 2 for trial 4 at elevated temperature

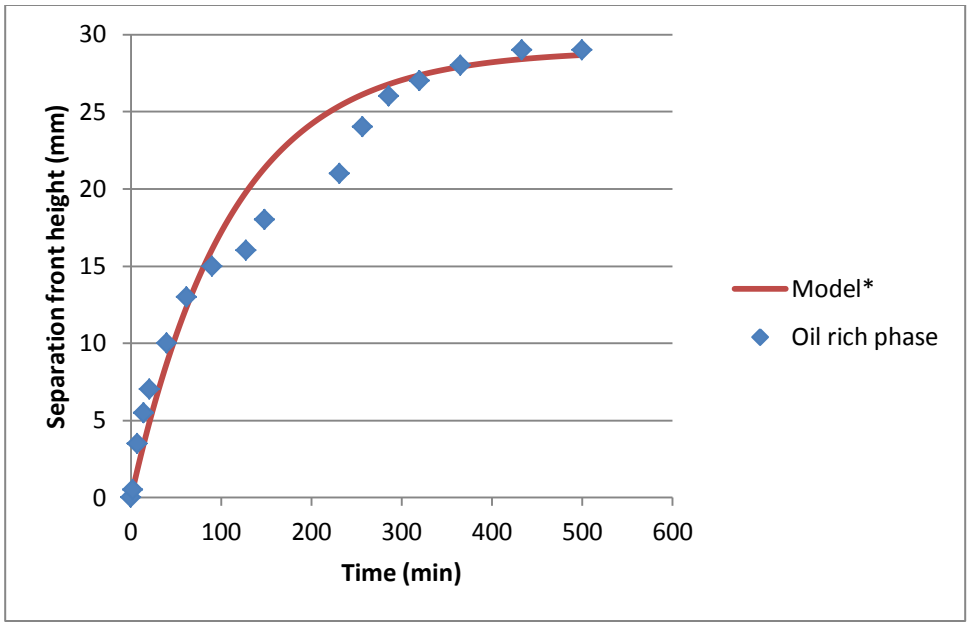

Figure 28: Settling clear front for the mixture data from table 47 at 67 °C
***height* = 29 ∗ (1 − *EXP*(−0.009 ∗ *t*)) This is the model equation found from the data. It is a power curve representing the increase in the top oil rich phase of the mixture as time increases.**

Figures 29 and 30 are graphical representations of the normalized separation front height of the top oil rich phase of all mixture and emulsions.

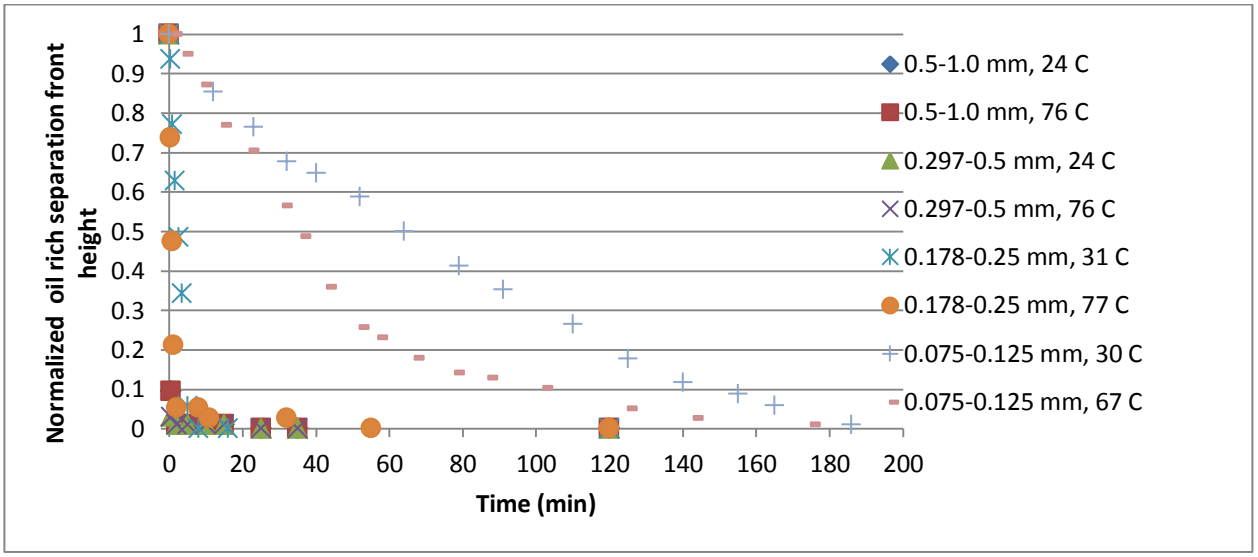

Figure 29: Normalized separation front for all trials of each non emulsion mixture

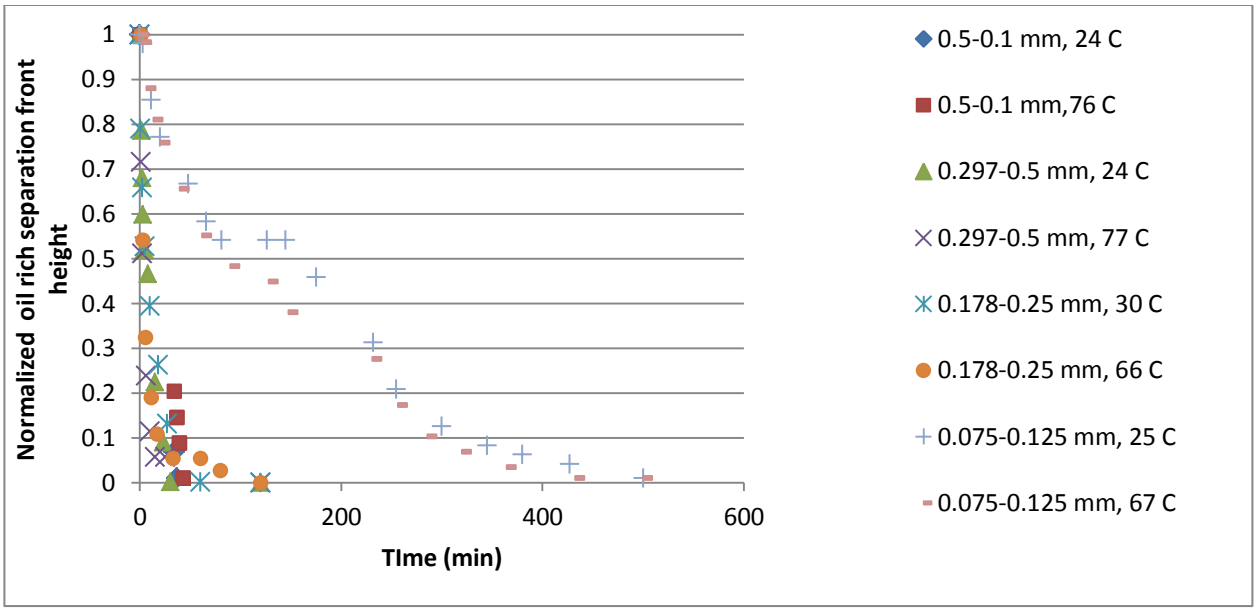

Figure 30: Normalized separation front for all trials of each emulsion

The final figure is a comparison of the smallest coal particle size emulsion and non-emulsion mixtures.

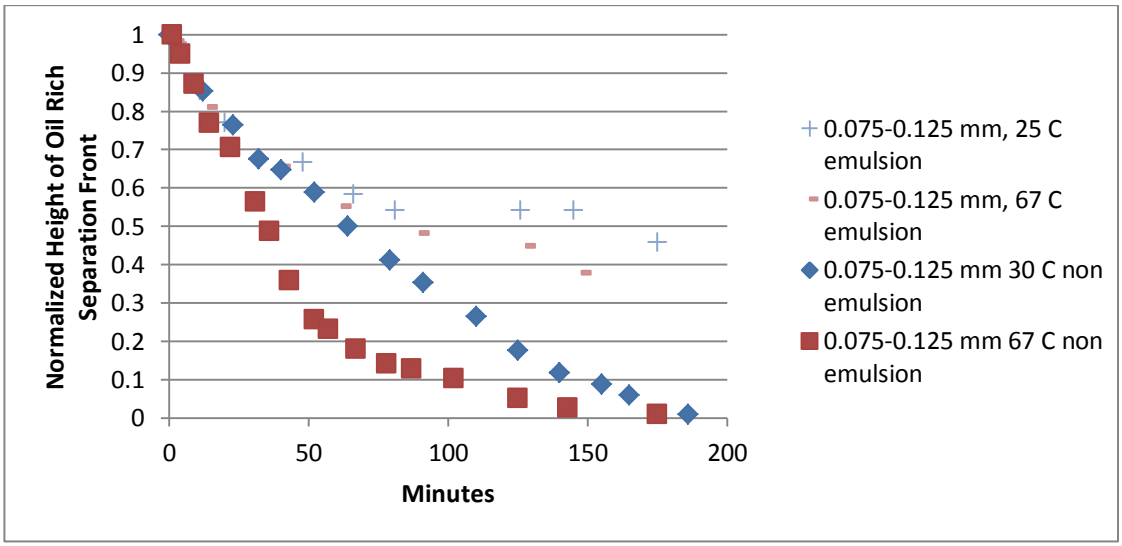

Figure 31: Comparison of trial 4 emulsion and non-emulsion mixture normalized separation fronts using the 0.075-0.125 mm coal particle diameter range

4.5.2 Mass and Volume Fractions

Table 48 is a collection of all mass fraction and volume fractions calculated used in Trial 1.

Table 48: Mass and Volume Fractions of the mixtures in Trial 1

	Mass Fraction Mixture 1	Volume Fraction Mixture 1	Mass Fraction Mixture 2	Volume Fraction Mixture 2
Oil	0.680661578	0.76314519	0.542596349	0.612796927
Coal	0.319338422	0.23685481	0.254563895	0.190191725
Water	-	-	0.202839757	0.197011348-
Total	100	100	100	100

Table 49 is a collection of all mass fraction and volume fractions calculated used in Trial 2.

Table 49: Mass and Volume Fractions of the mixtures in Trial 2

	Mass Fraction Mixture 1	Volume Fraction Mixture 1	Mass Fraction Mixture 2	Volume Fraction Mixture 2
Oil	0.671267252	0.755305054	0.536609829	0.607731427
Coal	0.328732748	0.244694946	0.262788365	0.196885759
Water	-	-	0.200601805	0.195382814
Total	100	100	100	100

Table 50 is a collection of all mass fraction and volume fractions calculated used in trial 3.

Table 50: Mass and volume fractions of the mixtures in trial 3

	Mass Fraction Mixture 1	Volume Fraction Mixture 1	Mass Fraction Mixture 2	Volume Fraction Mixture 2
Oil	0.682230869	0.764449413	0.541709578	0.611573205
Coal	0.317769131	0.235550587	0.252317199	0.188444683
Water	-	-	0.205973223	0.199982113

Total	100	100	100	100

Table 51 is a collection of all mass fraction and volume fractions calculated used in trial 4.

Table 51: Mass and volume fractions of the mixtures in trial 4

	Mass Fraction Mixture 1	**Volume Fraction Mixture 1**	**Mass Fraction Mixture 2**	**Volume Fraction Mixture 2**
Oil	0.686552803	0.76803332	0.553422532	0.623690908
Coal	0.313447197	0.23196668	0.252666279	0.188371397
Water	-	-	0.193911189	0.187937695
Total	100	100	100	100

4.6 Discussion

As was seen with wood-oil mixtures, emulsification led to more stable fuel mixtures. Specifically, the creation of the emulsion always decreased both settling velocity and settling front maximum, with the largest decreases seen in mixtures using smaller particle sizes. It was seen once again that temperature of the mixture and particle size of the solid affect the settling velocity and the maximum settling front for both emulsified and non-emulsified mixtures. Specifically settling velocity and the maximum settling front decreased as particle size decreased, while increasing mixture temperature increased settling velocity and the maximum settling front, for the same theorized reasons as with wood. The settling observed was not considered to be hindered settling due to the concentration of solids in the emulsions being low. Also a general form for a model equation that can predict the settling of an emulsion was obtained.

4.7 Conclusions

The coal settling experiments confirmed all of the conclusions found in the wood settling experiments in that emulsification of a composite mixture, having smaller solid fuel particle size and lower mixture temperatures, all aid in mixture stability.

CHAPTER 5 - VISCOSITY MODELING OF COMPOSITE FUELS

5.1 Introduction

Viscosity is a fuel property that if not properly accounted for, can lead to a complete halt in the combustion process of various power plants. This is due to two main reasons. The first being that fuel in every application is not stored at the site of combustion. It is always stored in a tank at varying distances from the combustion site. Because of this fact, the fuel must be transported to the combustion site. If the fuel is too viscous to allow for this transportation, combustion will not be able to occur regardless of pump power. Besides pipeline transportation, viscosity also is a factor in how effectively fuels can combust. The fuel oil in question needs to be viscous enough to be atomized and the less viscous the fuel, the greater the level of atomization can be reached.

As was explained earlier, the cheapest fuel oils are normally the heaviest and therefore the most viscous. Many industrial plants end up storing these fuels in large outdoor or underground tanks. These tanks and their contents are therefore at whatever temperature their surrounding is. The easiest way to deal with a fuel with high viscosity is too raise the temperature of the fuel because as viscosity decreases in fluids as temperature increases. This is a strategy that many current fuel oil using industrial plants currently employ. [1] When designing a fuel, it is best to have as low as a viscosity as possible. If the viscosity of the fuel is low enough, pre heating is not required, which equates to more energy and money saved as the preheating step requires an initial kicker of some other energy source being consumed.

The ability to accurately predict the viscosity of a theoretical fuel is a valuable tool and will be discussed in the following chapter.

5.2 Coal Oil Mixtures

To begin, coal-oil mixture (COM) viscosity data was analyzed from an experiment performed by Timbalia [2]. The coal used was #8 Pittsburgh coal and the oil used was graded as #6 fuel oil. The viscosity of the fuel oil as well as the COM was found using a Brookfield RVT model viscometer, using spindle number one. The viscosity for the COM was found at 25 ^{o}C for the following weight percent values by coal: 20, 40, 50 and 55. The mesh size of the coal particles used was -200 to +325. The following is a graph of the data collected [2]:

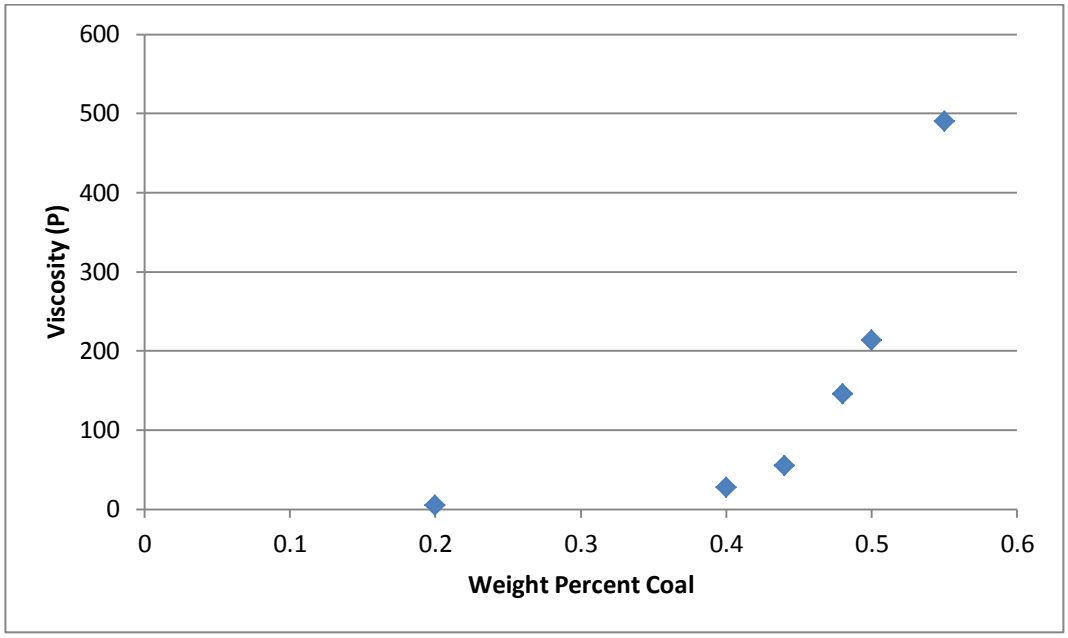

Figure 32: Viscosity of varying COM mixtures at 25 C [2]

The following is a description of the COM at different coal weight percentages [2]. All descriptions of data are taken from Timbalia's work as this was not an experiment that was physically performed.

First the sheer thinning of each COM will be discussed as that information is not presented in figure 32. The raw # 6 fuel oil was deemed a Newtonian fluid because no shear thinning could be observed when the RPM of the spindle in the viscometer was raised. At 20% coal, an insignificant change was observed in viscosity. At 40% coal the COM was found to have a nominal non-Newtonian characteristic. When the 40% COM was stressed with a shear rate for a long period of time, there was no change in the viscosity. At 50% coal, there was no doubt about observing shear thinning characteristics. Timbalia noted that when 50% COM was placed under a constant shear rate for a long period of time, the viscosity value slightly decreased. For 55% coal, once again shear thinning was observed, but when the COM was agitated at a constant rate for a long period of time, a decrease in viscosity was shown followed by an increase in viscosity. Timbalia characterized this as the thixotropic breakdown of the material with time. This phenomenon was also noticed in 50% coal mixtures but was almost negligible in 20 and 40% coal mixtures. It was also noted by Timbalia through further experiments that the viscosity of the COM mixture increased with particle size decrease while decreasing with temperature increase.

At this point the data was used to make a model equation that could predict the viscosity of a COM mixture with similar properties (particle size, fuel oil type and temperature) at any variation of coal to oil ratio.

To start, the following slurry viscosity equation taken from literature by Thomas was used [3]:

$$\frac{\mu_m}{\mu_L} = \mathbf{1} + \boldsymbol{K_1\varphi} + \boldsymbol{K_2\varphi} + \boldsymbol{K_3\varphi} + \boldsymbol{K_4\varphi} + \cdots \tag{5.1}$$

In this equation, μ_m is the slurry viscosity, μ_L is the viscosity of the liquid in the slurry, K are constants and φ is the volume fraction of coal in the mixture. Thomas concluded that any K values after K_2 were extremely difficult to find and did not result in a significant accuracy change in the calculation of μ_m. In his paper Thomas provided generic K values to be used, K_1 being equal to the Einstein constant of 2.5 and K_2 ranging from 10.05 to 14.1 [3], the range for K_2 found by Guth and Simha [4]. The following are the predicted values using equation 5.1 with the generic values:

Table 52: Predicted viscosity using Thomas equation 5.1 and the minimum and maximum K_2 values

Coal by Weigh Fraction	Experimental Viscosity (P)	Predicted Viscosity with K_2=10.05 (P)	Predicted Viscosity with K_2=14.1 (P)
0.2	4.64	6.776455863	8.196313483
0.4	27.2	12.75762795	16.04501057
0.44	55	14.14641031	17.86943492
0.48	145	15.60586717	19.78734107
0.5	212.8	16.36306289	20.78262539
0.55	489.6	18.33943109	23.38112221

The generic values provided by the Thomas viscosity equation do not provide accurate results. Thomas also provided another equation, to be used in slurry mixtures with medium to high concentration values:

$$\frac{\mu_m}{\mu_L} = 1 + K_1\varphi + K_2\varphi + Aexp(B\varphi) \quad (5.2)$$

Where Thompson defined A and B as constant values of 0.00273 and 16.6 respectively. Using this equation gives the following results:

Table 53: Predicted viscosity using Thomas equation 5.2 and the minimum and maximum K_2 values

Coal by Weight Fraction	Experimental Viscosity (P)	Predicted Viscosity with K_2=10.05 (P)	Predicted Viscosity with K_2=14.1 (P)
0.2	4.64	6.851545069	8.271402688
0.4	27.2	14.0834263	17.37080892
0.44	55	16.61402389	20.3370485
0.48	145	20.27879916	24.46027307
0.5	212.8	22.83698625	27.25654875
0.55	489.6	33.26701179	38.30870291

Again, generic model equation values supplied by Thomas did not end up accurately predicting viscosity, even with an equation was better suited to the modeling situation.

If the Thomas modeling equations were tailored to fit the current slurry conditions, they would undoubtedly perform better. Specifically the constants can be selected to provide better results. While equation 5.2 did not predict the slurry viscosity well, it did perform better than equation 5.1 and therefore it will be the equation that is altered.

Equation 5.2, besides already performing better than equation 5.1, also has two more constants, A and B. It will be these two constants that are altered to create a more accurate model equation. The following is the process used to solve for the correct A and B constants

The first step was to rearrange equation 5.2:

$$\frac{\mu_m}{\mu_L} - 1 + K_1\varphi + K_2\varphi = Aexp(B\varphi) \quad (5.3)$$

Once equation 5.3 is in this form, the relationship between A, B and φ can be used to solve for A and B by using the known variable values from data taken from Timbalia's experiment. This can be done by plotting the left hand side (LHS) of equation 5.3 vs. φ in excel and fitting functions through the resulting points. Excel can give the equation of these functions that best fit through the points and they can then be used to solve for A and B. An example of the step follows:

$$\boldsymbol{Zexp(Yx) = Aexp(B\varphi)} \tag{5.4}$$

$$\boldsymbol{where\ x\ is\ volume\ fraction\ coal, Z\ and\ Y\ are\ contants},$$

$$so$$

$$\boldsymbol{Z = A, Y = B} \tag{5.5}$$

The functions that provided the most accurate fits were the exponential function and the power function as can be seen below in figures 33 and 34:

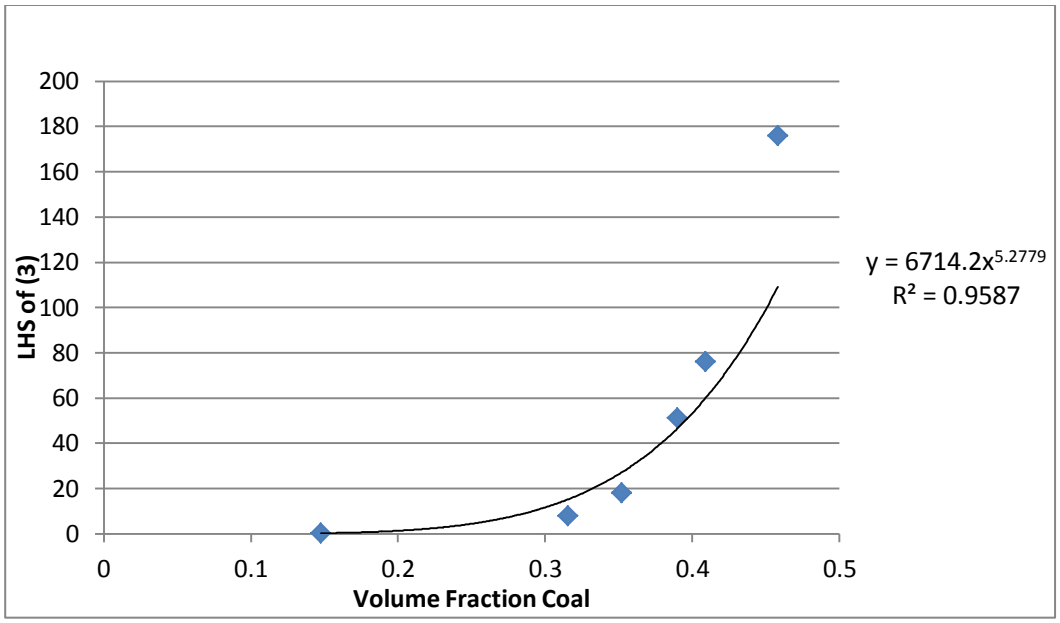

Figure 33: Excel power function fit of LHS of equation 5.3 varying volume percent coal

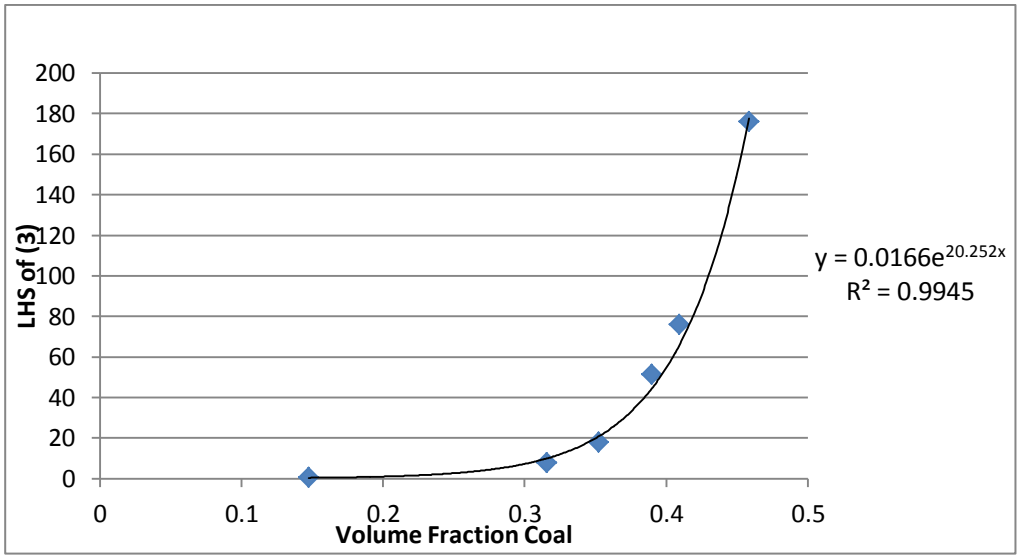

Figure 34: Excel exponential function fit of LHS of equation 5.3 varying volume percent coal

The exponential graph having the higher R^2 was expected as the original equation from Thomas had an exponential function as part of the expression. The new model equation ends as follows:

$$\boldsymbol{\mu_m = \mu_L\left(1 + 2.5\varphi + 10.05\varphi + 0.0166exp(20.252\varphi)\right)} \qquad (5.6)$$

The following are the predicated viscosities when using the generalized K values from Thomas, as well as the modified A and B values found above:

Table 54: Predicted viscosity using modified Thomas equation

Coal by Weight Fraction	Experimental Viscosity (P)	viscosity of mixture (P)
0.2	4.64	4.555334073
0.4	27.2	32.71431005
0.44	55	62.47725572
0.48	145	127.2605773
0.5	212.8	185.212469
0.55	489.6	495.4865598

This model equation is for the specific circumstance provided in Timbalia's experiment. The predicted viscosities provided by the modified Thomas equation provide estimates that are accurate enough to be useful in actual applications. This is due to the fact the exact viscosity value of a potential fuel does not need to be known. What is important is if it is below a certain critical viscosity point. If a predicted value is near this point, then further steps can be taken to ensure the fuel will reach it's required viscosity. The following is an error analysis of the above data:

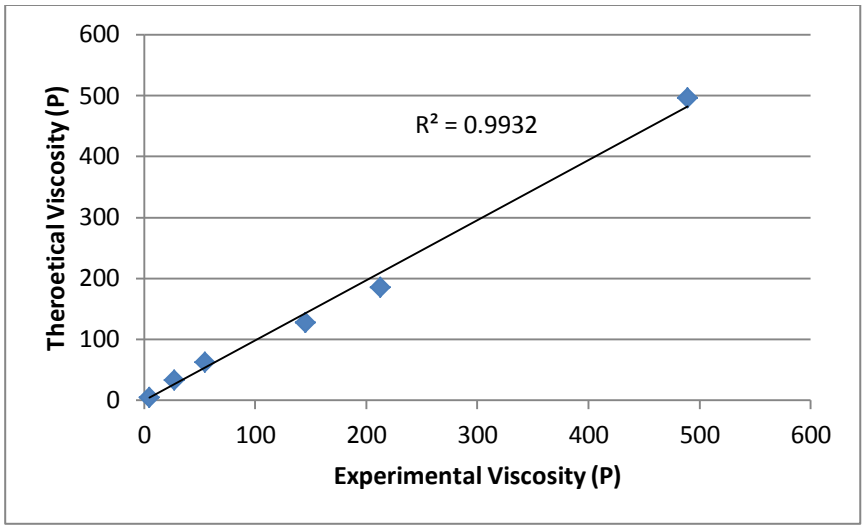

Figure 35: Comparison of experimental viscosity and theoretical viscosities predicted by modified Thomas equation

With this degree of accuracy, as long as predicted values remained below 90% of the no flow value, no precautionary steps would need to be taken.

5.3 Coal Oil Water Emulsion

The next task will be to predict the viscosity of a coal-oil-water emulsion, (COWE). An experiment as well as data will be referenced from Majumder et al [5]. The coal was taken from Bihar, India and was ground and passed through the following mesh sizes: −100+150, −150+200, −200+240. Diesel oil having a density of 829.6 kg/m^3 was used as well as distilled water. The equipment used for the viscosity examination was a custom built apparatus [5]. The data to be used in the following modeling procedure shows the viscosity of a specific emulsion vs. it's weight percent of water [5]. Each set of data is separated by weight percent coal.

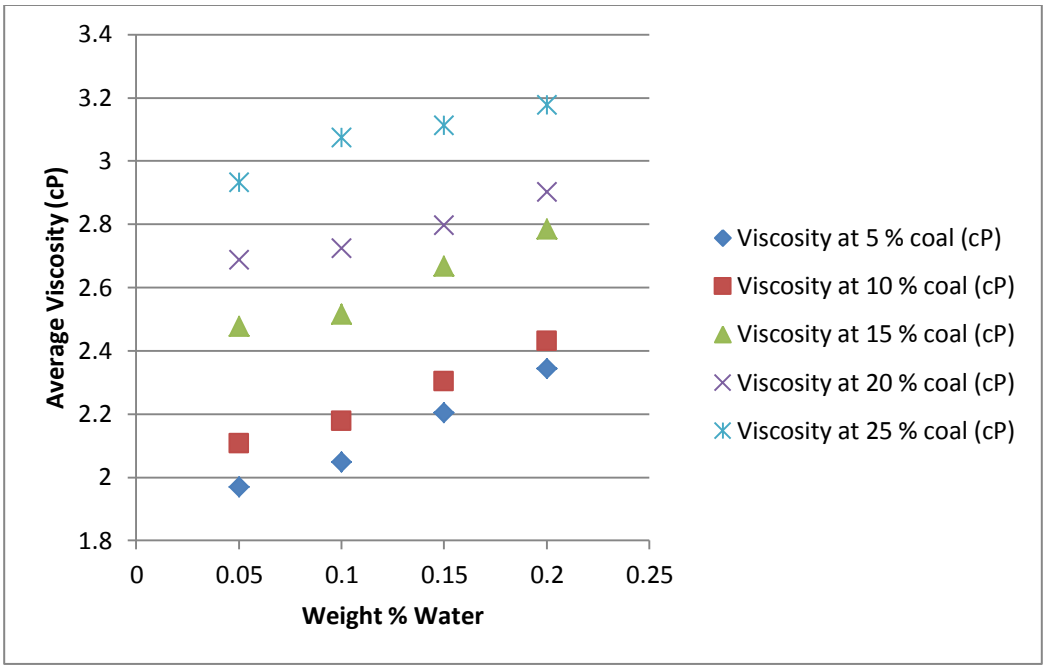

Figure 36: Average emulsion viscosity varying water mass percent, data series varying by coal concentration [5]

Some key experimental results not apparent in the above data relating to viscosity are as follows. When solid concentrations of the COWE are 10% and below, changing particle size does not noticeably affect the viscosity. But when the solids concentration is 15% or above, decreasing particle size, increases viscosity. The greater the solids concentration the more apparent this change is. It is theorized that this is due a decrease in the fluidity of the COWE as a result of the increase in irregularity of the surfaces of the particles [5].

The following equation was given to predict viscosity of emulsions [5]:

$$\frac{\mu_{sL} d_p}{T C_c} = \mathbf{2.131} \left(\frac{d_p^3 C_w^2}{C_c} \right)^{0.253} \left(\frac{d_p^5 C_c \omega^2}{T} \right)^{0.057} \tag{5.7}$$

Where d_p is the diameter of the particle, μ_{sL} is emulsion viscosity, T is the torque, C_c is the mass concentration of the coal, C_w is the mass concentration of the water, ω is

the angular velocity used by the custom viscosity measurement device. Because the apparatus used in the experiment was unavailable, the above equation must be altered because some of the variables cannot be accounted for such as the torque and angular velocity. The following is that process.

$$\frac{\mu_{sL} d_p}{TC_c} = 2.131\left(\frac{d_p^3 C_w^2}{C_c}\right)^{0.253}\left(\frac{d_p^5 C_c \omega^2}{T}\right)^{0.057}$$

$$\mu_{sL} = 2.131\frac{TC_c}{d_p}\left(\frac{d_p^{0.759} C_w^{0.506}}{C_c^{0.253}}\right)\left(\frac{d_p^{0.285} C_c^{0.057} \omega^{0.114}}{T^{0.057}}\right)$$

$$\boldsymbol{\mu_{sL} = 2.131 C_w^{0.506} C_c^{0.804} d_p^{0.017} \omega^{0.114} T^{0.943}}$$

$$\boldsymbol{\mu_{sL} = 2.131 C_w^{0.506} C_c^{0.804} d_p^{0.017}} \quad (5.8)$$

Due to the fact that the exponent of the particle diameter is very small and large changes in viscosity due to particle size changes were not reported [5], it will be ignored, leaving:

$$\boldsymbol{\mu_{sL} = 2.131 C_w^{0.506} C_c^{0.804}} \quad (5.9)$$

When equation 5.9 was used in prediction calculations, it performed poorly. This was expected as variables were completely removed from the original equation. In order to account for the removal of T and ω, an iterative process will be used to fit for new constants that will allow for accurate viscosity predictions.

Staring with a general form of equation 5.9 gives

$$\boldsymbol{\mu_{sL} = k C_w^m C_c^n} \quad (5.10)$$

Where m and n are the specific constants that will be solved for as follows. The first step is to take the data given in figure 37, and plot viscosity vs. coal concentration and vary by water concentration:

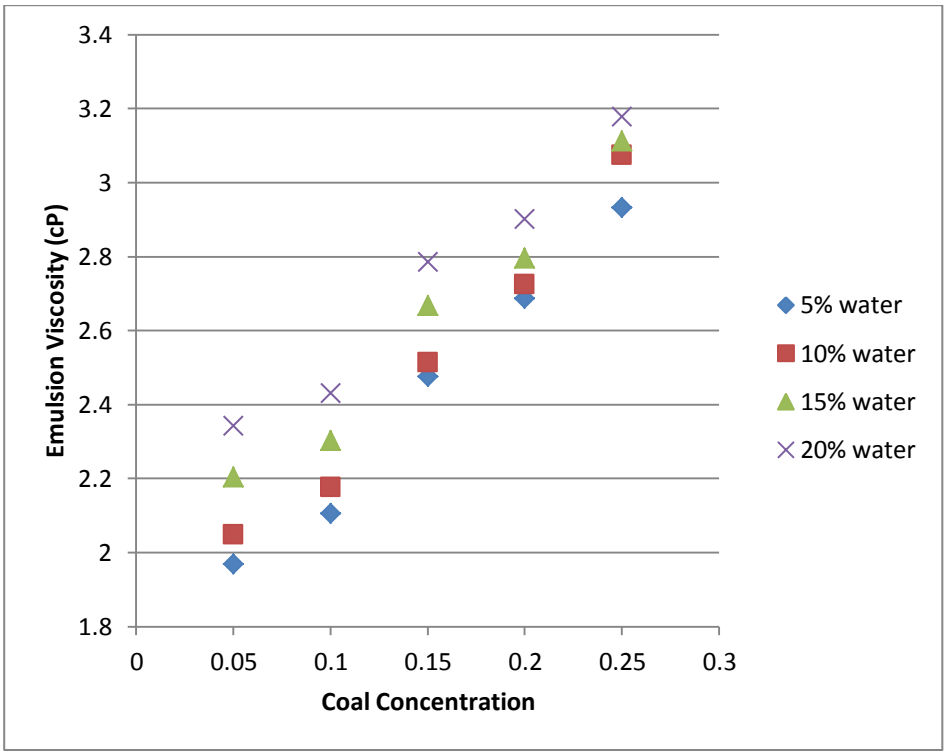

Figure 37: Emulsion viscosity varying coal concentration, data series varying by water concentration [5]

Because equation 5.10 is a power function, the excel power function trend lines will be fit through each data series.

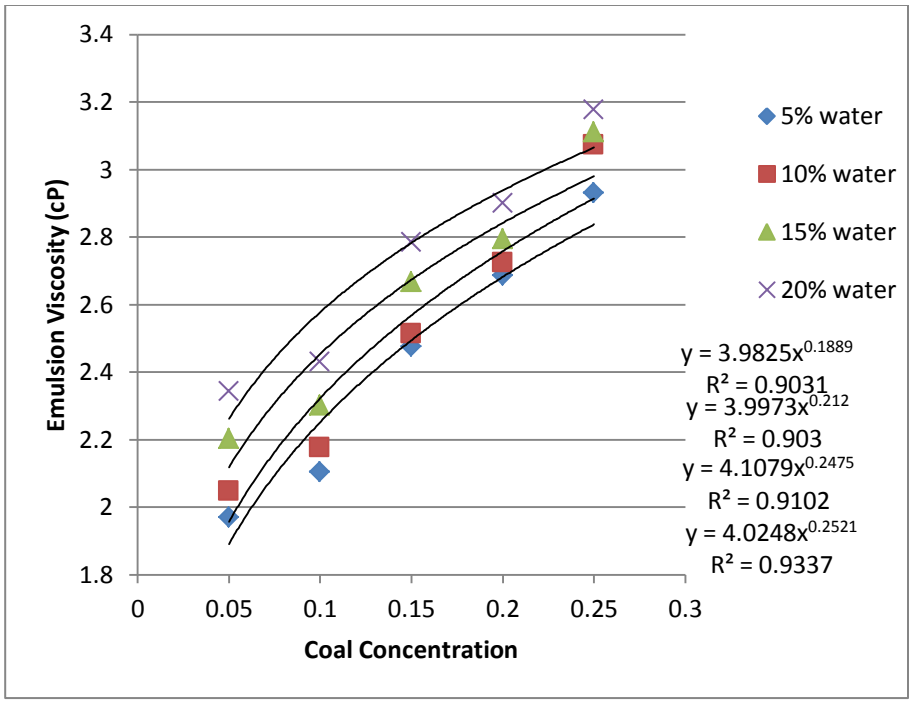

Figure 38: Power function trend lines for data from Majumder

At this point each individual power function equation can be taken and compared to equation 5.10 in the following manor:

$$\mu_{sL} = kC_w^{0.506}C_c^n = k'C_c^n = 3.9825x^{0.1889}$$

$$giving: k' = 3.9825, n = 0.1889$$

Using this approach, repeat for the all four power functions. The results are as follows:

Table 55: n and k' for 1st iteration 1st step

Mass Fraction Water (Cw)	k'	n
0.05	4.0248	0.2521
0.1	4.1079	0.2475
0.15	3.9973	0.212
0.2	3.9825	0.1889

The final value for the first iteration of n is then found by averaging the 4 n's giving 0.23. To find k the following process is used:

$$k_i' = kC_w^{0.506}; i = 1,2,3,4$$

Resulting in the following:

Table 56: k for 1st iteration 1st step

k'	k
4.0248	18.32590716
4.1079	13.17103376
3.9973	10.43913626
3.9825	8.991550891

Then the k values are averaged giving a value of 12.73.

The next step is to take the averaged k and n values and repeat the process except this time instead of solving for the coal concentration constant, the water concentration is solved for:

$$\mu_{sL} = kC_w^m C_c^{.23} = k'C_w^m$$

This results in:

Table 57: k', m, and k values for 1st iteration 2nd step

Mass Fraction Coal (C_C)	k'	k	k average	m
0.05	2.7986	5.493323909	4.869481142	0.1227
0.1	2.8051	4.710568767	-	0.1002
0.15	3.1334	4.80284194	-	0.0834
0.2	3.1122	4.471189952	-	0.052
0.25	3.4767	4.750135225	-	0.0562

With the m solved for, k is the only constant left that needs to be found. The first calculation led to a k value of around 12 and k value of around 5. Thus the process needs to be repeated, using the new m and n values until two k values are solved for that are almost equal.

The process is complete when the k values for both the first and 2nd step of an iteration reach an equal value. In this case it only took two iterations until k had reached an acceptable value in both steps:

Table 58: Results of viscosity prediction iterations

	Iteration Set 1	Iteration Set 2
n	0.225125	0.225125
k	12.73190702	4.84007543
m	0.0829	0.0829
k	4.869481142	4.869481142

The values n and m as well as the average k at the end of the 2nd iteration and then taken and plugged into equation 5.10:

$$\mu_{sL} = kC_w^m C_c^n \rightarrow 4.855 C_c^{0.225} C_w^{0.0829} \quad (5.11)$$

This is the final form of the equation that will be used to predict the emulsion viscosity. The following table compares the experimental and the theoretical viscosities as well as graphical analysis of that data. The table is displayed graphically in figure 39.

Table 59: Experimental and Theoretical viscosity comparison for a COWE

Experimental	Theoretical
1.969	1.929
2.105	2.255
2.476	2.471
2.686	2.636
2.932	2.772
2.048	2.044
2.176	2.389
2.515	2.617
2.725	2.792
3.074	2.936
2.204	2.113
2.302	2.470
2.667	2.706

2.795	2.888
3.112	3.036
2.343	2.164
2.430	2.530
2.785	2.772
2.902	2.957
3.177	3.110

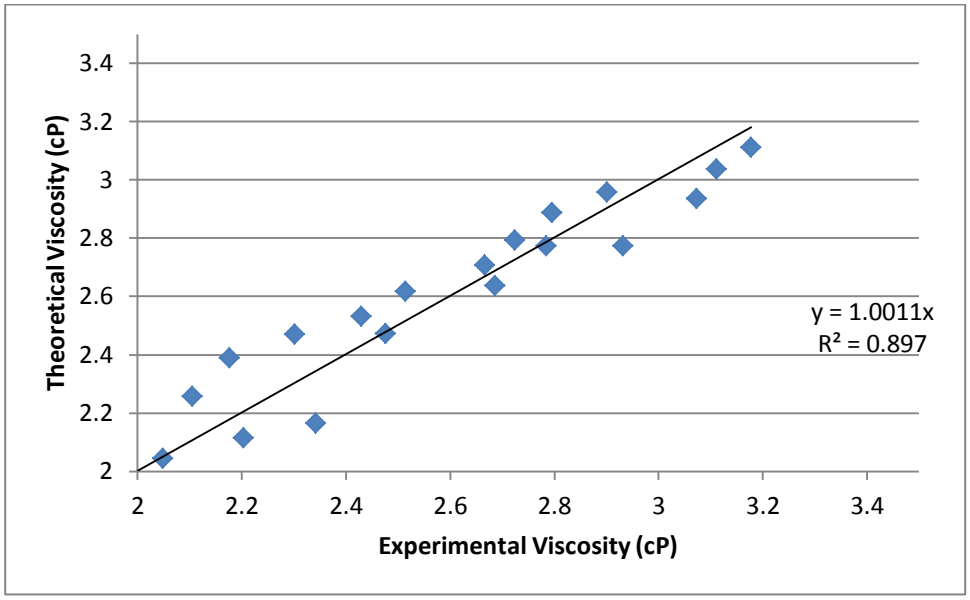

Figure 39: Accuracy graph for viscosity models

With the degree of accuracy displayed above, useful modeling of COWE's can be done, but if the predicted viscosity value ends up being with 75% of the critical viscosity point, pre cautionary measures would need to be taken before fuel production.

5.4 Discussion

Relatively accurate model equations were created for both a specific slurry situation as well as a specific emulsion situation. While in reality there will be countless different types of fuel mixtures at different temperatures, it is clear that using similar methods to the ones demonstrated in this chapter, relatively accurate

viscosity predicting equations can be created for virtually any mixture. This is because the equations used above are functions of a combination of solids mass percent, solids concentration and liquid concentration, which are easy values to obtain, the method above should be able to be employed for almost any combination of solids and fuels. For example if wood were to be used instead of coal, volume percent's and concentrations would be as trivial to find as they would be for coal. They only difference in viscosity calculations would be a few physical properties such as density.

In both cases the model results provided accurate enough predictions for the task at hand. As explained elsewhere, when predicting the viscosity for potential fuels, the most important factor is that the viscosity is below a certain value in which otherwise it would be un-combustible due to lack of flow. If the predicted values are far enough below this critical viscosity point, these model equations are accurate enough to not have to worry about potentially heating the fuel mixture. If the predicted values are close to the critical viscosity point, the fuel producer can either alter the concentrations of solids and liquids or can plan on using heat to lower viscosity. If the predicted viscosity is much higher than the critical viscosity, it is safe to assume that that fuel mixture probably is not a good option.

5.5 Conclusion

When composite fuels are constructed, attention will have to be given the composition ratio of solids to liquids, depending on what viscosity the intended process requires the fuel to be at. The following equation was found to predict viscosity of a given solid-liquid mixture with enough accuracy to give a good idea of

what a viscosity a prospective fuel will have. The methodology used to find the equation can be repeated to find an equation for most liquid-solid species.

5.6 Nomenclature

A and B	constants for the Thomas equation
C_c	Concentration of coal, $kg/m3$
C_w	Concentration of water, $kg/m3$
d_p	Diameter of particle mm
K	Power constants
$m\ and\ n$	Constants being solved for in Majumder equation
T	Torque N/m^2
φ	Volume fraction of coal in the mixture
μ_m	slurry viscosity $kg/m\ s$
μ_L	Viscosity of liquid, $kg/m\ s$
μ_{sL}	Viscosity of suspension, $kg/m\ s$
ω	Angular velocity of fluid at a distance, r, from the inner cylinder, $radians/s$

5.7 References

[1] URI boiler building, Craig. Personal interview. 12 Nov. 2012.

[2] Timbalia, Avanti. “Solvent Refined Coal and Coal-Oil Mixtures.” Master’s Thesis, Ohio University 1981

[3] Thomas, David G. "Transport characteristics of suspension: VIII. A note on the viscosity of Newtonian suspensions of uniform spherical particles." *Journal of Colloid Science* 20.3 (1965): 267-277.

[4] Guth, Eugene, and R. Simha. "Untersuchungen über die viskosität von suspensionen und lösungen. 3. über die viskosität von kugelsuspensionen." *Colloid & Polymer Science* 74.3 (1936): 266-275.

[5] Kumar Majumder, Subrata, et al. "Studies on flow characteristics of coal–oil–water slurry system." *International Journal of Mineral Processing* 79.4 (2006): 217-224.

CHAPTER 6 - LIQUID DROPLET COMBUSTION MODELING

6.1 Introduction

Now that the benefits of an emulsion in regards to the viscosity and stability of composite combustion mixtures have been examined, the next step is to look at the actual effects composite fuels have on combustion properties. In order to accomplish this, the composite fuel combustion process will be separated into multiple parts: Liquid combustion, solid combustion, emulsion combustion and emulsion-solid combustion. Once the first three parts are successfully modeled, the final model, emulsion-solid combustion, composite combustion, will be able to be completed.

The following section will detail the method used to create the model of the liquid combustion process. To begin with, a set of assumptions must be made [3]. These assumptions allow simplification of the required calculations which in turn affect the overall accuracy of the model. The model still can and does produce accurate results which can in turn be used with confidence in other portions of this thesis.

6.2 Physical Model Description

The following is the list of assumptions:

1.) The burning droplet is surrounded by a spherically symmetric flame and exists in a quiescent, infinite medium
2.) The effects of convection are ignored. Radiation heat transfer is negligible
3.) The liquid fuel is a single component liquid with zero solubility for gases
4.) Pressure is constant at 1 atmosphere

5.) The gas phase consists of three species: Fuel vapor, oxidizer and combustion products

6.) Fuel and oxidizer are assumed to react in stoichiometric proportions to the flame, while the chemical kinetics are so fast the flame is idealized as an infinitesimally thin sheet

7.) The Lewis number is assumed to be 1

8.) The gas phase thermal conductivity, specific heat and density are all constants. (k_g, C_{pg}, ρ)

9.) The liquid fuel droplet is the only condensed phase

With these assumptions in place, a more detailed description of the combustion environment can be made.

To begin is a physical model of the environment being examined which is shown below in figure 40.

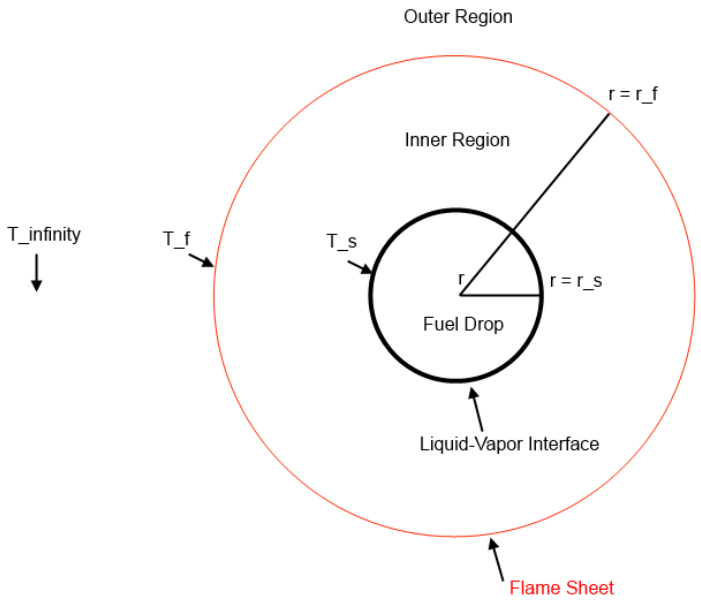

Figure 40: Liquid droplet physical model

Here is the droplet of liquid fuel of radius r_s surrounded by the flame sheet of radius r_f. Inside r_s is pure liquid fuel. The inner region, $r_f \geq r \geq r_s$, contains fuel vapor and combustion products while the outer region, $r_\infty \geq r \geq r_f$, contains oxidizer and combustion products. In regards to the inner region, the fuel concentration in air is highest near the droplet and decreases as the flame sheet is approached, while the product concentration is highest near the flame sheet and decreases with distance. This is due to the fact that the flame sheet is consuming fuel in the combustion reaction which also produces products which are dispersed to both sides of the flame sheet. It should be noted that due to the assumption that states the fuel has zero solubility for gases, the products do not diffuse into the fuel droplet, but remain in the inner region and serve as a medium through which heat and fuel must transfer through. The outer region shows a similar relationship except with oxidizer replacing fuel. The closer to the flame sheet, the less oxidizer is found in the air because it is being consumed in the combustion reaction while combustion products are being produced. This is shown graphically in figure 41.

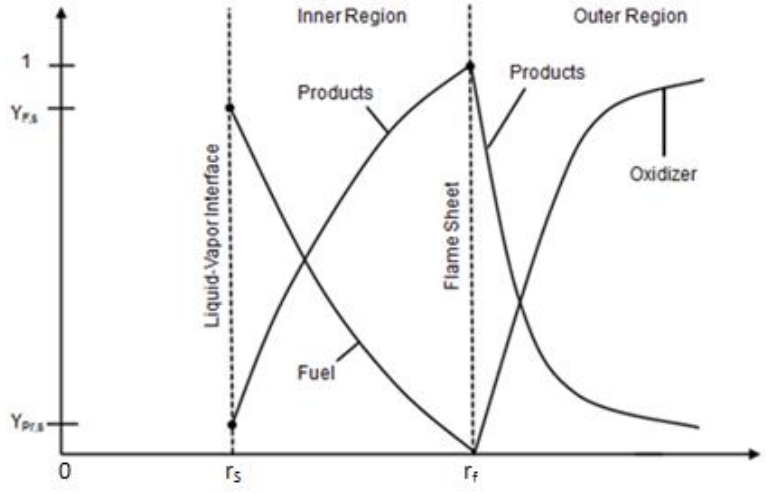

Figure 41: Component concentration profiles in different regions of model

The droplet will be assumed to follow the "onion" model [3] in that the bulk interior of the droplet will be assumed to be at the injection temperature, T_0, while a very thin outer most layer will be very close to the boiling temperature of the fuel, T_s. The outer most temperature, T_∞, is the average temperature of the furnace and is greater than T_s but less than that of the flame, T_f. T_∞ can be controlled and is normally between 811 and 1033 degrees Kelvin. T_∞ also directly will also influence T_f.

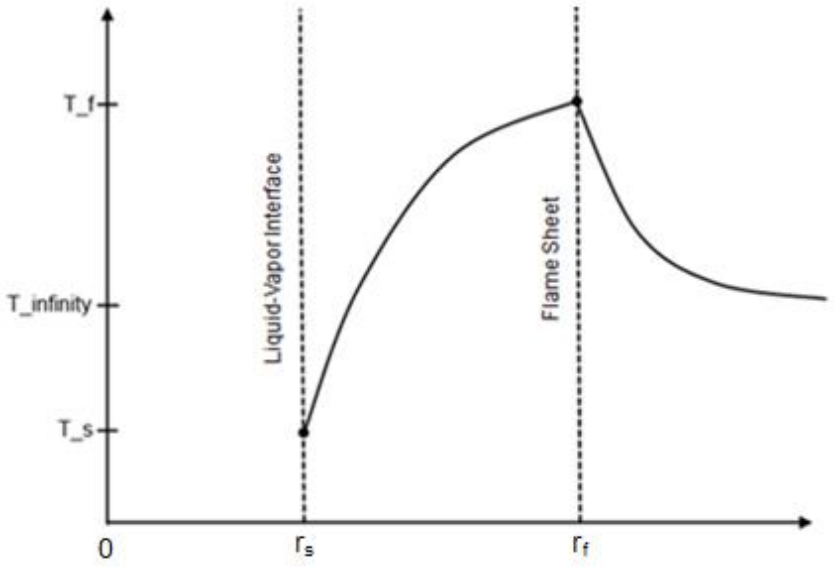

Figure 42: Temperature profile in different regions of model

6.3 Model Equations

The end goal of this model is to find the fuel mass burning rate $\dot{m}_F$ as well as the droplet life time t_d given the following controllable variables: Initial droplet size, T_∞, and oxidizer mass fraction at infinity, $Y_{Ox,\infty}$. Along the way to finding $\dot{m}_F$ and t_d, other important properties will be found including, flame radius and temperature, r_f

and T_f, droplet radius and temperature, r_s and T_s and fuel mass fraction at the droplet surface, $Y_{F,s}$.

To get these properties, a set of 5 conservation principles can be solved [1][2][3]. First the mass flow relationships can be examined at the flame sheet.

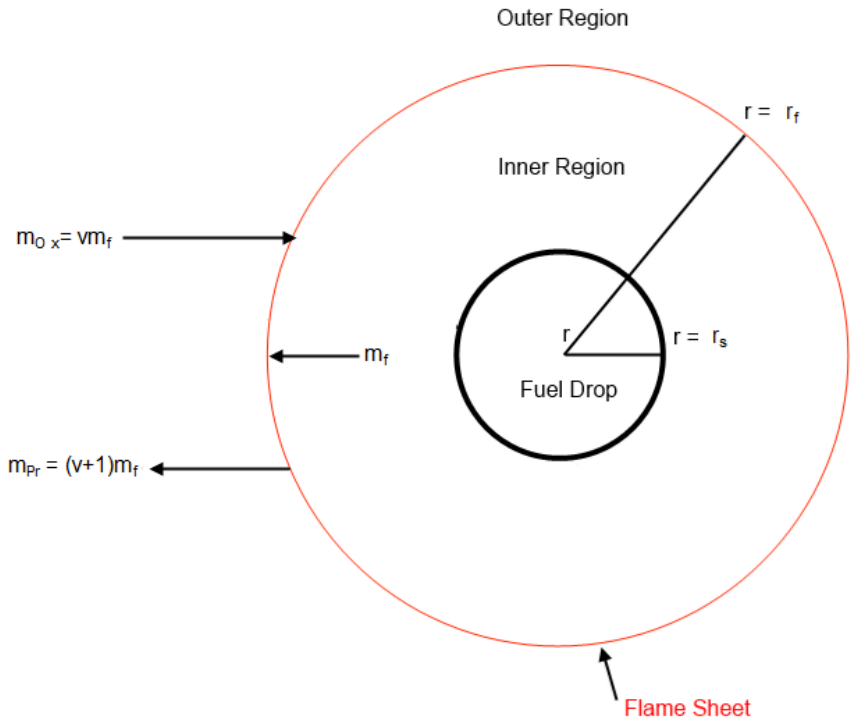

Figure 43: Mass flow relationships in fuel drop combustion model

By balancing the oxidizer species at the flame sheet, an expression for $\dot{m}_F$ can be found [3]:

$$\dot{m}_F = \frac{4\pi k_g r_s}{c_{pg}} \ln\left(1 + B_{o,q}\right) \tag{6.12}$$

Where k_g is the thermal conductivity of the all gas phase components in the system, r_s is the radius of the surface of the fuel droplet, c_{pg} is the specific heat of all gas phase components and $B_{o,q}$ is the Spalding Number which is [3]:

$$\boldsymbol{B_{o,q} = \frac{\Delta h_c}{v} + c_{pg}(T_\infty - T_s)} \quad \textbf{(6.2)}$$

Where Δh_c is the heat of combustion of the fuel and v is the oxidizer-fuel stoichiometric ratio. A fuel species conservation balance can be also be performed on the inner region to obtain the following equation for $Y_{F,S}$ [3]:

$$\boldsymbol{Y_{F,S} = \frac{B_{o,q} - \frac{1}{v}}{B_{o,q} + 1}} \quad \textbf{(6.3)}$$

Next we will examine the surface energy representation at the droplet surface as well as at the flame sheet.

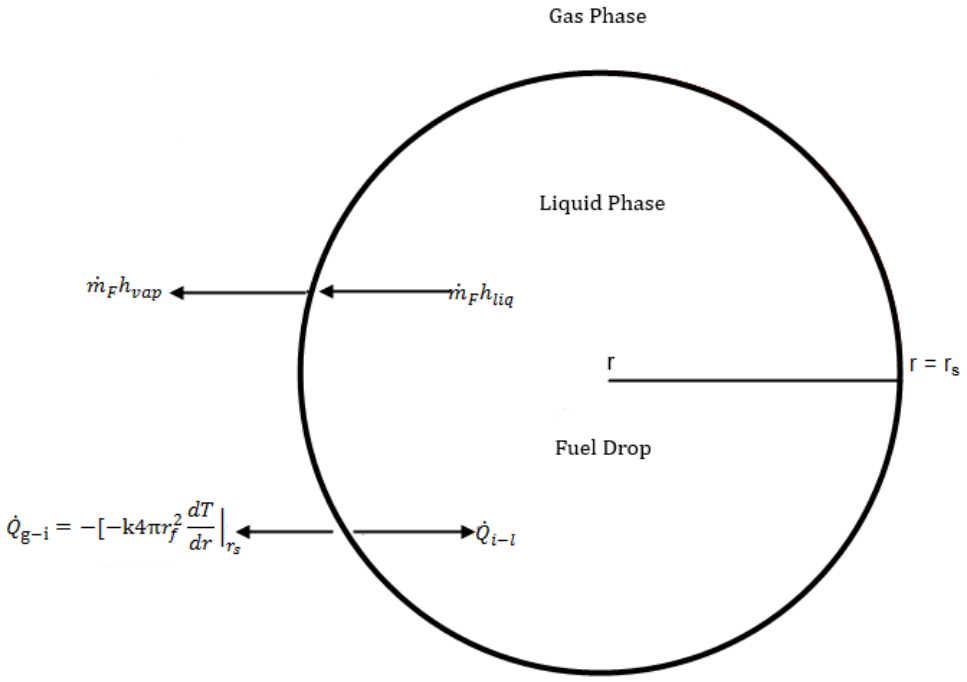

Figure 44: Energy balance at the liquid-vapor Interface

If an energy balance is performed at the droplet liquid-vapor interface, the following expression can be found for T_f [3]:

$$\boldsymbol{T_f = \frac{c_{pl}(T_s - T_0) + h_{fg}}{c_{pg}(1+v)}\left(vB_{o,q} - 1\right) + T_s} \quad \textbf{(6.4)}$$

Where h_{fg} is the latent heat of vaporization of the fuel and c_{pl} is the specific heat of the liquid fuel and T_0 is the injection temperature of the droplet. If the same balance is performed at the flame sheet, as is seen in the following figure an expression can be found for r_f.

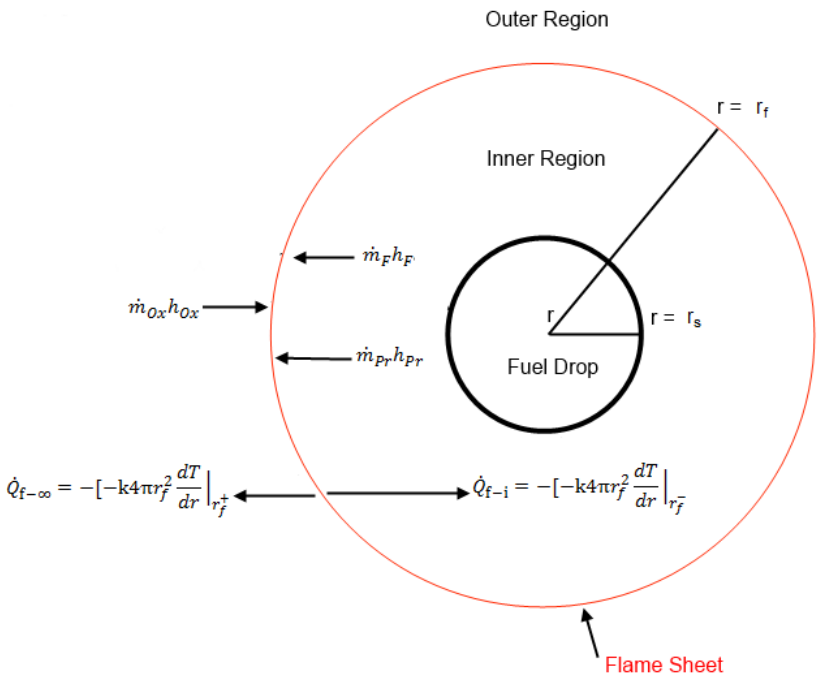

Figure 45: Energy balance at the flame sheet

With the expression taking the following form [3]:

$$\boldsymbol{r_f = r_s \frac{\ln(1+B_{o,q})}{\ln\left(\frac{1+v}{v}\right)}} \quad \textbf{(6.5)}$$

These 4 equations can all be solved with an initial assumption for T_s. Unless T_s is guessed reasonably accurately on the first try, the results will not be as accurate as they could be. To fix this issue, a fifth equation is used by analyzing the liquid-vapor phase equilibrium at the interface while applying the Clausius-Clapeyron?? equation. Initially the following expression is obtained [3]:

$$\boldsymbol{Y_{F,s} = \frac{Ae^{-\frac{B}{T_s}}MW_F}{Ae^{-\frac{B}{T_s}}MW_F + \left(P - Ae^{-\frac{B}{T_s}}MW_{Pr}\right)}} \quad \textbf{(6.6)}$$

Which is can be rearranged to solve for T_s to [3]:

$$\boldsymbol{T_s = \frac{-B}{\ln\left(\frac{MW_{Pr}Y_{F,s}P}{A(Y_{F,s}MW_F - Y_{F,s}MW_{Pr} - MW_F)}\right)}} \quad \textbf{(6.7)}$$

Where MW_F and MW_{Pr} represent molecular weight of the fuel and products respectively, P stands for pressure. If the Clausius-Clapyron equation is integrated two constant can be found. One constant, A, will be called the pressure constant and the other constant, B, is the temperature constant. They are expressed as follows [3]:

$$\boldsymbol{A = 1.013 * 10^5 e^{\frac{h_{fg}MW_F}{R_u T_b}}} \quad \textbf{(6.8)}$$

$$\boldsymbol{B = \left(\frac{h_{fg}MW_F}{R_u}\right)} \quad \textbf{(6.9)}$$

Where R_u is the universal gas constant and T_b is the boiling temperature of the fuel. Once an initial T_s is supplied and equations 6.1-6.5 are solved, equation 6.7 can be used to provide and improved value of T_s. This new T_s can then be used to solve equations 6.1-6.5 again and the process can repeat until convergence is obtained.

Then to find the droplet radius at any given time during the droplet combustion process, the following equation is used, which is known as the D^2 law for spherical droplets [3]:

$$\boldsymbol{D^2(t) = D_0^2 - Kt} \tag{6.10}$$

When K, a constant, is the burning rate constant, the D^2 law becomes specific for droplet burning [3]:

$$\boldsymbol{K = \frac{8k_g}{\rho_l c_{pg}} \ln(1 + B_{o,q})} \tag{6.11}$$

6.4 Initial Calculation Parameters

In order to perform the above calculations, extensive physical properties of the fuels being combusted need to be known. Soybean oil has not been used long as a fuel, so properties from a combustion standpoint are not easy to find and in some cases assumptions had to be made. The variation found in any liquid fuel, whether a fuel oil or a vegetable will be present due to varying processing techniques as well different harvesting areas. Because of this it should be kept in mind that a lot of the properties listed are averages and differing values can be found. Regardless, the properties presented in this section should be close enough to any other obtainable property values. Each property that required some sort of extensive method or assumptions to be made will now be addressed for both soybean oil and diesel.

c_{pl} for soybean oil was found using the following equation [5]:

$$\boldsymbol{c_{pl}\ (kJ/kg * K) = \ 1.8583 + 0.0024T} \tag{6.12}$$

c_{pl} for diesel was found using the following equation [6]:

$$c_{pl}\ (kJ/kg*K)\ = \frac{(264+6.33T-0.00296T^2)}{1000} \quad \textbf{(6.13)}$$

In regards for what temperature to use, since this is a specific heat of the fuel and specific heat will not change immensely with temperature, a single average T will be used. This T will be chosen by using the following equation:

$$T = \frac{(T_0+T_s)}{2} \quad \textbf{(6.14)}$$

Since T_s is not yet known at this point, a value should be assumed slightly below the boiling temperature of the fuel. It should be noted that this is the method used when selecting a temperature for any temperature dependent liquid properties.

The liquid density, ρ_l, of soybean oil was found by taking the density value at 293 K and the $\frac{d\rho_l}{dt}$ value and using them in the following equation [7]:

$$\rho_l\ \left(\frac{kg}{m^3}\right) = \rho_{l,293\ K} + \frac{d\rho_l}{dt}(T-293) \quad \textbf{(6.15)}$$

The ρ_l for diesel was found using the following equation: [6]

$$\rho_l\ \left(\frac{kg}{m^3}\right) = \left(\frac{840}{1+0.00067(T-288)}\right) \quad \textbf{(6.16)}$$

Where T is found using equation 6.12.

Combustion parameters were found using the following method. For any oxygenated hydrocarbon fuel, combustion can be expressed as [3]:

$$C_xH_yO_z + a(O_2 + 3.76N_2) \rightarrow + \frac{y}{2}CO_2 + a*3.76N_2 \quad \textbf{(6.17)}$$

$$a = x - \frac{z}{2} + \frac{y}{4} \quad \textbf{(6.18)}$$

At the flame sheet the oxidizer and the fuel are assumed to combine stoichiometrically [3]:

$$\mathbf{1}\ \boldsymbol{kg\ fuel} + \boldsymbol{v}\ \boldsymbol{kg\ oxidizer} = (\boldsymbol{v}+\mathbf{1})\ \boldsymbol{kg\ products} \tag{6.19}$$

Then [3]

$$\boldsymbol{v} = \frac{\boldsymbol{m_{Ox}}}{\boldsymbol{m_F}} = \frac{\boldsymbol{4.76aMW_{air}}}{\boldsymbol{MW_F}} \tag{6.20}$$

This method is used for both soybean oil and diesel, but where the problem arises, specifically for soybean oil, is in figuring out what x, y and z are, as the chemical formula for soybean oil does not exists due to its varying composition. The first step is to figure out the molecular weight for soybean oil. An average value of 872.33 g/mol was found [8]. Then the average composition of processed soybean oil was found [7].

Table 60: Composition of processed soybean oil. Total percent shown is 0.998

	%	C	H	O
Linoleate	0.545	18	32	2
Oleate	0.23	18	34	2
Palmitate	0.11	16	32	2
Linolenate	0.072	19	32	2
Sterate	0.041	18	36	2

The average chemical formula was found by using a molecular weighting method:

Carbon: $0.545 * 18 + 0.23 * 18 + 0.11 * 16 + 0.072 * 19 + 0.041 * 18 = 17.816$

Hydrogen: $0.545 * 32 + 0.23 * 34 + 0.11 * 32 + 0.072 * 32 + 0.041 * 36 = 32.56$

Oxygen: $0.545 * 2 + 0.23 * 2 + 0.11 * 2 + 0.072 * 2 + 0.041 * 2 = 1.996$

Resulting in an average chemical formula of $C_{17.816}H_{32.56}O_{1.996}$. The expected molecular weight of 872.33 g/mol was then divided by the weight of the chemical formula, 278.736 to give a value of 3.13. This number was then multiplied with $C_{17.816}H_{32.56}O_{1.996}$ to give an empirical formula for soybean oil of $C_{56.76}H_{101.91}O_{99.96}$. This multiplier of around 3 makes sense because soybean oil is mostly made up of triglycerides. Since $C_{17.816}H_{32.56}O_{1.996}$ is the average formula for one fatty acid chain, it would make sense then to reach the correct molecular weight, it would be multiplied by 3, essentially giving the triglyceride weight. Now that the formula for soybean oil is known, a and v can be solved.

When finding the combustion parameters for diesel the average chemical formula is much better documented and was simply looked up as $C_{12}H_{23}$ [6]. In this case the molecular weight was calculated using the formula for diesel and a and v

The $c_{pg}$was found using the following assumptions. Since the gas phase consists of fuel vapor and combustion products for the inner region and oxidizer and combustion products for the outer region, it is a widely varying value depending on distance r from r_s. Because of this an attempt will be made to find a single average value. The approach taken in this thesis is to use the $c_{pg}$of the combustion products. This will end up leading to accurate results being obtained. One reason this is a good assumption is that the combustion products, unlike the oxidizer and fuel vapor are on both sides of the flame sheet and in high concentrations. Another reason for this assumption is that the c_{pg} does not reliably exist in the literature. In one source [3], even when the calculation was performed using a known fuel (heptane) and therefore a c_{pg} was known, the results were less accurate than if the c_{pg} of just the combustion

products were used. The c_{pg} of major combustion products $CO_2$and N_2 are widely available in the literature. c_{pg} of the gas phase ended up taking the following form:

$$\boldsymbol{c_{pg}\ (kJ/kg*K) = \left(a*3.76*MW_{N_2}\right)c_{pg,N_2}(T) + \left(\frac{y}{2}*MW_{CO_2}\right)c_{pg,CO_2}(T)} \quad \textbf{(6.21)}$$

The temperature at which c_{pg} was found for these products was found by averaging droplet surface temperature and the flame temperature [3]:

$$\boldsymbol{T = \frac{(T_s+T_f)}{2}} \quad \textbf{(6.22)}$$

Again T_s is initally assumed to be slightly lower than fuel boiling temperature and T_f is initially assumed to be around 2200 K. These assumptions are close enough to get accurate results, even though the real temperatures, once solved for, will be different.

The heat conductivity of soybean oil and diesel, k_F, also had to be found making certain assumptions. This was because once again, literature values of k_F were not available. There were however ample sources containing the liquid thermal conductivity of both fuels. When comparing known liquid hydrocarbon fuel thermal conductivities to their respective gaseous thermal conductivities at room temperature, it was seen that they differed by around an order of magnitude. So since the thermal conductivities of the liquid fuels were known, they were reduced by a factor of 10 to achieve the k_F at room temperature and then the $T^{1/2}$ dependence law was used to obtain the k_F at the correct temperature [4].

$$\boldsymbol{k_F(kW/m*K) = (k_{F,293}*0.1)\left(\frac{T}{293}\right)^{\frac{1}{2}}} \quad \textbf{(6.23)}$$

Where

$$\boldsymbol{T = \frac{(T_s + T_f)}{2}} \quad \textbf{(6.24)}$$

Meanwhile the k of air, k_{ox}, was easily obtainable from the literature. Then to find k_g the following weighting equation was used [4]:

$$\boldsymbol{k_g = 0.4k_F(T) + 0.6k_{ox}(T)} \quad \textbf{(6.25)}$$

The h_{fg} and h_c for soybean oil and diesel were average values taken from the literature [6][7].

Table 61 displays the initial parameters for both soybean oil and diesel:

Table 61: Pure fuel combustion parameters

Soybean oil		**Diesel**	
$T_f\ guess\ (K)$	2200	$T_f\ guess\ (K)$	2200
$T_{avg} at\ Flame\ (K)$	1386.575	$T_{avg}\ at\ Flame\ (K)$	1368.2
$T_{avg} at\ surface\ (K)$	433.075	$T_{avg}\ at\ surface\ (K)$	414.7
$h_{fg}\ (KJ/kg)$	211	$h_{fg}\ (KJ/kg)$	254
MW_F	872.33	MW_F	167.3
MW_{air}	28.85	MW_{air}	28.85
MW_{Pr}	30.00	MW_{Pr}	29.77
$T_{boil}\ (K)$	573.15	$T_{boil}\ (K)$	536.4
$T_0\ (K)$	293	$T_0\ (K)$	293
$B_{o,q}$	3.82	$B_{o,q}$	3.82
K	7.55^{-7}	K	7.55^{-7}
v	12.30	v	14.57
$c_{p,N_2}\ (kJ/kg * K)$	1.21	$c_{p,N_2}\ (kJ/kg * K)$	1.21
$c_{p,CO_2}\ (kJ/kg * K)$	1.26	$c_{p,CO_2}\ (kJ/kg * K)$	1.25
$c_{p,l}\ (kJ/kg * K)$	2.90	$c_{p,l}\ (kJ/kg * K)$	2.38
$c_{p,g}\ (kJ/kg * K)$	1.240	$c_{p,g}\ (kJ/kg * K)$	1.233
$\rho_F\ at\ 293\ K\ (kg/m\text{^}3)$	926.1	$\rho_F\ at\ 293\ K\ (kg/m\text{^}3)$	774.273
$d\rho/dt\ \ (kg/m\text{^}3)$	−0.643	$\rho_l\ (kg/m\text{^}3)$	774.273
$\rho_l\ \ (kg/m\text{^}3)$	836.032	$k_F\ at\ 293\ (W/m * K)$	0.015

$k_F\ at\ 293\ K\ (W/m*K)$	0.015	$k_F\ average\ (W/m*K)$	0.032
$K_F\ average\ (W/m*K)$	0.0333	$k_{ox}\ (W/m*K)$	0.080
$k_{ox}\ (W/m*K)$	0.081	$k_g\ (kW/m*K)$	6.083^{-5}
$k_g\ (kW/m*K)$	6.2^{-5}	$R_u\ (kJ/kmol*K)$	8.315
$R_u\ (kJ/kmol*K)$	8.315	$h_c\ (kJ/kg)$	43400
$h_c\ (kJ/kg)$	38220	$P\ (Pa)$	101300
$P\ (Pa)$	101300	$T_{critical}\ (K)$	726.9

6.5 Results

The following section will detail the results of the model explained above when varying the two controllable variables, initial fuel droplet size and furnace temperature.

While the results of the calculations will mostly be presented via graphs, a small sample of the results will be shown in tabulated form as it is sometimes hard to glean exact values from a graph. Below are results, tables 62 and 63, for both soybean oil and diesel. Each table has 3 rows, the first row being the smallest initial fuel droplet size at the highest furnace temperature, followed by mid-range values for both, ending with the largest initial fuel drop size and lowest furnace temperature.

Table 62: Some soybean oil combustion modeling results

$r_s\ (m)$	$T_\infty\ (K)$	A (Pa)	$B\ (K)$	$B_{o,q}$	$Y_{F,s}$	$\dot{m}_f\ (kg/s)$	$T_f\ (K)$	$r_f\ (m)$	$T_s\ (K)$	$t_d\ (s)$
1.00E-05	1.03E+03	6.02E+21	2.21E+04	3.98E+00	7.83E-01	1.01E-08	3.26E+03	2.05E-04	6.42E+02	6.19E-04
1.00E-04	9.33E+02	6.02E+21	2.21E+04	3.85E+00	7.77E-01	9.96E-08	3.17E+03	2.02E-03	6.42E+02	6.28E-02
6.00E-04	8.10E+02	6.02E+21	2.21E+04	3.70E+00	7.70E-01	4.87E-07	3.06E+03	9.89E-03	6.41E+02	1.35E+00

Table 63: Some diesel oil combustion modeling results

$r_s\ (m)$	$T_\infty\ (K)$	A	B	$B_{o,q}$	$Y_{F,s}$	$\dot{m}_f\ (kg/s)$	$T_f\ (K)$	$r_f\ (m)$	$T_s\ (K)$	$t_d\ (s)$
1.00E-05	1.03E+03	1.39E+09	6.11E+03	4.96E+00	8.21E-01	1.11E-08	3.22E+03	2.69E-04	4.95E+02	4.40E-04
1.00E-04	9.33E+02	1.39E+09	6.11E+03	4.81E+00	8.16E-01	1.09E-07	3.13E+03	2.65E-03	4.94E+02	4.46E-02
6.00E-04	8.10E+02	1.39E+09	6.11E+03	4.62E+00	8.10E-01	6.35E-07	3.01E+03	1.30E-02	4.93E+02	1.14E+00

The following 3 graphs are the results of maintaining a constant furnace temperature of 933 K while varying the initial droplet radius from 10 μm to 500 μm. Droplet sizes are optimum size range taken from the literature that have historically provided good flow and combustion properties. The first graph shows that with increasing initial particle size the flame sheet radius also increases, linearly. Also the diesel flame sheet radius increases faster with increasing initial particle size.

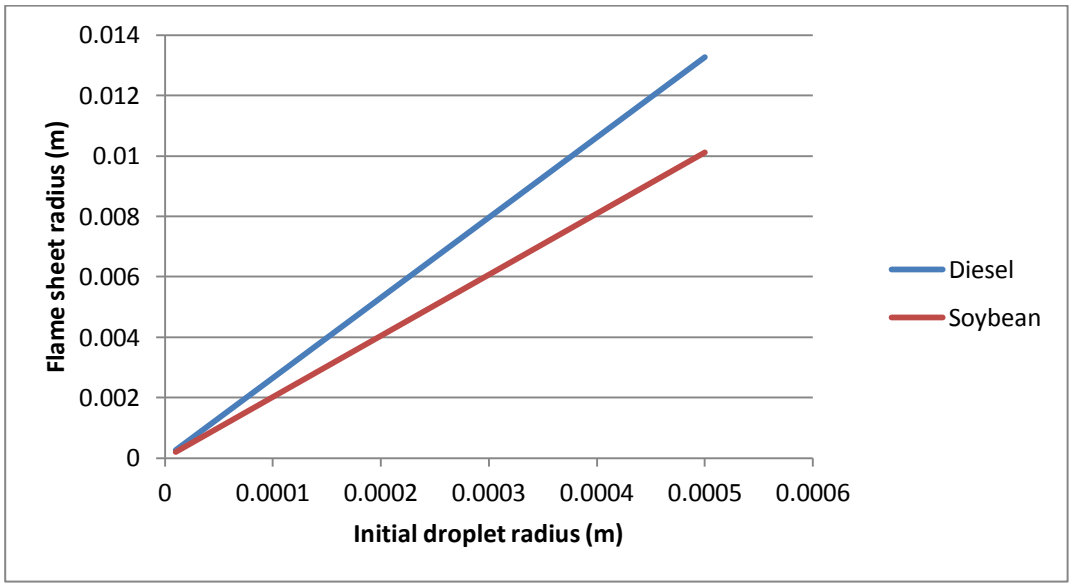

Figure 46: Radius of the flame sheet for both soybean oil and diesel droplets varying with droplet size at 933 K

Figure 47 shows that as initial particle size increases the droplet burn rate also increases linearly.

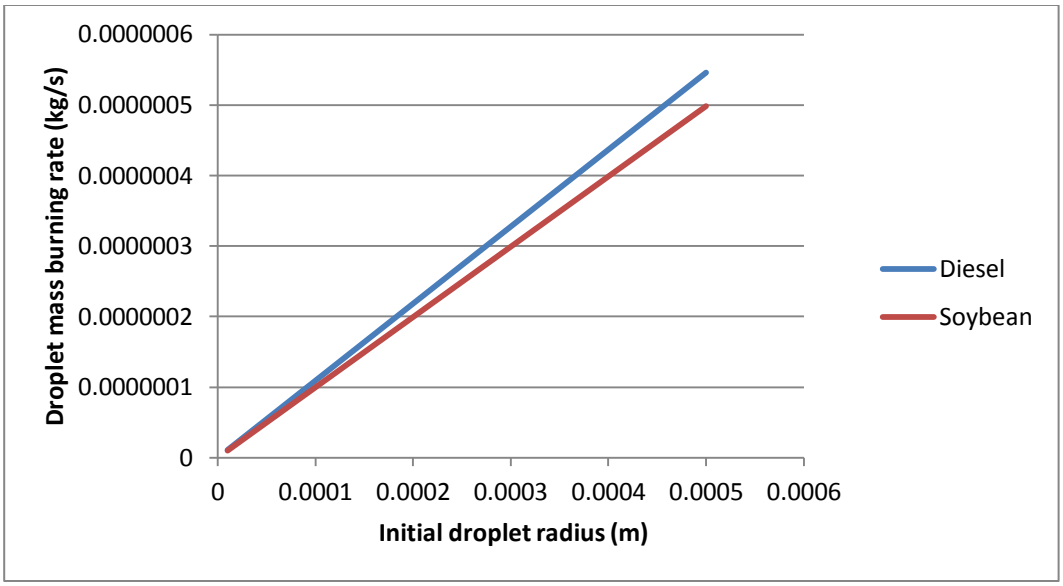

Figure 47: Mass burning rate dependency on droplet size at 933 K

The last graph of this series shows the total droplet combustion time increasing exponentially with initial particle size. Diesel is shown to completely combust in a shorter amount of time than soybean oil at all initial particle sizes.

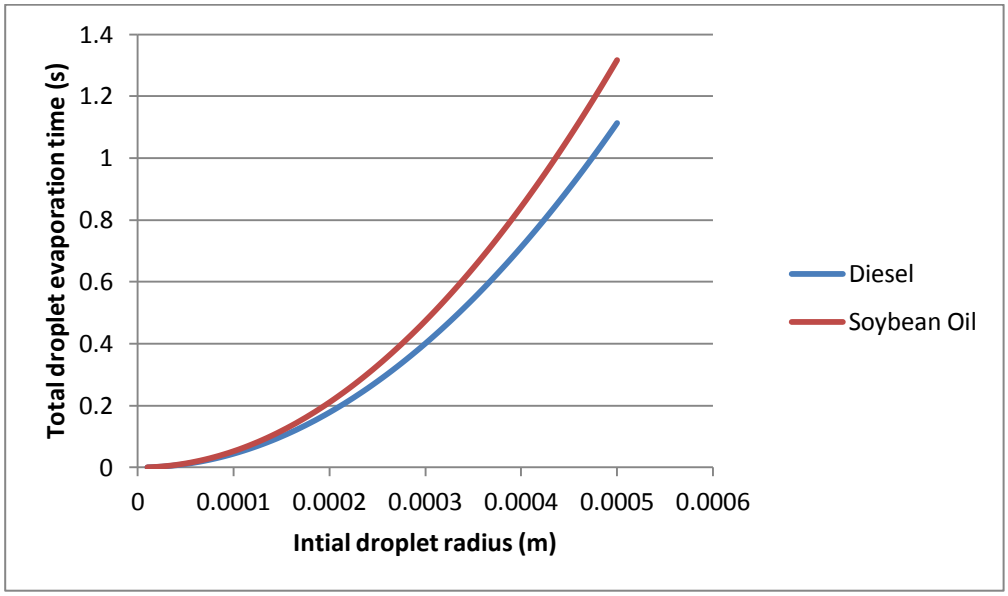

Figure 48: Total combustion time for various droplet sizes at 933 K

The next set of graphs will show the results when initial droplet size is kept constant at 100 μm while the furnace temperature is varied between the normal operating ranges of 811-1033 K. The first graph of this series shows the flame temperature increasing linearly with the furnace temperature.

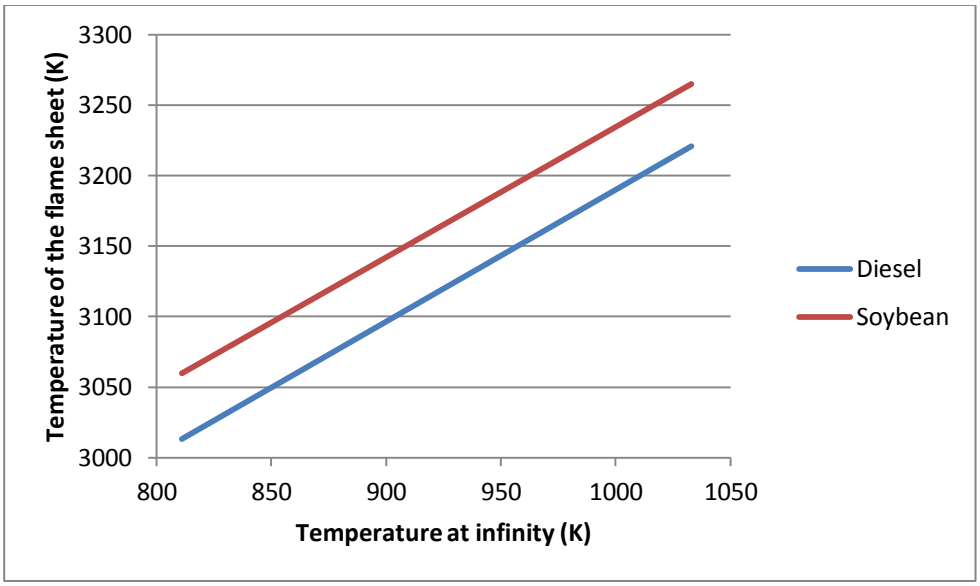

Figure 49: Temperature at the flame sheet at furnace temperatures of 811 to 1033 K for 100 μm fuel droplets

Figure 50 shows that the surface temperature increases minimally and linearly with furnace temperature.

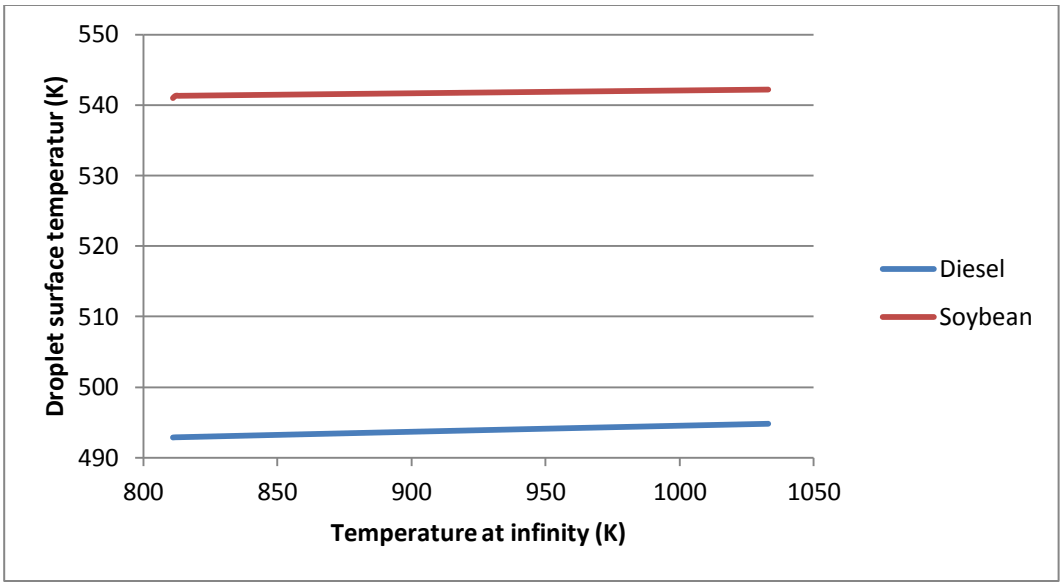

Figure 50: Temperature at the droplet surface at furnace temperatures of 811 to 1033 K for 100 µm fuel droplets

Figure 51 shows that the fuel mass fraction at the droplet surface increases linearly with furnace temperature.

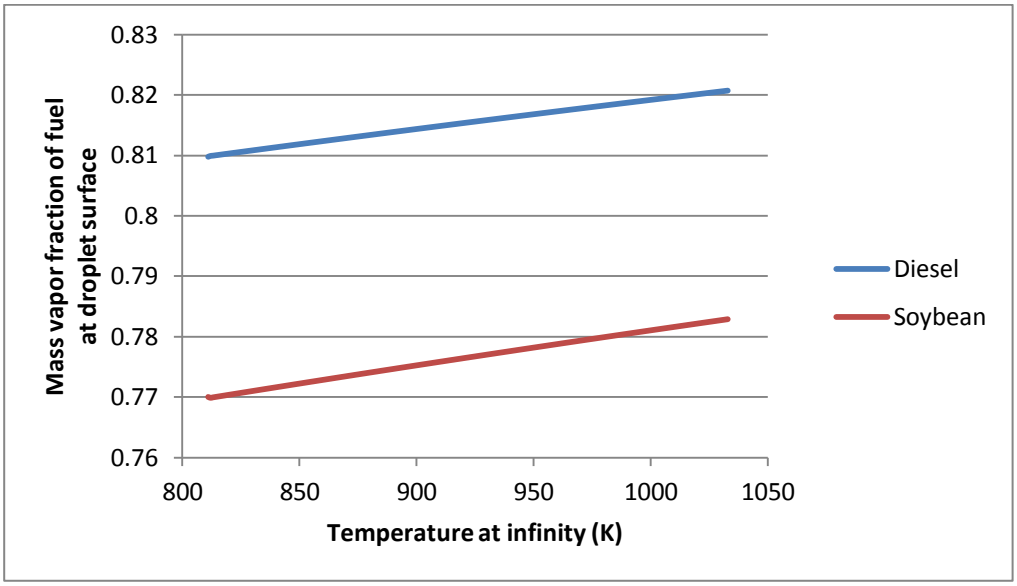

Figure 51: Mass vapor fraction of fuel at the droplet surface at furnace temperatures of 811 to 1033 K for 100 µm fuel droplets

Figure 52 shows flame sheet radius increases minimally and linearly with furnace temperature.

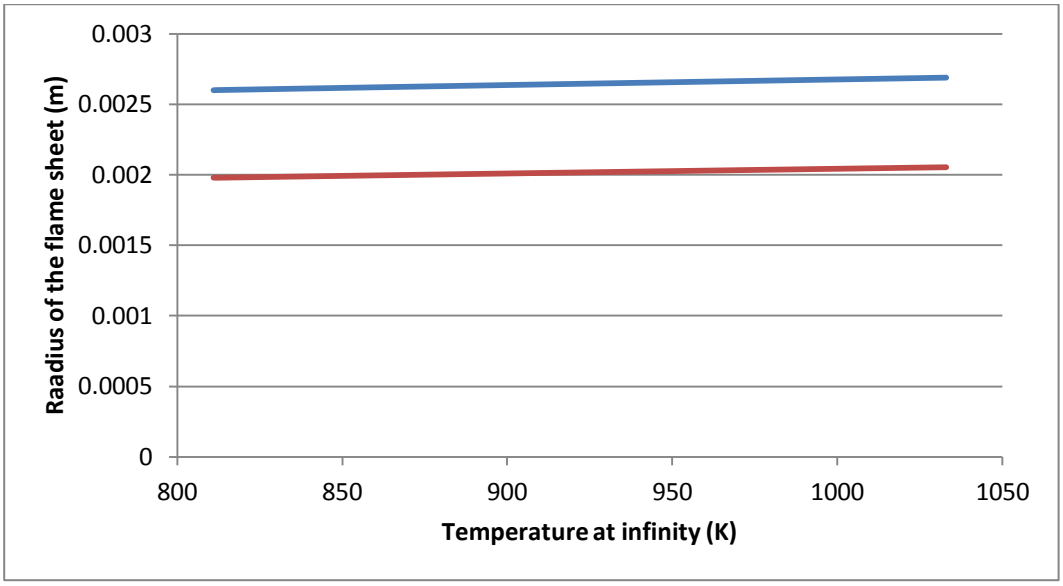

Figure 52: Flame sheet radius at furnace temperatures of 811 to 1033 K for 100 µm fuel droplets

Figure 53 shows droplet burn rate increases linearly with furnace temperature.

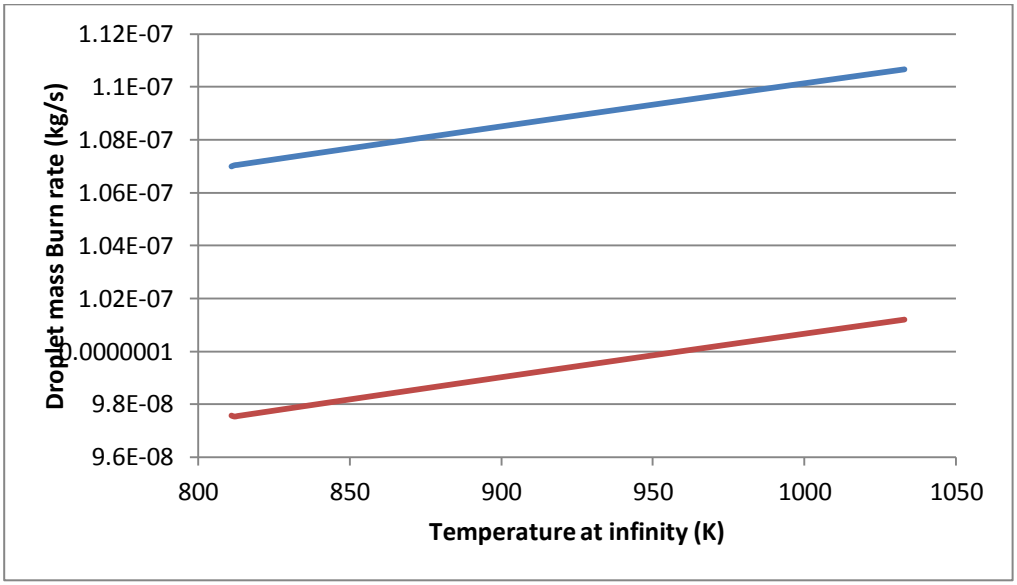

Figure 53: Droplet mas burning rate at furnace temperatures of 811 to 1033 K for 100 µm fuel droplets

Figure 54 shows total droplet combustion time decreases linearly with furnace temperature.

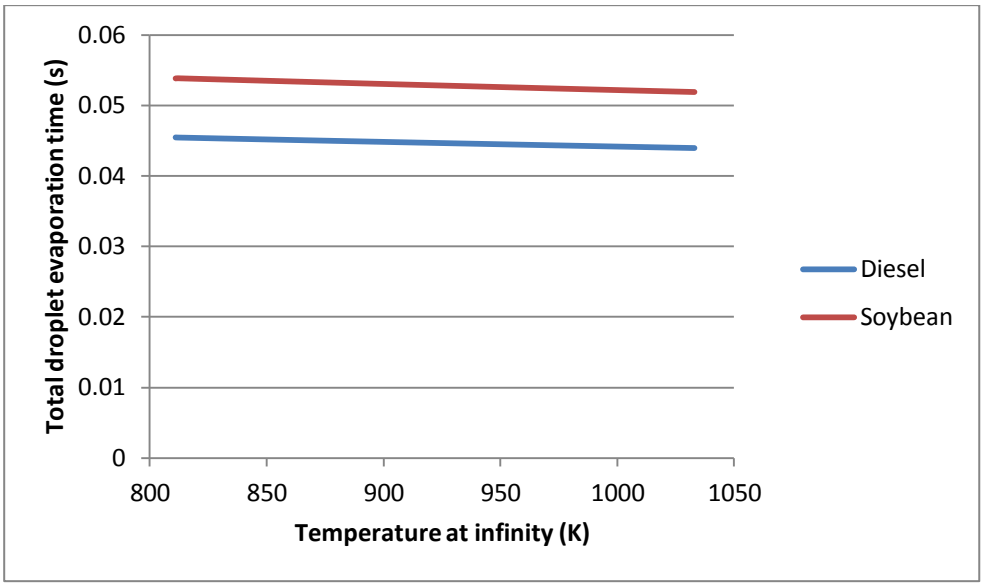

Figure 54: Total droplet combustion time at furnace temperatures of 811 to 1033 K for 100 µm fuel droplets

The last set of graphs examine the entire life of the fuel droplet. Both fuels were examined at three differing initial particle sizes and furnace temperature combinations. All three scenarios had the same general shape to the results as well as the diesel oil droplet combusting faster and being smaller at all times except for t_0.

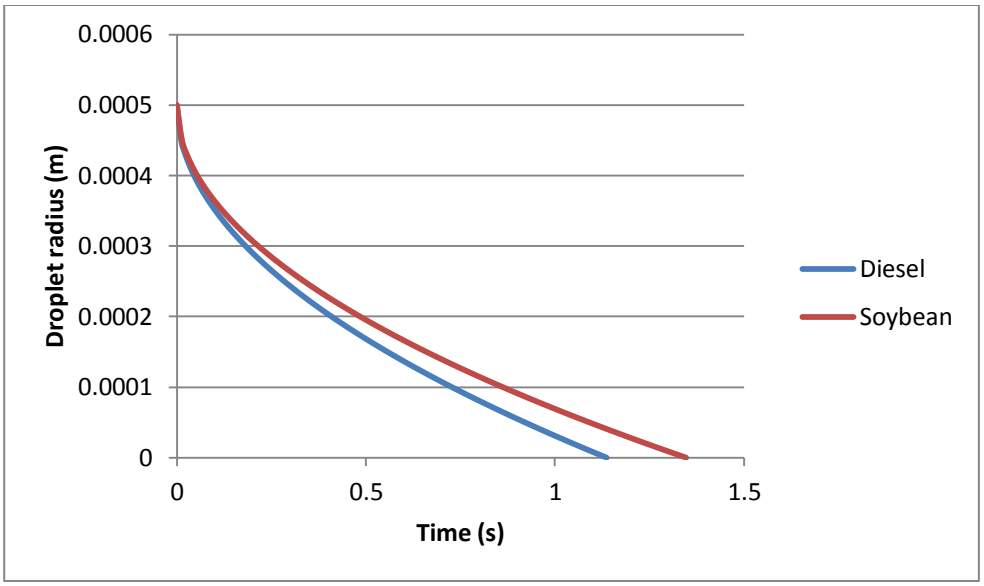

Figure 55: Droplet size through combustion lifetime at furnace temperature of 811 K

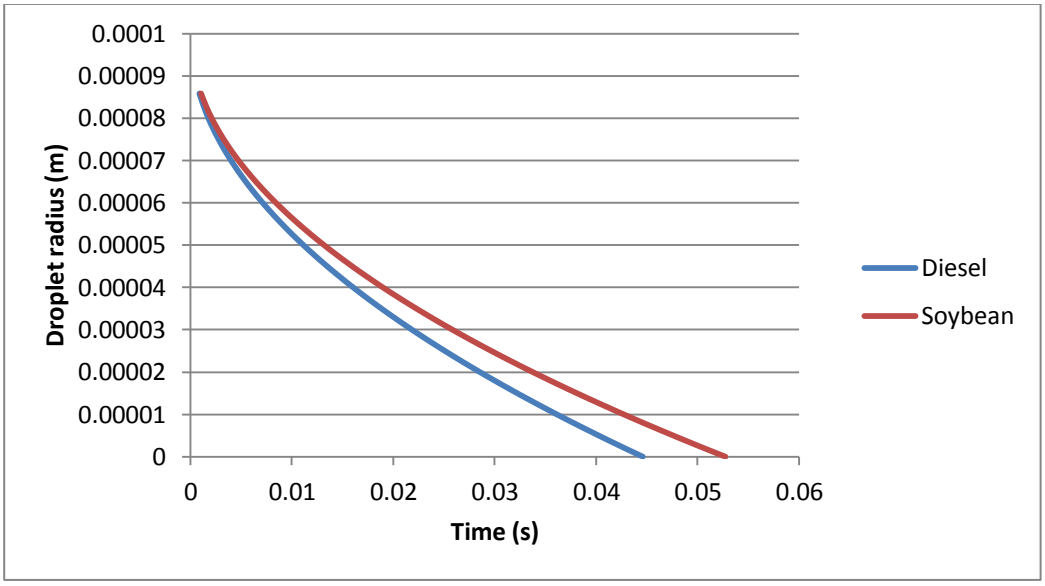

Figure 56: Droplet size through combustion lifetime at furnace temperature of 933 K

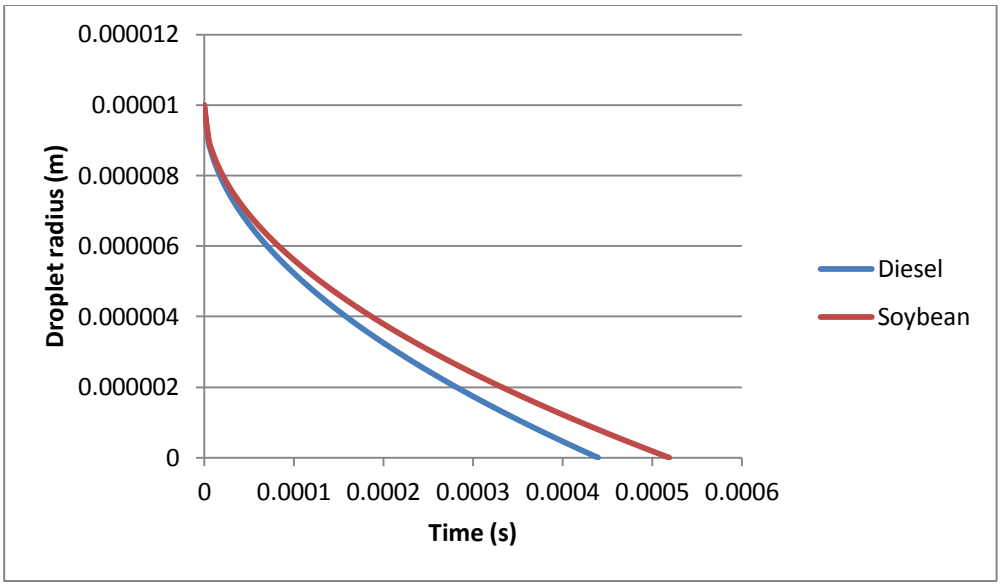

Figure 57: Droplet size through combustion lifetime at furnace temperature of 1033 K

6.6 Discussion

The results will now be discussed by figure:

Figure 46: Flame sheet radius linearly increasing with initial particle size is expected because a spherical flame sheet surrounding the fuel droplet is a model assumption. So as the droplet radius increases so must the flame sheet in order to encompass it.

Figure 47: The greater the fuel droplet mass, the greater the surface area of the drop, which will lead to faster fuel vaporization as well as a hotter flame temperature due to more fuel mass. The greater flame temperature will then lead to a faster droplet burn rate . Diesel is shown to burn at a greater rate as well as showing a greater increase with initial particle size which is also expected as diesel is a more volatile fuel than soybean oil.

Figure 48: The larger the droplet is at the beginning of combustion, the longer total droplet combustion time will take. Since diesel is a more volatile fuel it will combust faster than soybean oil. Soybean oil does have a higher flame temperature and latent heat of combustion, but the higher volatility of diesel leads to an overall faster burn.

Figure 49: This is expected as flame temperature is known to be dependent not only on fuel, but also on the temperature of the surrounding area where the combustion is occurring. Here soybean oil burns hotter than diesel oil, which is expected as denser fuels normally burn hotter. It should be noted that the flame temperature values of both fuels increase at the same rate, because flame temperature is only increasing due to the change in furnace temperature, which is completely independent of the fuel type.

Figure 50: This would be expected because as long as combustion is occurring, surface temperature will always be very close to the boiling temperature of the fuel regardless of any varying parameters. It is also expected that soybean oil has a higher surface temperature as it also has a higher boiling temperature.

Figure 51: This was expected as the fuel mass fraction at the droplet surface is essentially equal to the vapor pressure of the fuel and vapor pressure is dependent on temperature. It was expected that diesel would have a higher fuel mass fraction at the droplet surface as it is more volatile fuel than soybean oil.

Figure 52: It was not expected that flame sheet radius would vary with furnace temperature. This is because the ambient temperature will marginally cause the fuel to increase or decrease in size.

Figure 53: An increased furnace temperature increases the speed at which the fuel droplet vaporizes as well as increases the flame temperature. Both of these increases lead to a greater droplet burn rate. Diesel still has a larger droplet burn rate than soybean oil, but droplet burn rate is increasing at the same rate for both fuels as furnace temperature is a fuel independent property.

Figure 54: This is expected as an increased furnace temperature increases the speed at which the fuel droplet vaporizes as well as increases the flame temperature. Both of these increases lead to a smaller total droplet combustion time. Diesel still has a smaller total droplet combustion time than soybean oil, but the total droplet combustion time is decreasing at the same rate for both fuels as furnace temperature is a fuel independent property.

Figures 55-57: Again furnace temperature's effect on droplet combustion time is shown. At higher furnace temperatures droplet's decrease in size faster, due to a faster combustion process.

The combustion model generated has been concluded to produce accurate results. This is based on comparison with literature as well as the results all making sense physically. The results obtained here can be used with confidence in other parts of this thesis.

6.7 Conclusions

All pure droplet combustion model results make sense. Diesel is predicted to be a more volatile and faster burning fuel than soybean oil. The model used in this section can be used in further sections with confidence.

6.8 Nomenclature

A	Clausius-Clapeyron constant (m^2)
B	Clausius-Clapeyron constant (K)
$B_{o,q}$	Spalding Number
c_p	Specific heat $(kJ/kg * K)$
D	diameter of fuel droplet (m)
h_c	heat of combustion (kJ/kg)
h_{fg}	Latent heat of vaporization (kJ/kg)
k	Thermal conductivity $(kW/m * k)$
K	Combustion rate constant (m^2/s)
$\dot{m}_F$	Mass burning rate of the fuel (kg/s)
MW	Molecular weight
P	Pressure (Pa)
r	Radius (m)
R_u	Universal gas constant $(kJ/kmol * K)$
T	Temperature (K)
Y	Mass fraction
ρ	density (kg/m^3)
v	Oxidizer to fuel stoichiometric ratio

Subscripts

d	droplet
f	flame
F	Fuel
g	Gas
l	Liquid
Pr	Products
s	Surface
∞	Far removed from the surface
0	initial

6.9 References

[1] Godsave, G.A.E., "Studies of the Combustion of Drops in a Fuel Spray: The Burning of Single Drops of Fuel," *Fourth Symposium (International) on Combustion*, Willkiams & Wilkins, Baltimore, MD, pp 818-830, 1953.

[2] Spalding, D.B., "The Combustion of Liquid Fuels*," Fourth Symposium (International) on Combustion*, Williams & Wilkins, Baltimore, MD, pp 847-864, 1953.

[3] Turns, Stephen R. *An introduction to combustion*. Vol. 499. New York: McGraw-Hill, 1996.

[4] Law, C.K., and Williams, F.A., "Kinetics and Convection in the Combustion of Alkane Droplets," Combustion and Flame, 19(3): 393-406 (1972).

[5] Gunstone, Frank, ed. *Vegetable oils in food technology: composition, properties and uses*. Wiley. com, 2011.

[6] Sazhin, Sergei S. "Advanced models of fuel droplet heating and evaporation." *Progress in energy and combustion science* 32.2 (2006): 162-214.

[7] Pharos Hammond, Earl G., et al. "Soybean oil." *Bailey's Industrial Oil and Fat Products* (2005): 577-672.

[8] "Triglyceride Molecular Weight Calculator » Biodiesel Fuel Education Program." *Biodiesel Fuel Education Program*. N.p., 2013. Web. 17 June 2013.

CHAPTER 7 - SOLID PARTICLE COMBUSTION MODELING

7.1 Introduction

This next chapter will explore the basics of solid particulate fuel combustion, specifically focusing on coal and wood. It should be noted that the equations used hear are general enough to be used for many different types of solid fuels. Coal and wood were chosen due to their familiarity and abundance.

The combustion of a solid fuel can be broken down into many steps, these steps differing based on the exact solid fuel used. Because of this a simple linear model will be chosen consisting of following steps: Drying, devolatilization, combustion of the volatiles, and combustion of char.

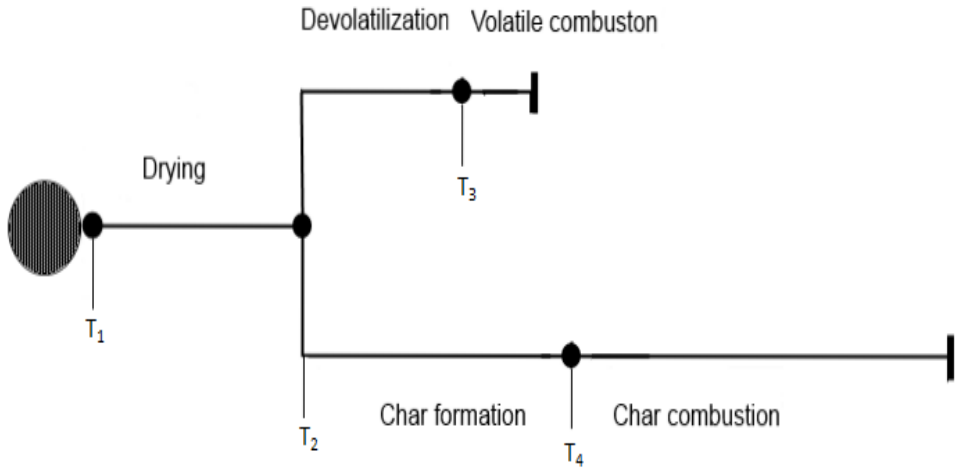

Figure 58: Linear model of solid combustion

For this combustion model, the solid particles will not be assumed to be pre-dried, they are injected into the furnace with their normal moisture content. Drying will begin as soon as the surface particle temperature is above that of the boiling temperature of water, at the furnace conditions. This temperature is represented as T_1. At some time t, the particle temperature will reach T_2. It is at this temperature and

time that devolatilization/combustion of the volatiles begins simultaneously with char formation. Char is the carbon heavy portion of coal after the moisture and the volatile portions have vaporized. It is important to note that the char formation step continues during the volatile combustion step because some volatiles will combust before complete devolatilization of the particle is reached. After the volatiles have combusted, at some time t and temperature T_3, the char will undergo combustion. This step is the most energy dense as well as the longest step of the solid combustion process. The following figure shows the general make up of a solid fuel particle.

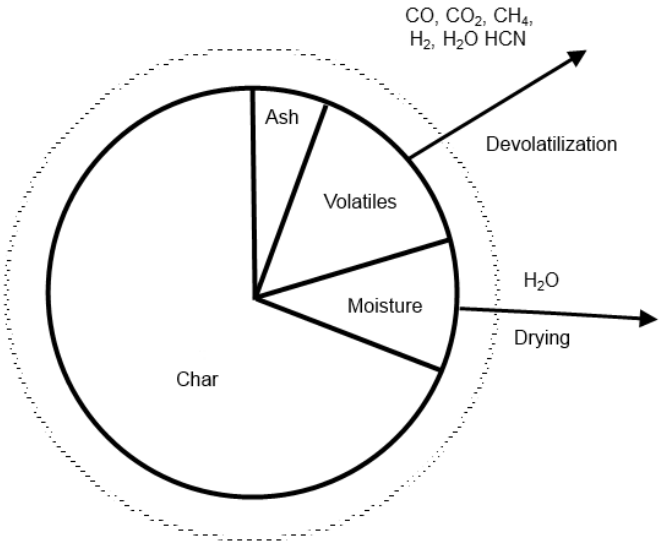

Figure 59: Breakdown of general carbon and hydrocarbon solid fuel

7.2 Modeling Assumptions

The model chosen to represent combustion has been briefly discussed. In the following section a more in depth look will be taken into each step. First a list of assumptions will be made.

1.) Drying will begin when the temperature of the particle reaches that of the boiling temperature of the water residing inside and on it

2.) Moisture consists mostly of free water, therefore drying of bound water will be neglected
3.) The particles are so small that a concentration of water within the particle is constant throughout
4.) Drying of free water will be modeled at a constant rate
5.) The majority of the drying process will end at around the time heavy devolatilization begins
6.) All heat transfer due to air flow will be assumed to be natural convection, low Reynolds number
7.) Char combustion rate is diffusion limited

7.2.1 Drying

When the particles are injected into the furnace, they will lose a majority of their moisture content due to the natural convection flow of the air, or other oxygen containing gas. The particle will have free water, which is bound via Van der Walls forces as well as bound water which is bound chemically to other molecules. As said in the assumptions, this model will focus on the evaporation of the free water. This is because the free water makes up the majority of the water content in coal and wood. Also the free water evaporates much easier than the bound water. What ends up occurring during the drying stage, is all the free water will evaporate and during the rest of the combustion process the bound water will slowly evaporate. With that in mind, the model for the drying of the free water will be presented.

It is important to note that the drying process will occur and be completed before the solid particle reaches its highest temperatures. For example an average ambient furnace temperature is 1000 K. As the particle heats up to this temperature it will undergo this drying step automatically, starting when the particle temperature reaches 373 K and ending well before it gets to 1000 K.

The drying rate can be defined as [1]:

$$\boldsymbol{R = -\frac{m_S}{A}\frac{dX}{dt}} \quad \textbf{(7.1)}$$

Where m_S is the mass of the solid, X is the moisture percent, A is the surface area of the solid and t is time. This equation when rearranged and integrated over the time interval for drying of X_1at $t_1 = 0$ to X_2 at $t_2 = t$ [1]:

$$\boldsymbol{t = \int_{t_1=0}^{t_2=t} dt = \frac{m_s}{A}\int_{X_2}^{X_1}\frac{dX}{R}} \quad \textbf{(7.2)}$$

The drying is assumed to be at a constant rate, so that both $X_1$and X_2 are greater than the critical moisture content X_C and $R = constant = R_C$. Integration of equation 7.2 for the constant-rate period gives [1]:

$$\boldsymbol{t = \frac{m_s}{AR_c}(X_1 - X_2)} \quad \textbf{(7.3)}$$

R_c is represented by [1]:

$$\boldsymbol{R_c = \frac{q}{A\lambda_w} = \frac{h(T_\infty - T_s)}{\lambda_w}} \quad \textbf{(7.4)}$$

Where q is heat, λ_w is the latent heat of vaporization of water, h is the heat transfer coefficient, T is the temperature of the furnace and T_s is the temperature of the solid. The heat transfer coefficient is made up of a conduction term, a convection term and a radiation term. In this environment heat transfer due to conduction will be assumed to

be negligible, leaving convection and radiation. The heat transfer coefficient for convection of an object being dried by flowing air will be represented by [1]:

$$\boldsymbol{h_c = 0.0204G^{0.8}} \quad \textbf{(7.5)}$$

where G is the mass velocity in $kg/h * m^2$ and should be assumed to be at natural convection flow rates. For radiation h is represented as [1]:

$$\boldsymbol{h_R = \varepsilon(5.676)\frac{\left(\frac{T_\infty}{100}\right)^4 - \left(\frac{T_S}{100}\right)^4}{T_\infty - T_S}} \quad \textbf{(7.6)}$$

Where ε is the emissivity of the solid. Equations 7.5 and 7.6 can be combined with equation 7.3 to give [1]:

$$\boldsymbol{t = \frac{m_s \lambda_w (X_1 - X_2)}{A(h_c + h_r)(T_\infty - T_s)}} \quad \textbf{(7.7)}$$

7.2.2 Devolatilization

Once the solid completes the drying phase and begins to approach the furnace temperature, heavy devolatilization will occur. To a small extent it is happening during drying, but this will be negated due to the majority of devolatilization occurring after drying has completed. Devolatilization is dependent on the solid species being combusted, porosity, size and temperature to name a few of the more important variables. Because wood and coal are so variable even within their own species, the devolatilization phase can become an extremely complicated process to model. With that in mind a simple, yet common approach based on reaction kinetics and the Arrhenius Law was taken to model both the release and the combustion of the volatiles [6]:

$$\boldsymbol{\frac{dV}{dt} = k(V_i - V)} \quad \textbf{(7.8)}$$

Where V_i is the maximum volatile mass in the solid and V is the current volatile mass. k is the rate constant and is expressed as:

$$\boldsymbol{k = A_0 e^{\left(-\frac{E_a}{RT}\right)}} \quad \textbf{(7.9)}$$

Where E_a is the activation energy, R is the universal gas constant, T is temperature and A_0 is the pre-exponential factor. Substitution of equation 7.9 into equation 7.10 and integration gives:

$$\boldsymbol{t = \frac{\ln\left(\frac{V}{V_i}\right)}{-k}} \quad \textbf{(7.10)}$$

The advantage of using this method is its simplicity. The disadvantage is that only temperature variance can be accurately accounted for. A_0 and E_a are specific values for specific solid fuels with certain characteristics. As long as the model stays within these parameters, it should remain accurate. A table of the kinetic parameters used is presented below [6]:

Table 64: Kinetic parameters used for devolatilization modeling [6]

Species	$A_0\ (s^{-1})$	$E_a\ \left(\frac{kJ}{mol}\right)$
Lignite coal	280	47.3
Bituminous coal	700	49.4
Anthracite	617	114
Wood	$7 * 10^7$	129.7

7.2.3 Char Combustion

Once the volatiles have vacated the solid, all that will remain is a solid is mostly made up of carbon, also known as char. As said before, it is this substance that contains the most energy of the combustion process as well as having the longest

combustion time. To begin with, the major reactions of char combustion will be presented:

$$\boldsymbol{C + \frac{1}{2}O_2 \rightarrow CO} \quad \textbf{(7.11)}$$

$$\boldsymbol{C + O_2 \rightarrow CO_2} \quad \textbf{(7.12)}$$

$$\boldsymbol{C + H_2O \rightarrow CO + H_2} \quad \textbf{(7.13)}$$

The first reaction, the creation of carbon monoxide, conditions the process of char combustion. The following expression shows the rate of char combustion versus. time [6]:

$$\boldsymbol{\frac{dm_c}{dt} = -\frac{kAM_C}{M_O}p_{O_2}^S} \quad \textbf{(7.14)}$$

Where m_c is the mass of the char, k is the reaction rate, $p_{O_2}^S$ is the parital pressure of oxygen at the surface of the particle , M_C is the molar mass of carbon and M_O is the molar mass of oxygen. In stationary conditions, the oxygen diffused from the gas phase to the particle surface is equal to that the oxygen consumed through the chemical reaction at the surface, leading to [6] :

$$\boldsymbol{\frac{k}{M_O}p_{O_2}^S = \frac{k_c}{RT}\left(p_{O_2} - p_{O_2}^S\right)} \quad \textbf{(7.15)}$$

k_c is the coefficient of transfer of material which normally is found in conjunction with the Sherwood number. At low Reynolds numbers $k_c = \frac{2D}{d}$. Then if equation 7.15 is resolved with respect to $p_{O_2}^S$ [6]:

$$\boldsymbol{p_{O_2}^S = \frac{\left(\frac{2D}{dRT}\right)p_{O_2}}{\frac{k}{M_O}+\frac{2D}{dRT}}} \quad \textbf{(7.16)}$$

Substituting equation 7.16 into equation 7.14 gives [6]:

$$\boldsymbol{\frac{dm_c}{dt} = -k\pi d^2\frac{M_C}{M_O}\frac{\left(\frac{2D}{dRT}\right)p_{O_2}}{\frac{k}{M_O}+\frac{2D}{dRT}}} \quad \textbf{(7.17)}$$

In order to be able to integrate this equation to find the time of char combustion a relationship must be expressed between the diameter of the char and the mass. This can be done by assuming the onion model, in that the combustion process is occurring at the particle surface only, and the density of the particle is constant. Then the following to relationships can be made [6]:

$$\boldsymbol{m_c = \frac{\pi d^3 \rho_c}{6}\ , d = \left(\frac{6m_c}{\pi \rho_c}\right)^{\frac{1}{3}}} \quad \textbf{(7.18)}$$

With this relationship and assuming that the char combustion process is diffusion limited equation 7.17 can be written as [6]:

$$\boldsymbol{\frac{dm_c}{dt} = -2\pi \left(\frac{6m_c}{\pi \rho_c}\right)^{\frac{1}{3}} M_C \frac{Dp_{O_2}}{RT}} \quad \textbf{(7.19)}$$

Integration of equation 7.19 gives [6]:

$$\boldsymbol{t = 0.785 \frac{\rho_c d_0^2}{Dp_{O_2}} \frac{RT}{M_C}} \quad \textbf{(7.20)}$$

7.3 Physical Properties

Unlike in the liquid combustion chapter, there are no methods behind any physical property parameters that need to be explained. All properties were gathered from various literature sources [1][3][4][5][6]. A table of the properties follows.

Table 65: Parameters for solid particle combustion

Drying		**Drying**	
$T_{evap}(K)$	273	$T_{evap}\ (K)$	273
$\rho_{particle,wet}\ (g/m\text{^}3)$	1500000	$\rho_{particle,wet}\ (g/m\text{^}3)$	551200
$velocity_{air}\ (m/h)$	0.65	$velocity_{air}\ (m/h)$	0.65
$\lambda_{water}\ (J/g)$	2270	$\lambda_{water}\ (J/g)$	2270
$\%\ moisture$	5.485714	$\%\ moisture$	30

$h_c\ (W/m\text{^}2 * k)$	1261.345	$h_c\ (W/m\text{^}2 * k)$	566.2500063
ε_solid	0.95	ε_solid	0.95
Devolatilization		**Devolatilization**	
$A_0\ (1/s)$	617	$A\_0\ (1/s)$	70000000
$E\ (kJ/mol)$	114	$E\ (KJ/mol)$	129.7
$R\ (kJ/mol * K)$	8314.46	$R\ (KJ/mol * K)$	8314.46
$\rho\ (kg/m\text{^}3)$	1421.993	$\rho_{dry}\ (kg/m\text{^}3)$	424
$\%\ char$	0.845571	$\%\ char$	0.195
$\%\ ash$	0.110286	$\%\ ash$	0.01
$\%\ volatile$	0.044143	$\%\ volatile$	0.795
Char		**Char**	
$M_C\ (kg/kmol)$	12.0107	$M_C\ (kg/kmol)$	12.0107
$R\ (kJ/kmol * K)$	8.31446	$R\ (KJ/mol * K)$	8.31446
$P_{o2}\ (kPa)$	21.27825	$P_{o2}\ (kPa)$	21.27825
$\rho_c\ (kg/m\text{^}3)$	1202.397	$\rho_c\ (kg/m\text{^}3)$	82.68

7.4 Model Results

The following section will detail the results of the model explained above when varying the two controllable variables, initial particle droplet size and furnace temperature for both Pennsylvania coal and white pine wood. The first set of graphs are the results of maintaining constant drying and furnace temperatures of 500 K and 1033 K while varying the initial droplet radius from 50 μm to 200 μm. Droplet sizes are optimum size range taken from the literature that have historically provided good flow and combustion properties. Figure 60 shows that the drying temperature will increase with initial particle size.

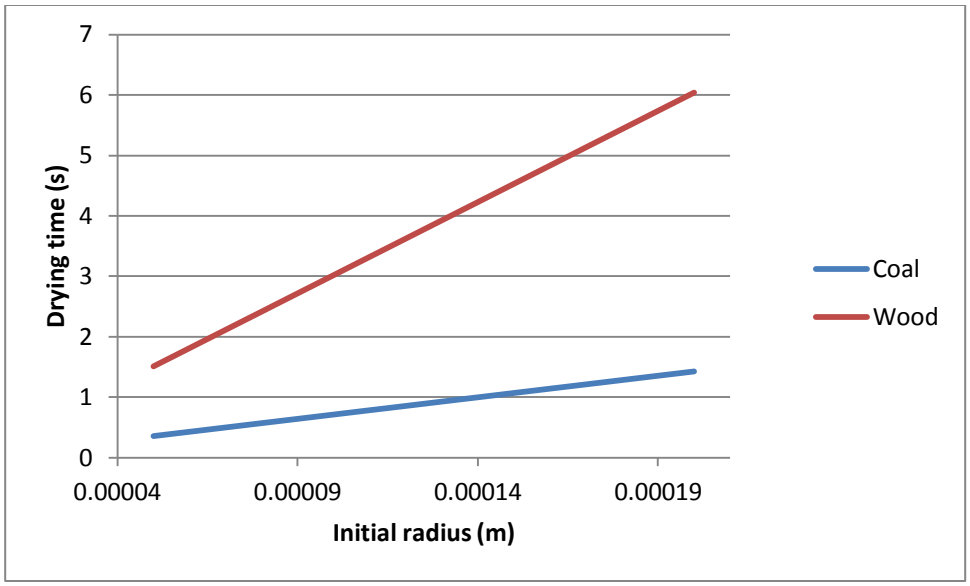

Figure 60: Time to dry a solid particle while varying the initial particle size at a furnace temperature of 933 K

Figure 61 shows the devolatilization time for coal and wood increases with initial particle size. The wood devolatilization times had to be represented on a separate figure due to the dramatic difference in devolatilization times.

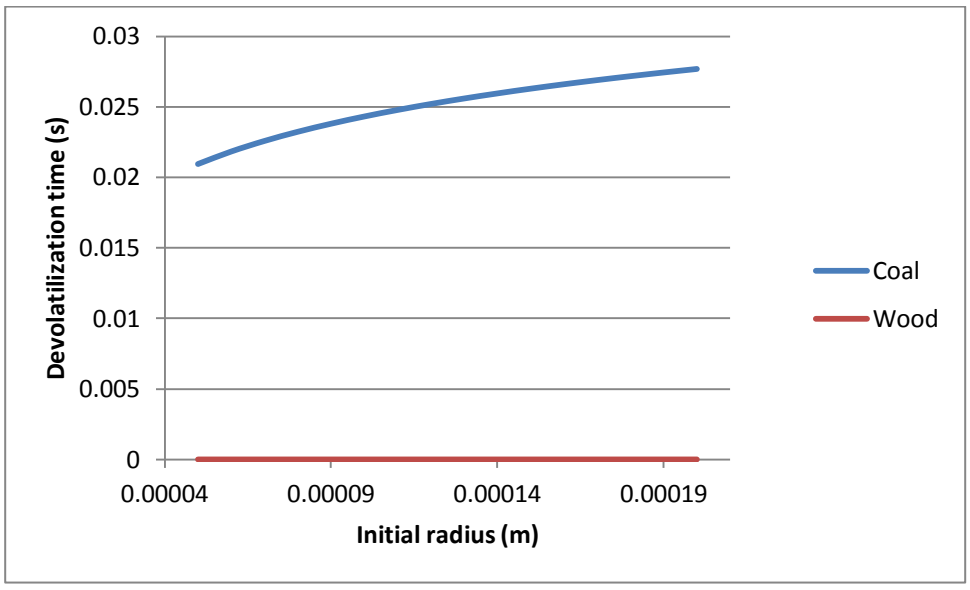

Figure 61: Devolatilization time for coal and wood while varying the initial particle size at a furnace temperature of 933 K

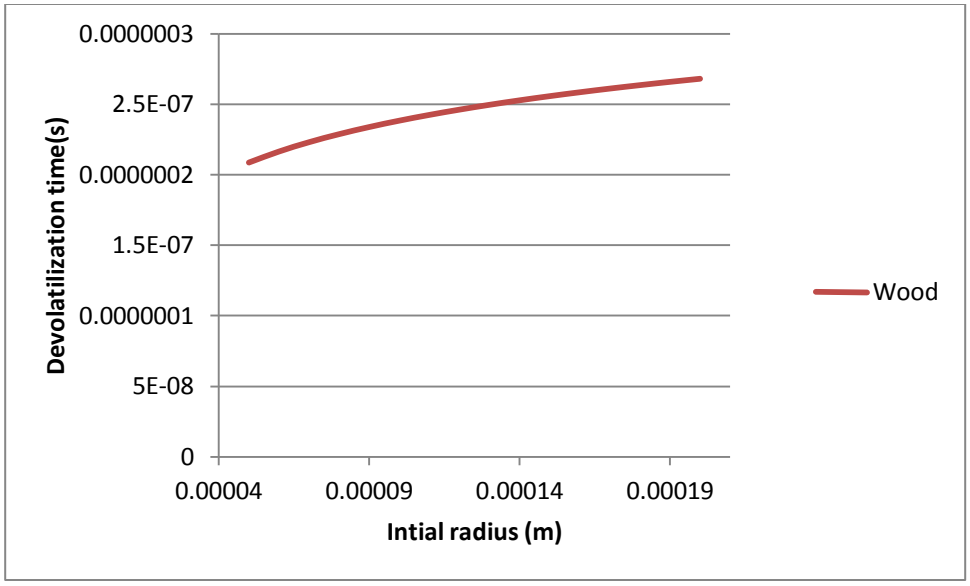

Figure 62: Devolatilization time wood while varying the initial particle size at a furnace temperature of 933 K

Figure 63 shows the char combustion time for both solid fuels increasing non-linearly as initial droplet size increases.

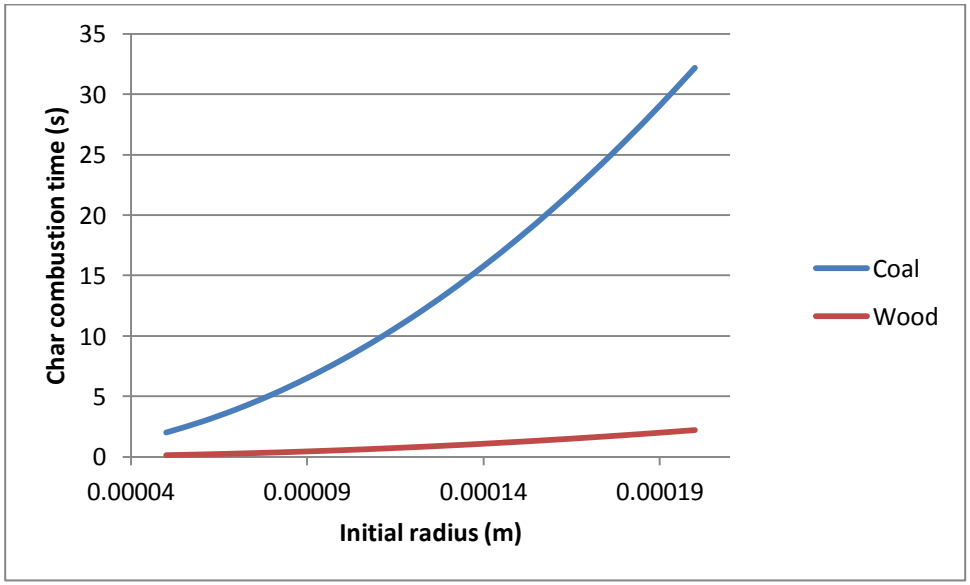

Figure 63: Char combustion time for coal and wood while varying the initial particle size at a furnace temperature of 933 K

Figure 64 shows the total combustion time for both solid fuels.

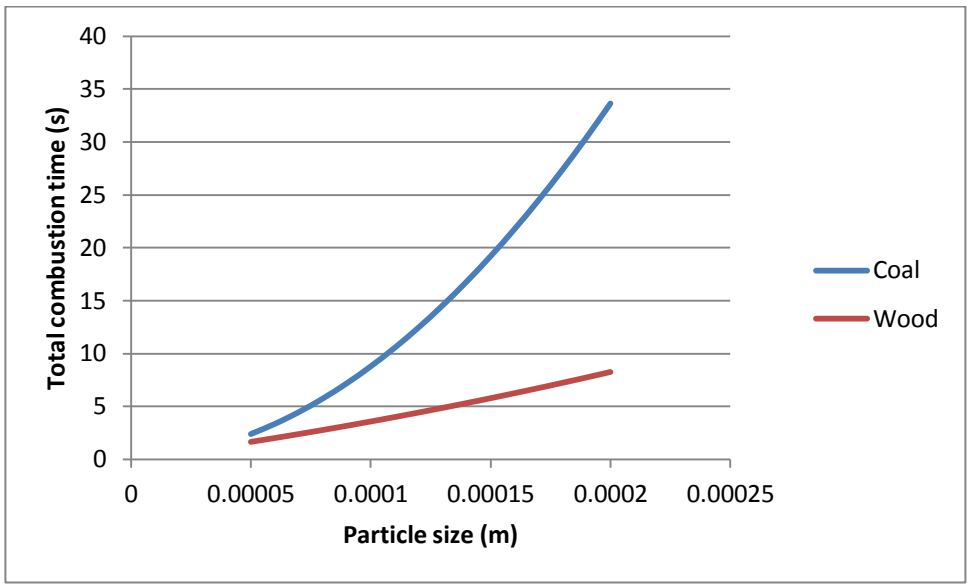

Figure 64: Total combustion time for coal and wood while varying the initial particle size at a furnace temperature of 933 K

Figures 65 and 66 show how furnace temperature can affect combustion.

Figure 65 shows that an increase in furnace temperature results in a decrease in drying time for both solids.

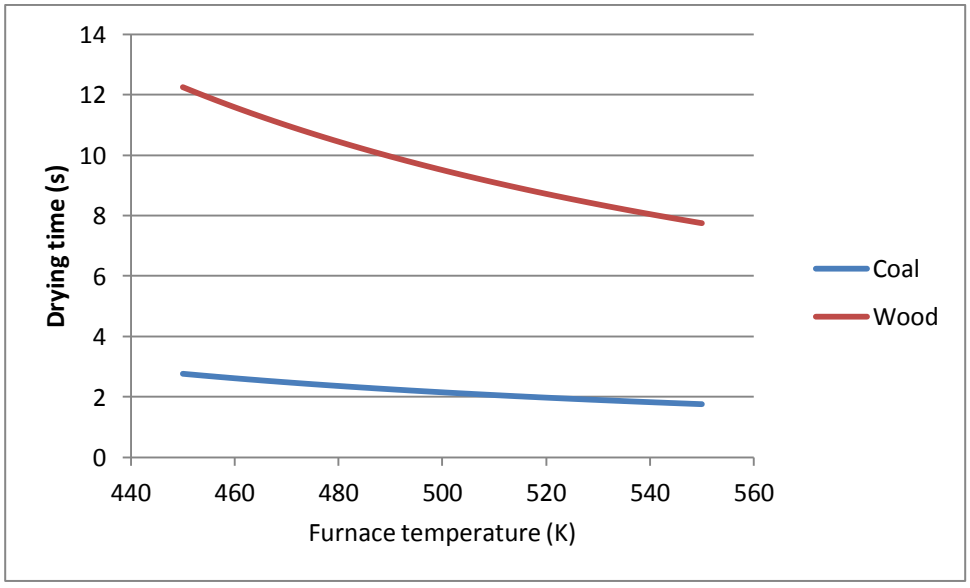

Figure 65: Drying time for coal and wood while varying the furnace temperature for solid fuel particle diameters of 0.0001 m

The furnace temperature range was too small to have noticeable any effect on devolatilization time, therefore graphical results are not shown. Figure 66 shows that increasing the temperature does decrease char combustion time for both solid fuels, but not by very much and the change is almost negligible for wood.

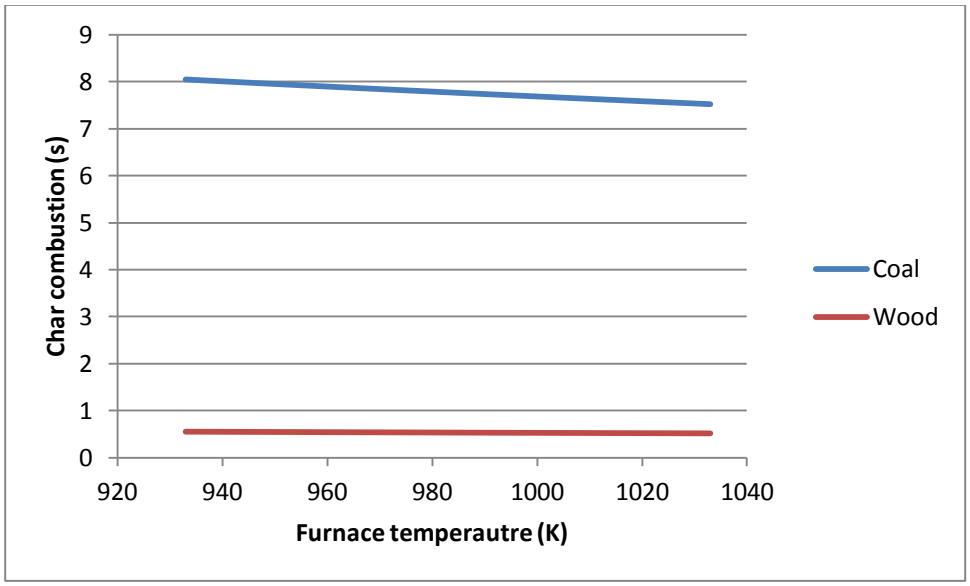

Figure 66: Char combustion time for coal and wood while varying the furnace temperature for solid fuel particle diameters of 0.0001 m

The following figures are the initial linear model representing solid combustion, except with temperature and time ranges added. Figure 67 shows the average temperatures of each step. Wood and coal are considered to undergo combustion at relatively similar temperatures at each step, so only one figure will be used to represent both fuels. The temperature range is due to the varying initial particle size range that can be used.

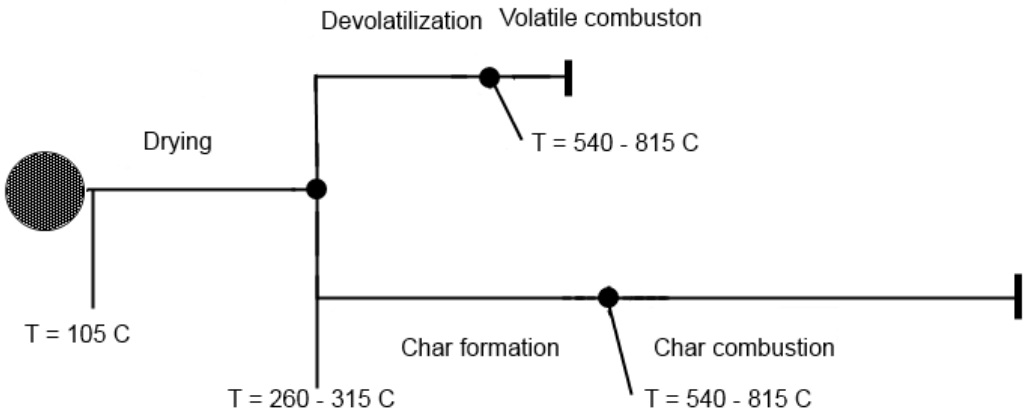

Figure 67: Liner combustion model with temperatures (coal and wood)

The next two figures are the linear model with times added, for both coal and wood. As the times vary considerably, two separate figures are needed. The time ranges are due to the initial particle size range and steady state combustion chamber temperature range.

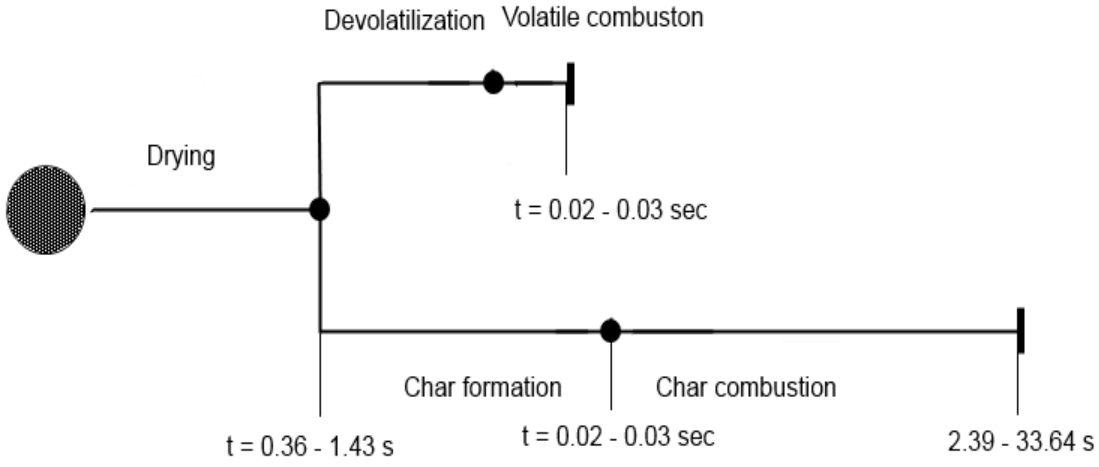

Figure 68: Liner combustion model with times (coal)

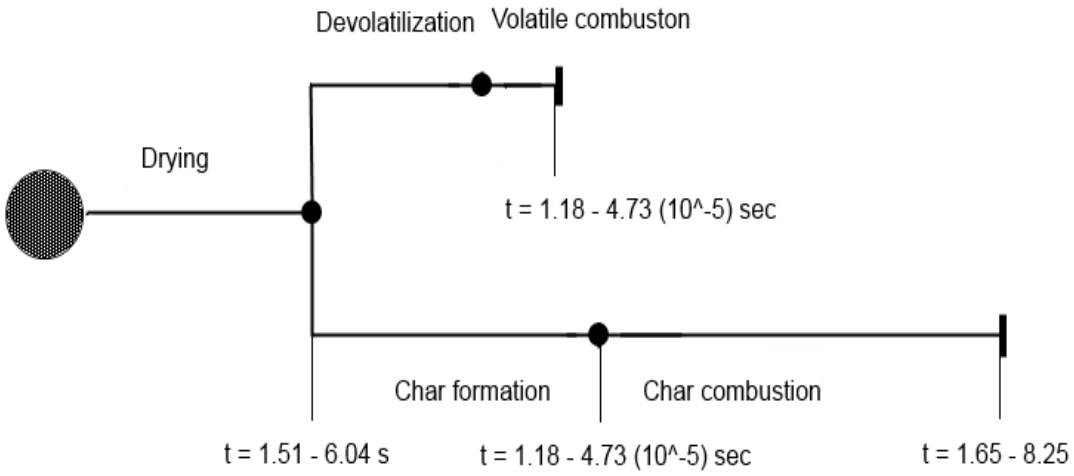

Figure 69: Liner combustion model with times (wood)

7.5 Discussion

The drying time of wood is expected to be slower than coal because wood has a much higher moisture content. Coal having a much longer char combustion time than wood is due to the fact that the majority of coal's mass is due to char. It was also interesting to note that coal started to see much larger increases in combustion time with increase in particle size over wood. Because of these results, if coal was being used as the solid in a solid-liquid fuel, the particle size range should be kept small. Wood on the other hand has a much greater particle range that can be used. Furnace temperature was seen to decrease both drying time and char combustion time for coal and wood. This would make sense as both of these process are temperature dependent. Wood drying time and coal char combustion time are influenced more heavily by the furnace temperature. In both of these cases sense the is believed to be a percentage decrease predicted by the model.

From the model results it is clear that in all combustion steps, increasing initial particle size will increase the overall combustion time and increasing the furnace

temperature will decrease the overall combustion time. Of the two controllable variables, particle size has more influence on rate, especially in the char combustion step. Because of these results, the smallest particle size that can be used should be used, due to the how long combustion begins to take as the particle sizes increase. Furnace temperature, can be controlled to further streamline the combustion process, but as long as the temperature is within the general accepted combustion furnace range (933-1033 K) combustion will occur at a fast enough rate. Wood seems to be a better choice when it comes to combustion time, as it is much faster than coal. This difference is noticeably smaller as the particles sizes are decreased.\

7.6 Conclusions

All solid combustion model results make sense. Wood has a faster char combustion time and slower volatile combustion time than coal due to wood having more volatiles than anthracite coal. The model used in this section can be used in further sections with confidence.

7.7 Nomenclature

Drying

A	Surface area of the solid (m^2)
G	Mass velocity ($kg/h * m^2$)
h	Heat transfer coefficient (W/m^2K)
h_c	Convection heat transfer coefficient (W/m^2K)
h_R	Raditation heat transfer coefficient (W/m^2K)
m_S	Mass of the solid (g)
q	Heat (J)

R	Drying rate (g/m^2s)
R_C	Constant drying rate (g/m^2s)
t	Time (s)
T	Temperature (K)
T	Temperature of the solid
T	Temperature of the furnace
X	Moisture percent
X_C	Critical moisture content
ε	Emissivity of the solid
λ_w	Latent heat of vaporization of water

Devolatilization

A	Surface area of the solid (m^2)
A_0	Pre-exponential factor $\left(\frac{1}{s}\right)$
E_a	Activation energy (kJ/mol)
k	Rate constant ($1/s$)
t	Time (s)
T	Temperature (K)
V	Volatile mass in the solid (kg)
V_i	Maximum volatile mass in the solid (kg)

Char combustion

k_c	Coefficient of transfer of material

m_c	Mass of char (kg)
M_C	Molar mass of carbon and $(kg/kmol)$
M_O	Molar mass of oxygen $(kg/kmol)$
p_{O_2}	Partial pressure of oxygen at infinity (kPa)
$p_{O_2}^S$	Partial pressure of oxygen at the surface of the particle (kPa)
R_U	Universal gas constant $(kJ/kmol * K)$
t	Time (s)
T	Temperature (K)
ρ_c	Density of char (kg/m^3)

7.8 References

[1] Geankoplis, Christie J. *Solutions Manual to Accompany Transport Processes and Separation Process Principles:(includes Unit Operations)*. Prentice Hall Professional Technical Reference, 2003.

[2] Rossberg, Manfred, et al. "Chlorinated hydrocarbons. Ullmann's encyclopedia of industrial chemistry." (2003).

[3] "Engineering ToolBox." *Engineering ToolBox*. N.p., n.d. Web. 5 Apr. 2013.

[4] Allen J. Johnson & George H. Auth, *Fuels and Combustion Handbook*, First ed., McGraw-Hill, New York, 1951

[5] "List and Values of Wood Fuel Parameters - Part 3." *Woodenergy.ie*. N.p., n.d. Web. 22 Jan. 2011. <http://www.woodenergy.ie/woodasafuel/listandvaluesofwoodfuelparameters-part3/>.

[6] Turns, Stephen R. *An introduction to combustion*. Vol. 499. New York: McGraw-Hill, 1997.

CHAPTER 8 - EMULSION DROPLET COMBUSTION MODELING

8.1 Introduction

This section will detail the method used to create the model of the emulsion combustion process. As with the other modeling sections, a list of assumptions must be made to simplify calculations. The list used for the emulsion combustion model have similarities to that of pure component combustion.

8.2 Physical Model Description

The following is the list of assumptions:

10.) The burning droplet is surrounded by a spherically symmetric flame and exists in a quiescent, infinite medium

11.) The effects of convection are ignored. Radiation heat transfer is negligible

12.) The fuel is a two component liquid with zero solubility for gases

13.) Pressure is constant at 1 atmosphere

14.) The gas phase consists of 4 species: Fuel vapor, oxidizer, water vapor and combustion products

15.) Fuel and oxidizer are assumed to react in stoichiometric proportions to the flame, while the chemical kinetics are so fast the flame is idealized as an infinitesimally thin sheet

16.) The Lewis number is assumed to be 1

17.) The gas phase thermal conductivity, specific heat and density are all constants. (k_g, C_{pg}, ρ)

18.) The liquid emulsion droplet is the only condensed phase

19.) The water and fuel emulsion is well mixed

20.) Vaporization occurs at the surface of the droplet

21.) The fractional vaporization rate of water and fuel will assumed to be equal to the initial liquid mass fraction of each component, and therefore constant or $\varepsilon_i = Y_{il}$

Because the conditions are very similar to pure liquid combustion, the emulsion droplet combustion process will be very similar to pure component combustion. The main differences are the liquid fuel composition and the vaporization process of the two components. There are two major modes that could be used to model the vaporization process, the distillation mode and the frozen steady depletion mode. [1][2]

In the distillation mode, components will vaporize at the surface at a rate dependent of their specific volatilities and independent of each other. The components also travel to the surface of the droplet quickly through convection. This mode normally leads to the more volatile component vaporizing first, causing a period of time where both components are vaporizing and a period of time where only the least volatile component is left vaporizing. In this case, water being more volatile, will vaporize before the fuel, in most cases bypassing of the micro-explosion phenomenon. [1][2]

For this thesis, the vaporization process chosen was the frozen steady depletion mode. In this mode, a component can only vaporize once the droplet surface has regressed to where it is located within the droplet because the components will not be moving within the droplet. Because the mixture being vaporized is an emulsion and is

assumed to be well mixed, the surface will always have a constant amount of both fuel and water being vaporized at any time. This allows for both realistic model results as well as more simplified calculations than the distillation mode would require. [1][2]

The same general model and theory will be used in emulsion combustion as pure fuel combustion. Because of this, most of the figures and explanations given in the pure liquid combustion chapter still hold true and will not be repeated. If needed please refer back to pure fuel combustion for these omitted references. The physical drop model will be shown below.

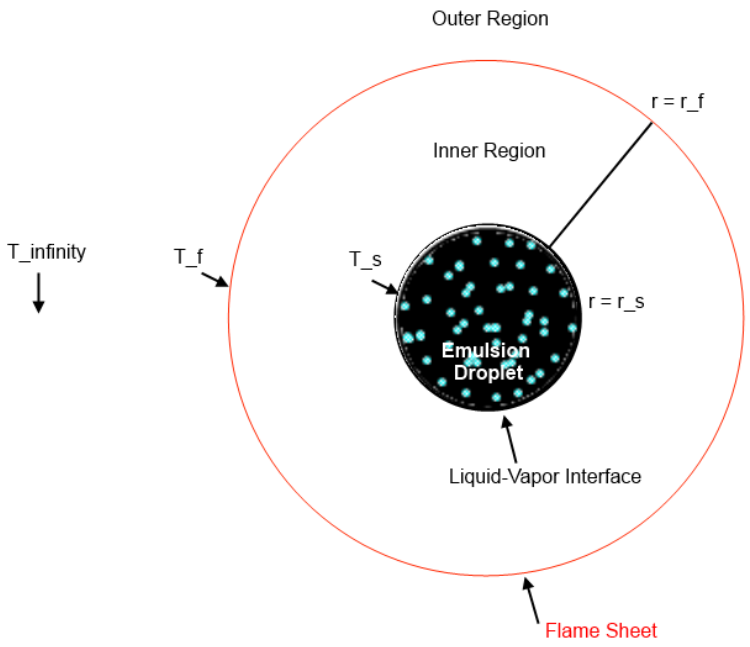

Figure 70: Physical model of emulsion droplet

8.3 Model Equations

The theory behind the modeling equations is as follows. The vaporization mode being the frozen steady depletion mode is key in understanding the theory used. To reiterate what has already been mentioned, the main aspect of the frozen mode is

that at any given time vaporization is occurring, $\varepsilon_i = Y_{il}$. This combined with the assumption that the emulsion will come into the furnace well mixed, means the surface will always have the same concentration as the body of the emulsion droplet, so $\varepsilon_i = Y_{il,s} = Y_{il} = Y_{il,0}$. Therefore the components of the emulsion are always vaporizing at a constant rate allowing the composition of the droplet to also be constant throughout the entire combustion process. Because the composition of the emulsion will be constant, it allows the same theory and equations to be used that were used previously in pure fuel combustion as long as the appropriate weighting factors are used.

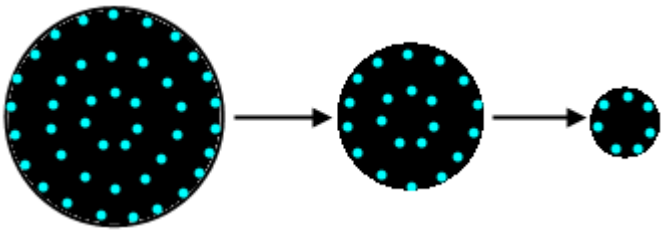

Figure 71: Emulsion droplet maintain surface concentration throughout vaporization

The majority of the combustion properties being solved for are dependent on parameters that are in turn dependent upon what fuel is being used and at what temperature it is. These combustion properties include $A, B, B_{o,q}, r_f, T_s$, and T_f. As was explained in the pure fuel combustion chapter, the parameters used to solve for these combustion properties are in reality not constant, but to ease calculations without sacrificing accuracy, constant average parameters were used. Obtaining constant parameters while using the distillation mode of vaporization would prove difficult because the emulsion concentration would always be changing. But because the frozen steady depletion mode is being used, the emulsion concentration is constant throughout the entire process, just like it was for the pure fuel combustion modeling,

so constant average parameters can be found. Because constant parameter values are being used, the six combustion variables can be found using very similar equations to what was used in pure fuel combustion, as long as the parameters are solved for using the correct weighting values which are solely dependent on the concentration of the components in the emulsion droplet and in some cases the surrounding temperature. This idea is seen in Law's papers as the equations used are actually the same equations used by Turns for pure fuel combustion, so this idea would seem to be valid. Also it allows the base property values already found for diesel and soybean oil to be used, instead of using similar, well defined substitutes such as hexadecane and dodecane as Law did [1][2][3].

There are two combustion variables being solved for that require further explanation; the emulsion droplet burning rate constant and the total droplet combustion time. Total droplet combustion time is dependent on the emulsion droplet burning rate and emulsion droplet burning rate is dependent on the vaporization rate of the components within the emulsion. Law and Williams [4] present the following correlation for burning rate of the fuel, $\dot{m}_f$, to the burning rate of the emulsion $\dot{m}_{emulsion}$:

$$\dot{\boldsymbol{m}}_{\boldsymbol{f,emulsion}} = \boldsymbol{\varepsilon_i}\dot{\boldsymbol{m}}_{\boldsymbol{f}} \tag{8.1}$$

And

$$\boldsymbol{\varepsilon_i} = \boldsymbol{Y_{is,l}} \tag{8.2}$$

Using these 2 equations along with our previous assumptions of constant vaporization rates we can get:

$$\dot{m}_{f,emulsion} = \varepsilon_{fuel}\dot{m}_f + \varepsilon_{water}\dot{m}_f = Y_{fl,0}\dot{m}_f + Y_{wl,0}\dot{m}_f \quad \textbf{(8.3)}$$

The vaporization fractions are equivalent to the mass fractions, so the emulsion droplet burning rate and therefore total droplet combustion time can be found by using the same equations as were used for pure fuel combustion as long as the initial mass fraction of the emulsion components are known.

Because it has been shown that the same model equations will work for both pure fuel and emulsion combustion, the equations and the theory behind how they were found, will be omitted from this section as they have already been explained extensively.

8.4 Initial Calculation Parameters

The parameter equations for emulsion combustion are dependent on the mass fraction of the emulsion droplet and are as follows. Because a lot of the parameters are temperature dependent which itself is emulsion concentration dependent, the temperature equations will be shown first.

For all liquid parameters the following equations are used [1][2][3]:

$$T = \frac{(T_0 + T_s)}{2} \quad \textbf{(8.4)}$$

$$T_s = \varepsilon_{fuel}T_{bp,fuel} + \varepsilon_{water}T_{bp,water} \quad \textbf{(8.5)}$$

For all gas parameters the following equation are used [3]:

$$T = \frac{(T_s + T_f)}{2} \quad \textbf{(8.6)}$$

T_f is again estimated to be 2200 K.

c_{pl} for soybean oil was found using the following [4]:

$$\boldsymbol{c_{pl}\,(kJ/kg*K) = \ 1.8583 + 0.0024T} \tag{8.7}$$

c_{pl} for diesel was found using the following equation [5]:

$$\boldsymbol{c_{pl}\,(kJ/kg*K) = \frac{(264+6.33T-0.00296T^2)}{1000}} \tag{8.8}$$

c_{pl} for water was found using the following equation [6]:

$$\boldsymbol{c_{pl}\,(kJ/kg*K) = 9*10^{-6}*T^2 - 0.0052*T + 4.9666} \tag{8.9}$$

Then for the emulsion c_{pl}:

$$\boldsymbol{c_{pl,emulsion}\ \left(\frac{kJ}{kg}*K\right) = c_{pl,fuel}*\varepsilon_{fuel} + c_{pl,water}*\varepsilon_{water}} \tag{8.10}$$

The liquid density, ρ_l, of soybean oil was found by taking the density value at 293 K and the $\frac{d\rho_l}{dt}$ value and using them in the following equation [7]:

$$\boldsymbol{\rho_l\ \left(\frac{kg}{m^3}\right) = \rho_{l,293\ K} + \frac{d\rho_l}{dt}(T-293)} \tag{8.11}$$

The ρ_l for diesel was found using the following equation [5]:

$$\boldsymbol{\rho_l\ \left(\frac{kg}{m^3}\right) = \left(\frac{840}{1+0.00067(T-288)}\right)} \tag{8.12}$$

The ρ_l for water was found using the following equation [6]:

$$\boldsymbol{\rho_l\ \left(\frac{kg}{m^3}\right) = -0.0028*T^2 + 1.3676*T + 839.42} \tag{8.13}$$

The ρ_l for the emulsion is then:

$$\boldsymbol{\rho_{l,emulsion}} \left(\frac{\boldsymbol{kg}}{\boldsymbol{m^3}}\right) = \boldsymbol{\varepsilon_{fuel}\rho_{l,fuel} + \varepsilon_{water}\rho_{l,water}} \quad \textbf{(8.14)}$$

Combustion parameters were found using the following method. For any oxygenated hydrocarbon fuel, combustion can be expressed as [3]:

$$\boldsymbol{\varepsilon_{fuel}C_xH_yO_z + \varepsilon_{water}H_2O + a(O_2 + 3.76N_2) \rightarrow + \frac{y}{2}CO_2 + a3.76N_2 +}$$

$$\boldsymbol{\varepsilon_{water}H_2O} \quad \textbf{(8.15)}$$

$$\boldsymbol{a = \varepsilon_{fuel}\left(x - \frac{z}{2} + \frac{y}{4}\right) + \varepsilon_{water}\left(0 - \frac{1}{2} + \frac{2}{4}\right)} \quad \textbf{(8.16)}$$

At the flame sheet the oxidizer and the fuel are assumed combine stoichiometrically to [3]

$$\boldsymbol{\varepsilon_{fuel}(1\ kg\ fuel) + v\ kg\ oxidizer = (v+1)\ kg\ products} \quad \textbf{(8.17)}$$

So [3]

$$\boldsymbol{v = \frac{m_{Ox}}{m_E} = \frac{4.76aMW_{air}}{MW_E}} \quad \textbf{(8.18)}$$

Where MW_E is the molecular weight of the emulsion and is found by knowing the initial mass concentration of the droplet and then converting to molecular weight. Molecular weights for diesel and soybean oil have already been found and the molecular weight of water is a known quantity.

The value of c_{pg} will be slightly altered by the addition of water but because the concentration of water compared to the concentration of CO_2 and N_2 in the product will be so small, the change will be considered negligible and the same equation will be used for c_{pg}

The k_g equation was altered in the following manor to account for the addition of water:

$$\boldsymbol{\varepsilon_{fuel}\left(0.4k_F(T)\right) + \varepsilon_{water}\left(0.4k_{water}(T)\right) + 0.6k_{ox}(T) = k_g} \quad \textbf{(8.19)}$$

k_{water} is widely available in the literature.

The h_{fg} and $h_c$for soybean oil and diesel average values were altered in the following manor:

$$\boldsymbol{\varepsilon_{fuel}h_{fg,fuel} + \varepsilon_{water}h_{fg,water} = h_{fg,emulsion}} \quad \textbf{(8.20)}$$

$$\boldsymbol{\varepsilon_{fuel}h_{c,fuel} + \varepsilon_{water}h_{c,water} = h_{fc,emulsion}} \quad \textbf{(8.21)}$$

The following are tables of the initial parameters for both soybean oil and diesel at concentrations of 80% fuel 20% water:

Table 66: Emulsion fuel combustion parameters

Soybean oil		**Diesel**	
$T_f guess\ (K)$	2200	$T_f\ guess\ (K)$	2200
$T_{avg} at\ Flame\ (K)$	1366.575	$T_{avg}\ at\ Flame\ (K)$	1351.875
$T_{avg} at\ surface\ (K)$	413.075	$T_{avg}\ at\ surface\ (K)$	398.375
$h_{ff}\ (KJ/kg)$	211	$h_{ff}\ (KJ/kg)$	254
$h_{fw}\ (kJ/kg)$	2270	$h_{fw}\ (kJ/kg)$	2270
$h_{fg}\ (KJ/kg)$	622.8	$h_{fg}\ (KJ/kg)$	658.2
MW_F	872.33	MW_F	168.3
MW_W	18	MW_W	18
MW_{air}	28.85	MW_{air}	28.85
MW_{Pr}	29.5169	MW_{Pr}	29.40326
MW_E	868.9455	MW_E	163.3893
$T_{boil,F}\ (K)$	573.15	$T_{boil,F}\ (K)$	536.4
$T_{boil,E}\ (K)$	533.15	$T_{boil,E}\ (K)$	503.75
$T_0\ (K)$	293	$T_0\ (K)$	293

v	9.83821	v	11.65518
$B_{o,q}$	2.70	$B_{o,q}$	3.02
K	6.53^{-7}	K	7.32^{-7}
$c_{p,N_2}\ (kJ/kg*K)$	1.211543	$c_{p,N_2}\ (kJ/kg*K)$	1.210214
$c_{p,CO_2}\ (kJ/kg*K)$	1.252173	$c_{p,CO_2}\ (kJ/kg*K)$	1.249643
$c_{p,H_2O}\ (kJ/kg*K)$	2.496345	$c_{p,H_2O}\ (kJ/kg*K)$	2.487525
$c_{p,l}\ (kJ/kg*K)$	3.150602	$c_{p,l}\ (kJ/kg*K)$	2.717438
$c_{p,g}\ (kJ/kg*K)$	1.254276	$c_{p,g}\ (kJ/kg*K)$	1.246644
$\rho_F\ at\ 293\ K\ (kg/m\text{^}3)$	926.1	$\rho_F\ at\ 293\ K\ (kg/m\text{^}3)$	782.1584
$d\rho/dt\ \ (kg/m\text{^}3)$	-0.643	$d\rho/dt\ \ (kg/m\text{^}3)$	-
$\rho_l\ \ (kg/m\text{^}3)$	864.4284	$\rho_l\ (kg/m\text{^}3)$	813.7008
$k_F\ at\ 293\ K\ (W/m*K)$	0.0153	$k_F\ at\ 293\ (W/m*K)$	0.0147
$K_F\ average\ (W/m*K)$	0.033034	$k_F\ average\ (W/m*K)$	0.031568
$k_{ox}\ (W/m*K)$	0.080129	$k_{ox}\ (W/m*K)$	0.079394
$k_g\ (kW/m*K)$	0.113492	$k_g\ (kW/m*K)$	0.112169
$k_w\ (kW/m*K)$	6.77E-05	$k_w\ (kW/m*K)$	6.67E-05
$R_u\ (kJ/kmol*K)$	8.31451	$R_u\ (kJ/kmol*K)$	8.31451
$h_{c,F}\ (kJ/kg)$	38220	$h_{c,F}\ (kJ/kg)$	43400
$h_c\ (kJ/kg)$	30576	$h_c\ (kJ/kg)$	34720
$P\ (Pa)$	101300	$P\ (Pa)$	101300
$T_{critical}\ (K)$	-	$T_{critical}\ (K)$	725.9

8.5 Results

The following section will detail the results of the model explained above when varying the two controllable operation variables, initial fuel droplet size and furnace temperature.

While the results of the calculations will mostly be presented via graphs, a small sample of the results will be shown in tabulated form as it is sometimes hard to glean exact values from a graph. Below are results for both soybean oil and diesel at 80% fuel and 20% water. Each table has 3 rows, the first row being the smallest initial

fuel droplet size at the highest furnace temperature, followed by mid-range values for both, ending with the largest initial fuel drop size and lowest furnace temperature.

Table 67: Some soybean oil/water emulsion combustion modeling results

$r_s\ (m)$	$T_\infty\ (K)$	A (Pa)	$B\ (K)$	$B_{o,q}$	$Y_{F,s}$	$\dot{m}_f\ (kg/s)$	$T_f\ (K)$	$r_f\ (m)$	$T_s\ (K)$	$t_d\ (s)$
1.00E-05	1.03E+03	1.71E+58	6.53E+04	2.79E+00	8.09E-01	9.04E-09	3.14E+03	1.38E-04	5.22E+02	6.01E-04
1.00E-04	9.33E+02	1.71E+58	6.53E+04	2.70E+00	8.02E-01	8.87E-08	3.05E+03	1.35E-03	5.22E+02	6.12E-02
5.00E-04	8.10E+02	1.71E+58	6.53E+04	2.58E+00	6.92E-01	4.33E-07	2.93E+03	6.59E-03	5.22E+02	1.57E+00

Table 68: Some diesel oil/water combustion modeling results

$r_s\ (m)$	$T_\infty\ (K)$	A	B	$B_{o,q}$	$Y_{F,s}$	$\dot{m}_f\ (kg/s)$	$T_f\ (K)$	$r_f\ (m)$	$T_s\ (K)$	$t_d\ (s)$
1.00E-05	1.03E+03	1.38E+16	1.29E+04	3.12E+00	8.37E-01	9.52E-09	3.12E+03	1.72E-04	4.83E+02	5.37E-04
1.00E-04	9.33E+02	1.38E+16	1.29E+04	3.02E+00	8.30E-01	9.35E-08	3.02E+03	1.69E-03	4.83E+02	5.47E-02
0.0005	8.10E+02	1.38E+16	1.29E+04	2.89E+00	8.21E-01	4.57E-07	2.91E+03	8.25E-03	4.82E+02	1.40E+00

The next section will present graphical comparisons of combustion variables for both soybean oil/water and diesel/water for all emulsion concentration ranges. The following 6 graphs are the results of maintaining a constant furnace temperature of 933 K while varying the initial droplet radius from 10 μm to 500 μm. Droplet sizes are optimum size range taken from the literature that have historically provided good flow and combustion properties. The first two graphs shows that with increasing initial particle size the flame sheet radius also increases, linearly. As the water content increases in both emulsion types, the rate of increase and total value of the flame sheet radius decreases.

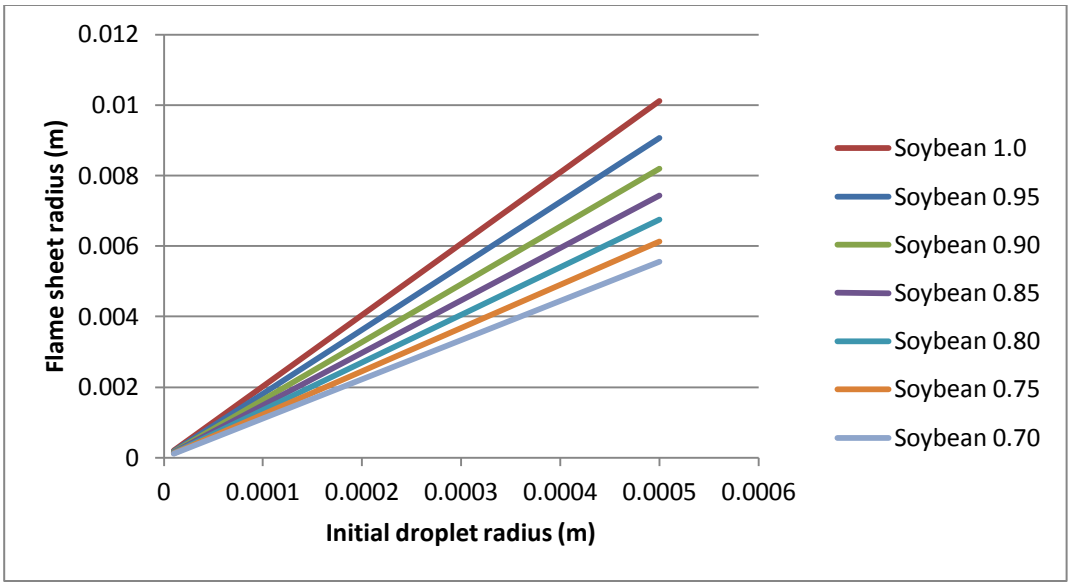

Figure 72: Radius of the flame sheet for a soybean-water emulsion droplet varying in droplet size at a furnace temperature of 933 K. Each data set represents a different emulsion concentration, with the number shown being the fuel oil concentration and the water concentration being the remainder.

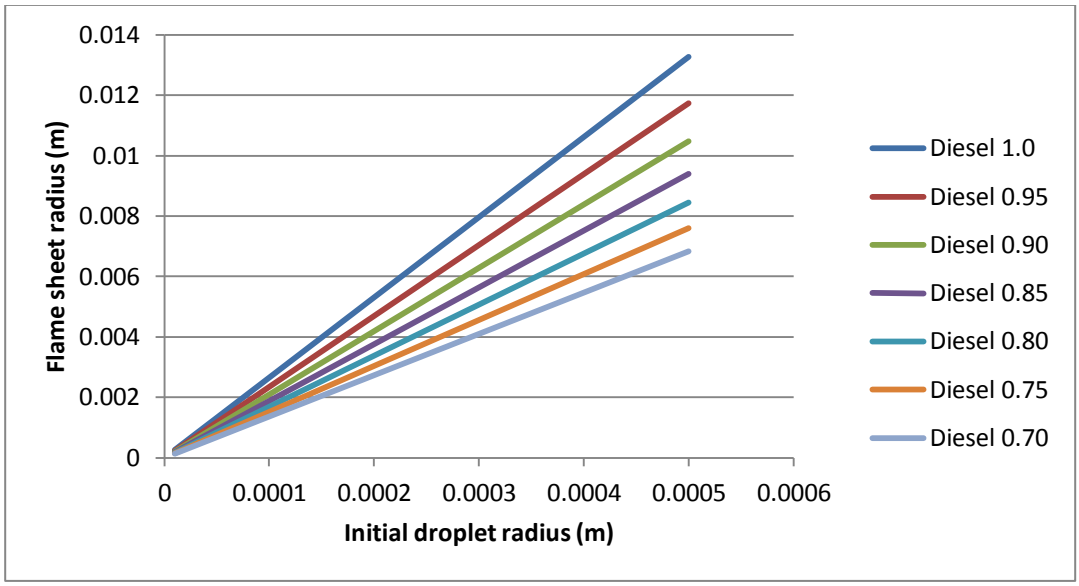

Figure 73: Radius of the flame sheet for a diesel-water emulsion droplet varying in droplet size at a furnace temperature of 933 K. Each data set represents a different emulsion concentration, with the number shown being the fuel oil concentration and the water concentration being the remainder.

Figures 74 and 75 show that as initial particle size increases, the droplet burning rate also increases linearly. For both emulsion types the droplet burning rate decreases as the water content increases.

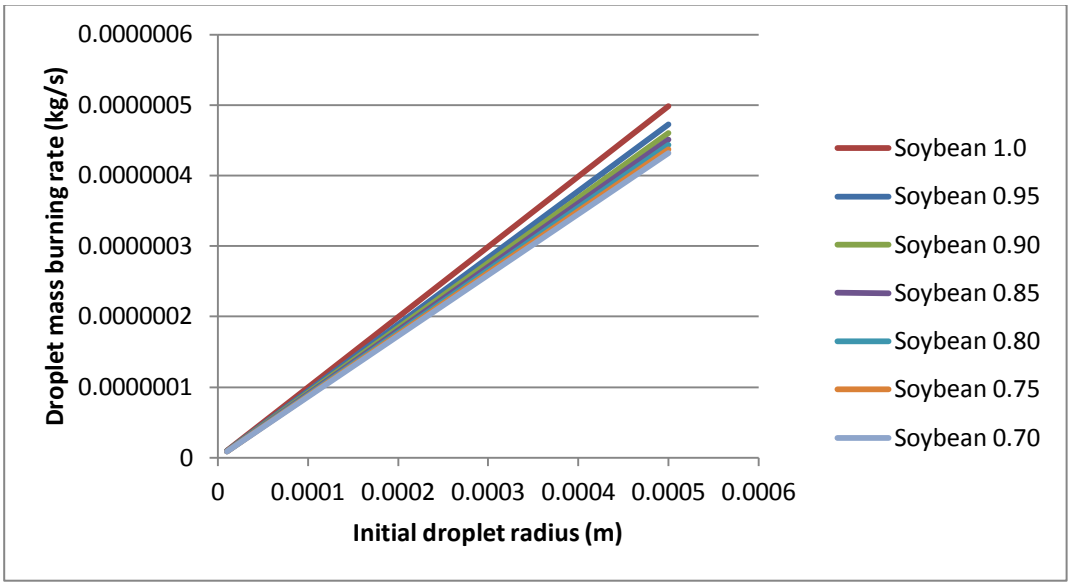

Figure 74: Burning constant for a soybean-water emulsion droplet varying in droplet size at a furnace temperature of 933 K. Each data set represents a different emulsion concentration, with the number shown being the fuel oil concentration and the water concentration being the remainder.

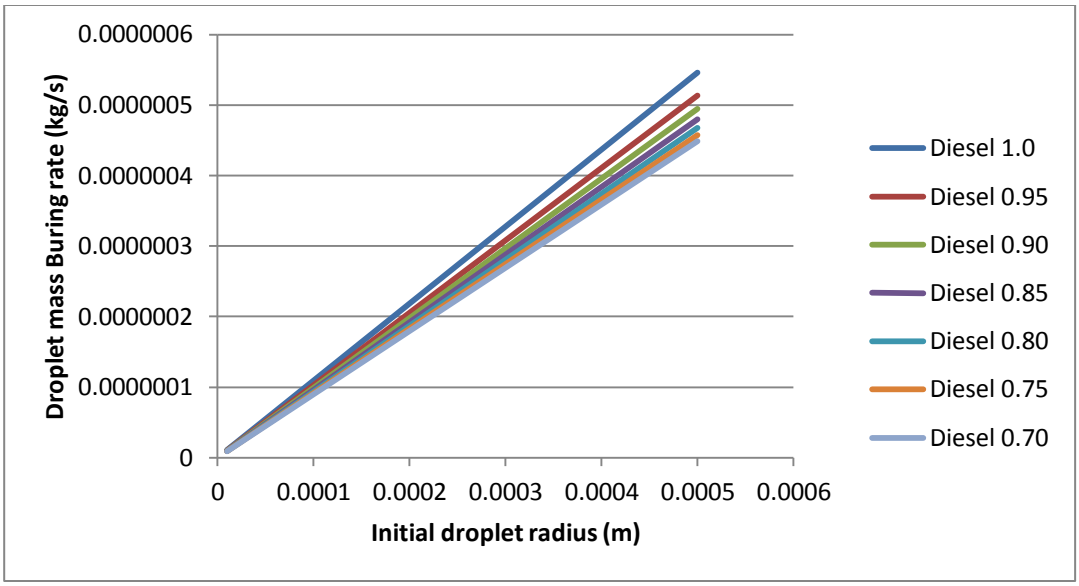

Figure 75: Burning constant for a diesel-water emulsion droplet varying in droplet size at a furnace temperature of 933 K. Each data set represents a different emulsion concentration, with the number shown being the fuel oil concentration and the water concentration being the remainder.

The last graphs shows the total droplet combustion time increasing exponentially with initial particle size. For both emulsion types, the total combustion time is increased with the addition of water.

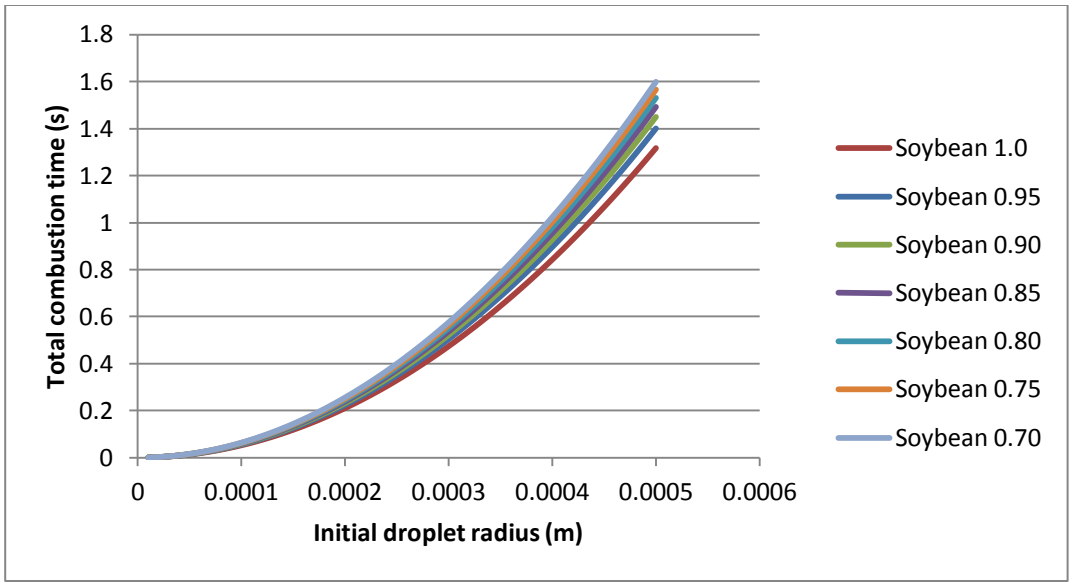

Figure 76: Total combustion time for a soybean-water emulsion droplet varying in droplet size at a furnace temperature of 933 K. Each data set represents a different emulsion concentration, with the number shown being the fuel oil concentration and the water concentration being the remainder.

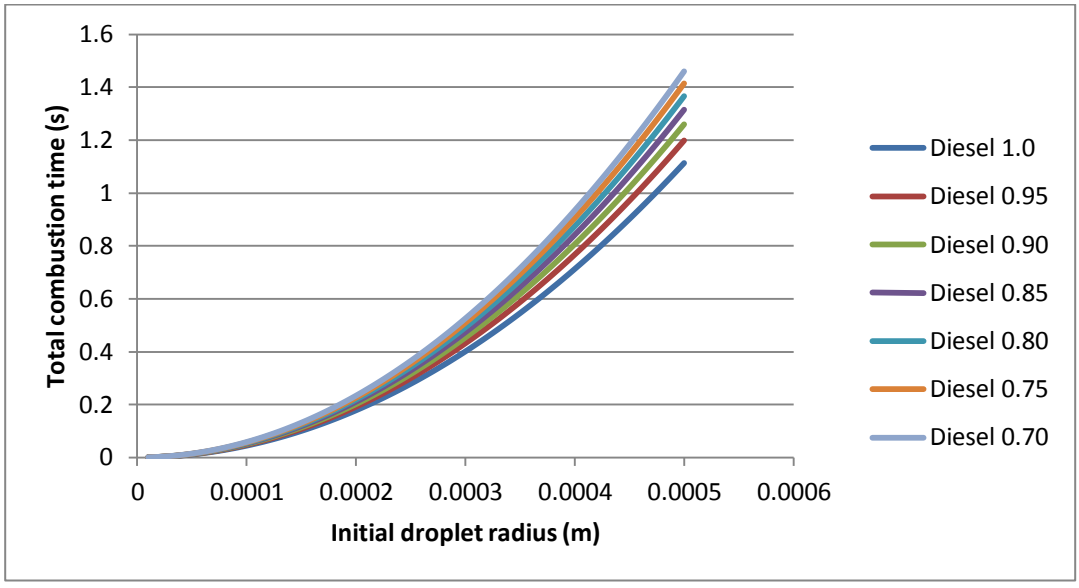

Figure 77: Total combustion time for a diesel-water emulsion droplet varying in droplet size at a furnace temperature of 933 K. Each data set represents a different emulsion concentration, with the number shown being the fuel oil concentration and the water concentration being the remainder.

The next set of graphs will show the results when initial droplet size is kept constant at 100 μm while the furnace temperature is varied between the normal operating ranges of 811-1033 K.

The first two graphs of this series shows flame temperature increasing linearly with furnace temperature. Both emulsion types show a decrease in flame temperature with increasing water content.

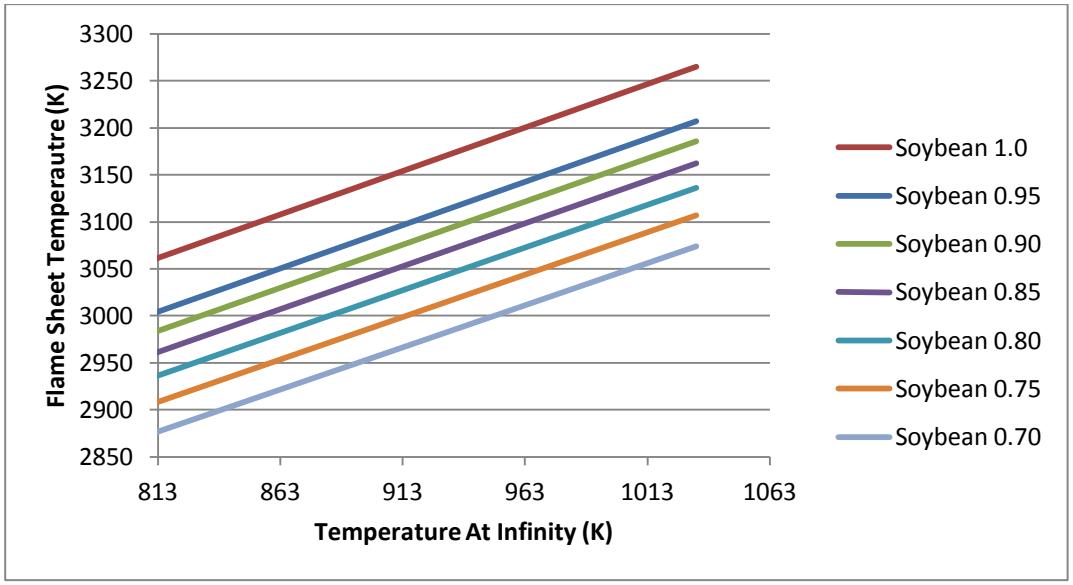

Figure 78: Flame temperature for a soybean-water emulsion droplet varying the furnace temperature for a droplet size of 0.0001 m. Each data set represents a different emulsion concentration, with the number shown being the fuel oil concentration and the water concentration being the remainder.

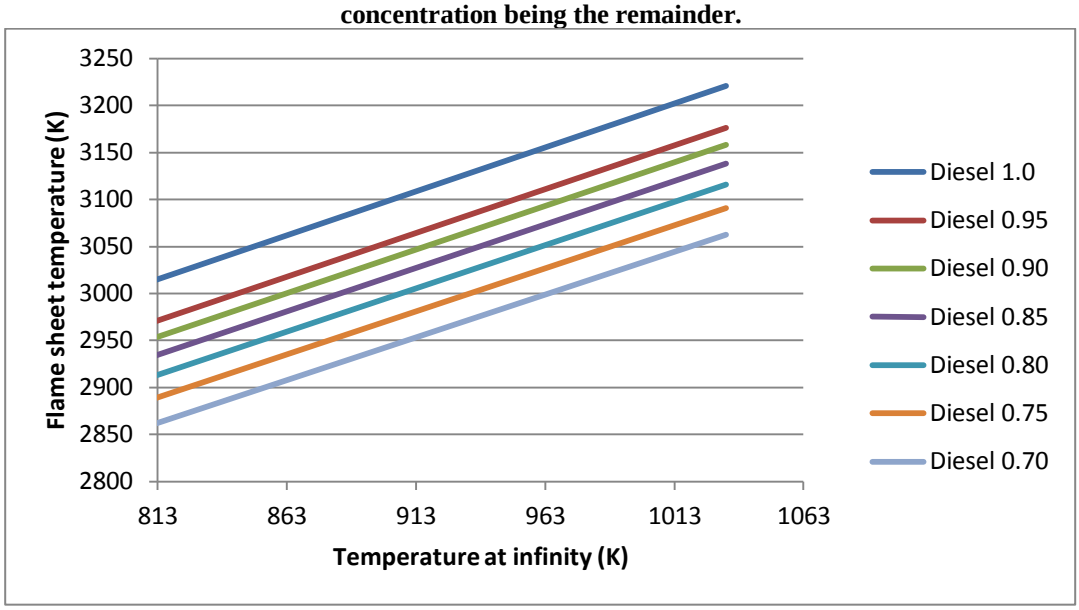

Figure 79: Flame temperature for a diesel-water emulsion droplet varying the furnace temperature for a droplet size of 0.0001 m. Each data set represents a different emulsion concentration, with the number shown being the fuel oil concentration and the water concentration being the remainder.

Figures 80 and 81 show surface temperature increases minimally and linearly with furnace temperature. Both emulsion types show a decrease in surface temperature with increasing water content.

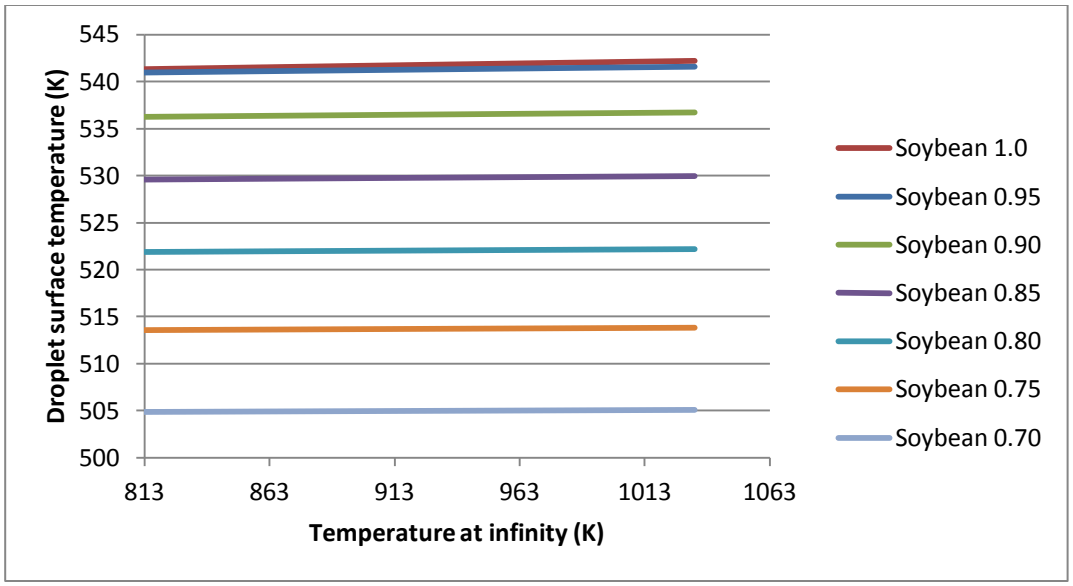

Figure 80: Surface temperature for a soybean-water emulsion droplet varying the furnace temperature for a droplet size of 0.0001 m. Each data set represents a different emulsion concentration, with the number shown being the fuel oil concentration and the water concentration being the remainder.

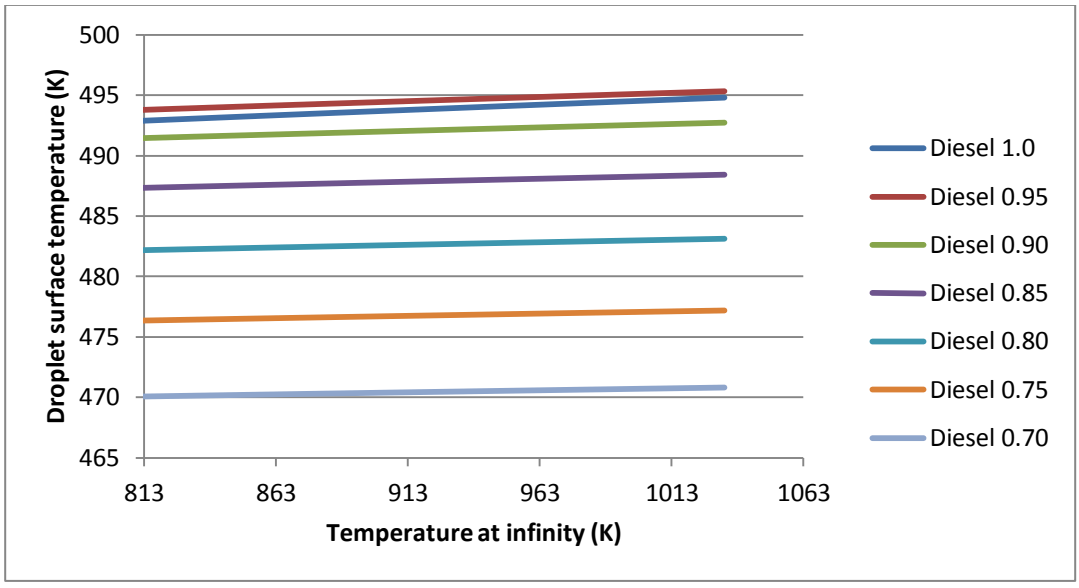

Figure 81: Surface temperature for a diesel-water emulsion droplet varying the furnace temperature for a droplet size of 0.0001 m. Each data set represents a different emulsion concentration, with the number shown being the fuel oil concentration and the water concentration being the remainder.

Figures 82 and 83 show that the flame sheet radius increases minimally and linearly with furnace temperature. Both emulsion types show a decrease in flame sheet radius with increasing water content.

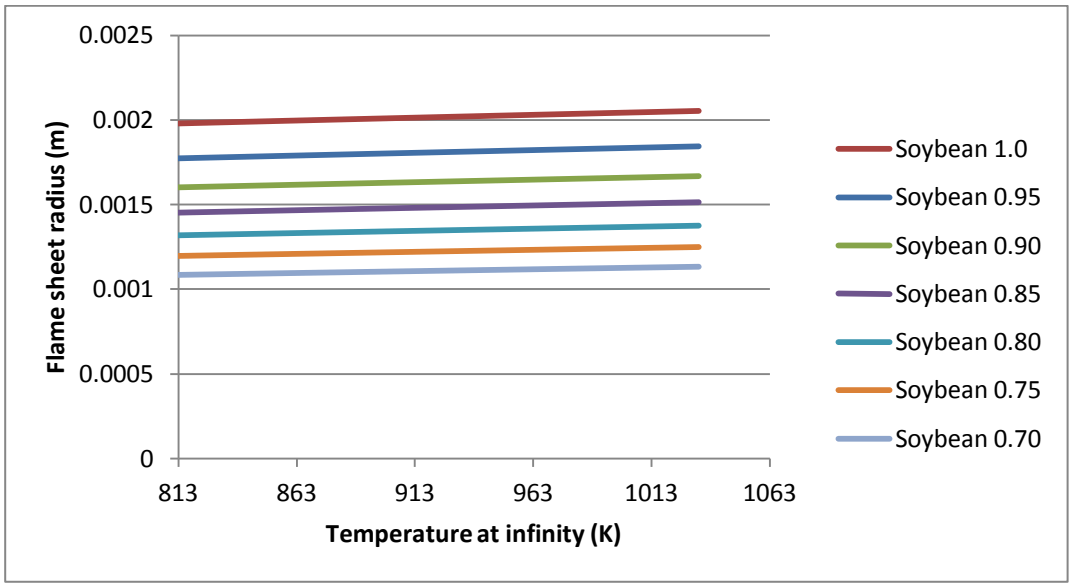

Figure 82: Flame sheet radius for a soybean-water emulsion droplet varying the furnace temperature for a droplet size of 0.0001 m. Each data set represents a different emulsion concentration, with the number shown being the fuel oil concentration and the water concentration being the remainder.

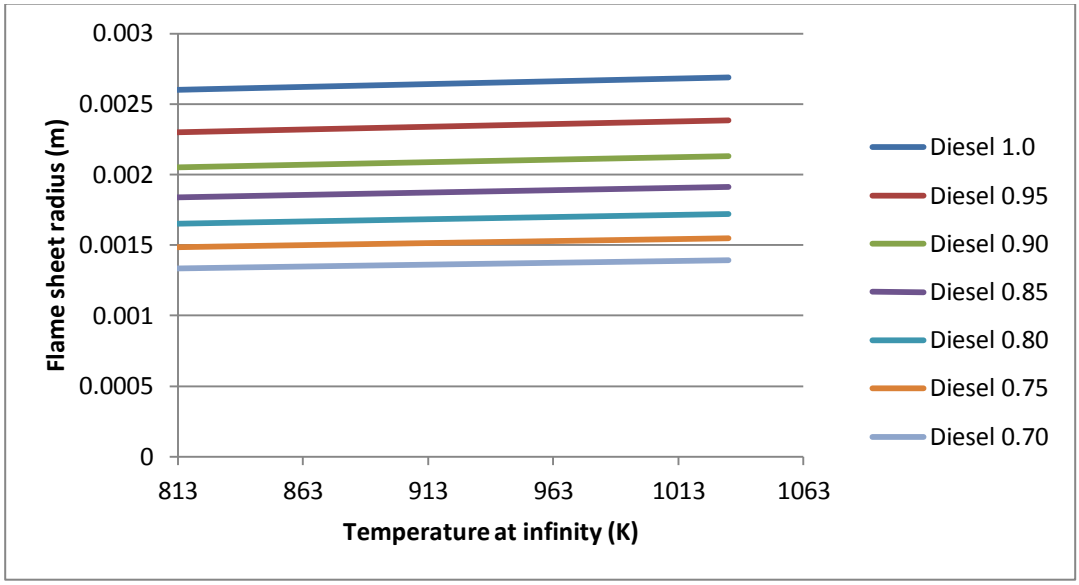

Figure 83: Flame sheet radius for a diesel-water emulsion droplet varying the furnace temperature for a droplet size of 0.0001 m. Each data set represents a different emulsion concentration, with the number shown being the fuel oil concentration and the water concentration being the remainder.

Figures 84 and 85 show that droplet burning rate increases linearly with furnace temperature. Both emulsion types show a decrease in droplet burning rate with increasing water content.

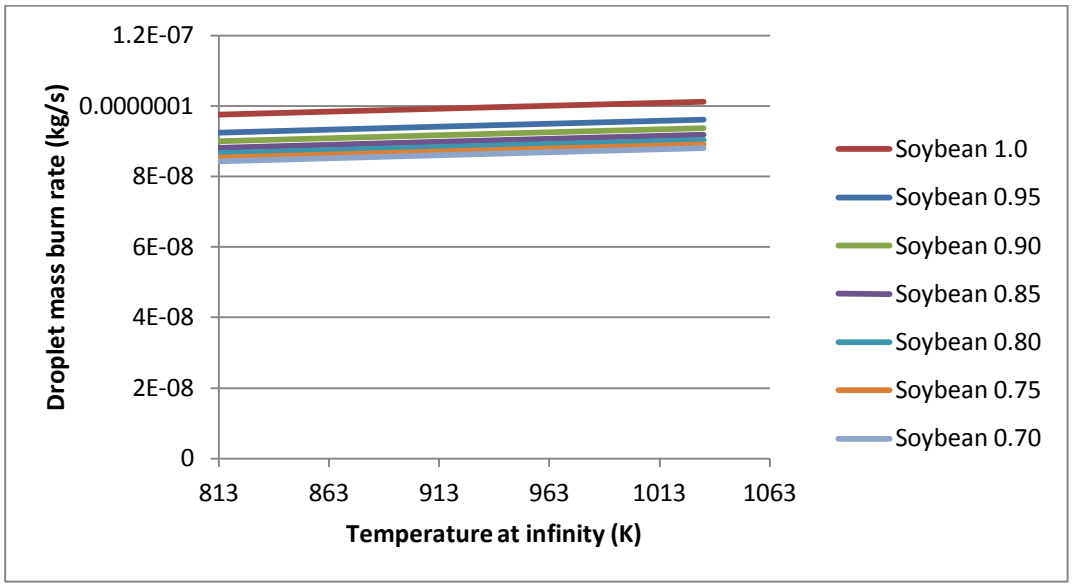

Figure 84: Burning rate for a soybean-water emulsion droplet varying the furnace temperature for a droplet size of 0.0001 m. Each data set represents a different emulsion concentration, with the number shown being the fuel oil concentration and the water concentration being the remainder.

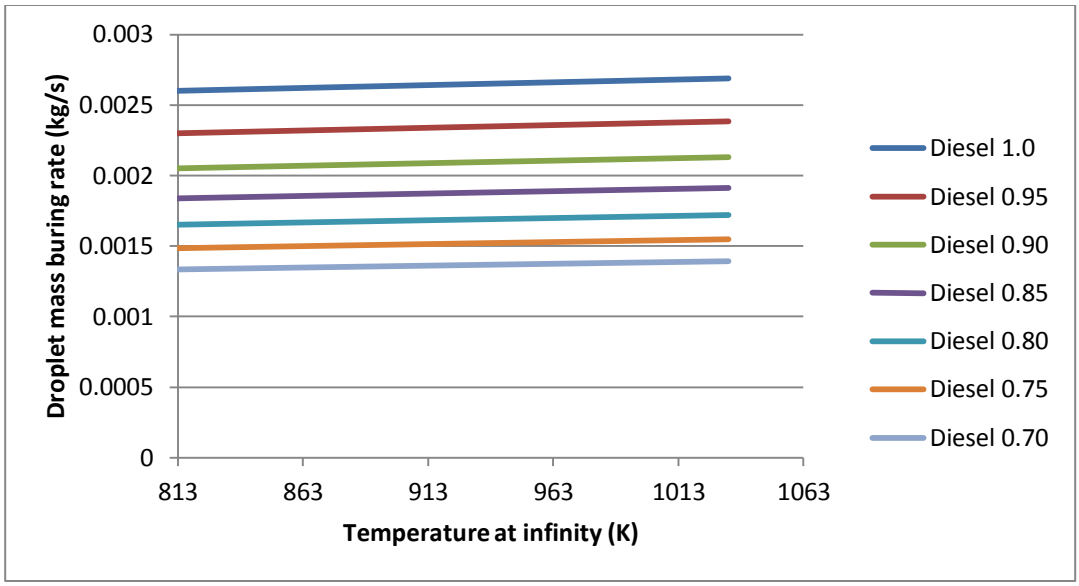

Figure 85: Burning rate for a diesel-water emulsion droplet varying the furnace temperature for a droplet size of 0.0001 m. Each data set represents a different emulsion concentration, with the number shown being the fuel oil concentration and the water concentration being the remainder.

Figure 86 and 87 show that found the total droplet combustion time decreases linearly with furnace temperature. Both emulsion types show an increase of total droplet combustion time with increasing water content.

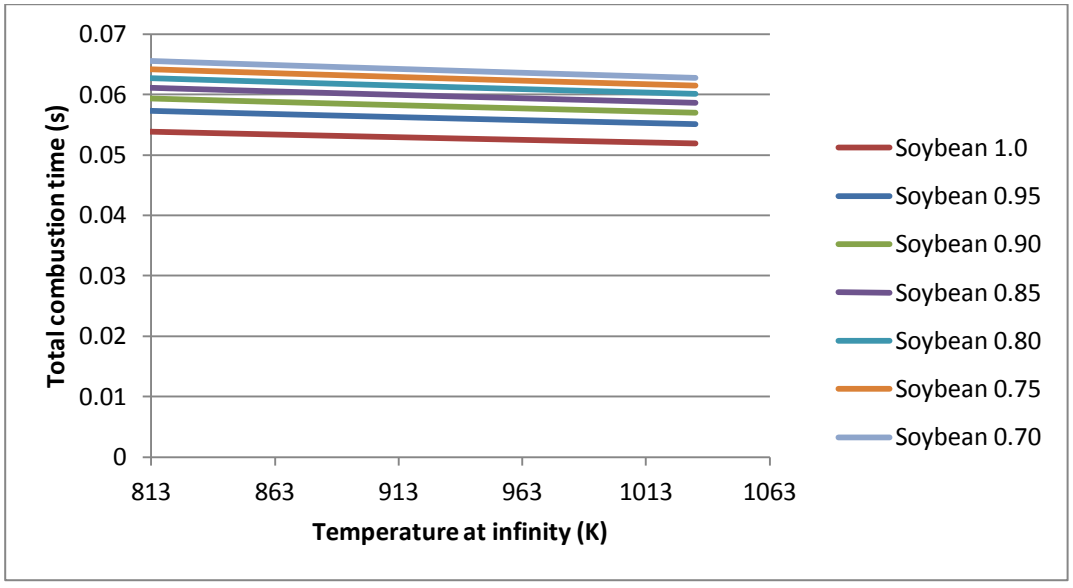

Figure 86: Total combustion time for a soybean-water emulsion droplet varying the furnace temperature for a droplet size of 0.0001 m. Each data set represents a different emulsion concentration, with the number shown being the fuel oil concentration and the water concentration being the remainder.

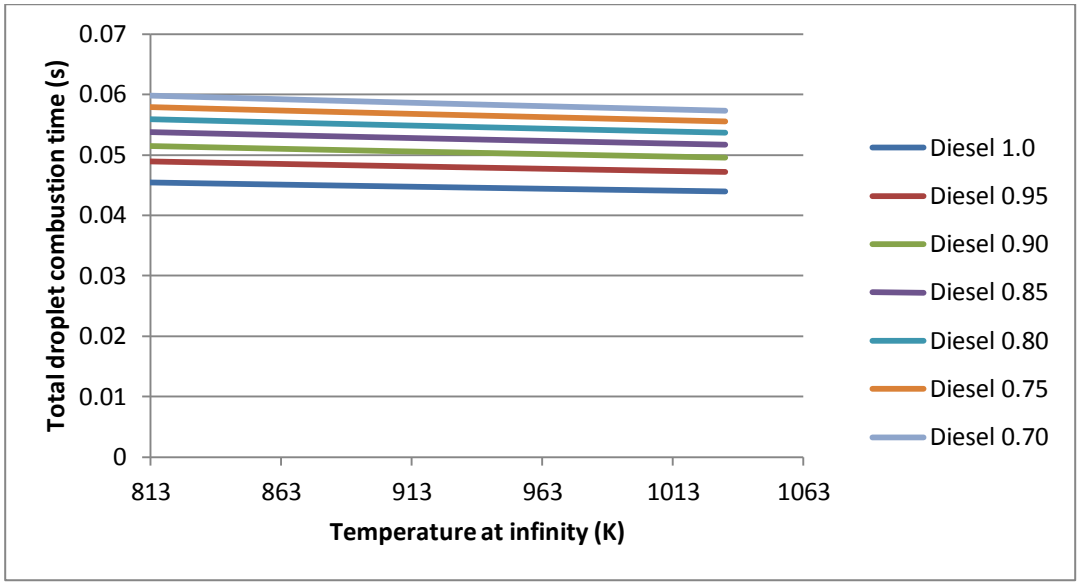

Figure 87: Total combustion time for a diesel-water emulsion droplet varying the furnace temperature for a droplet size of 0.0001 m. Each data set represents a different emulsion concentration, with the number shown being the fuel oil concentration and the water concentration being the remainder.

The last set of graphs are examining the radius of the droplet throughout its entire life. Both fuel emulsion types were examined at three differing initial particle sizes and furnace temperature combinations. All three scenarios had the same general shape to the results as well as an increase in water concentration resulting in an increase in droplet lifetime and radius at any given time.

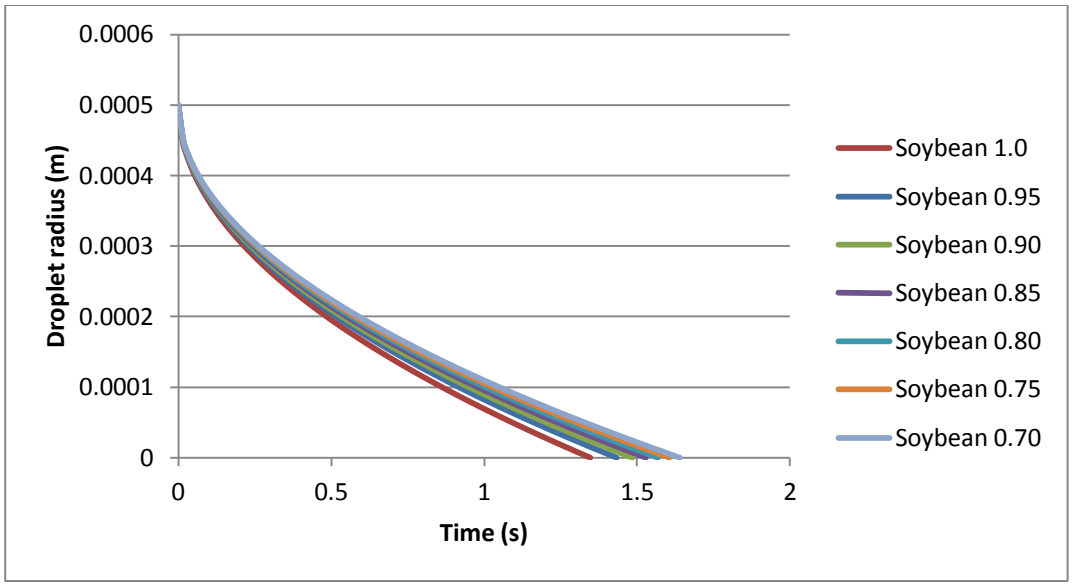

Figure 88: Soybean droplet size throughout combustion life at a furnace temperature of 813 K. Each data set represents a different emulsion concentration, with the number shown being the fuel oil concentration and the water concentration being the remainder.

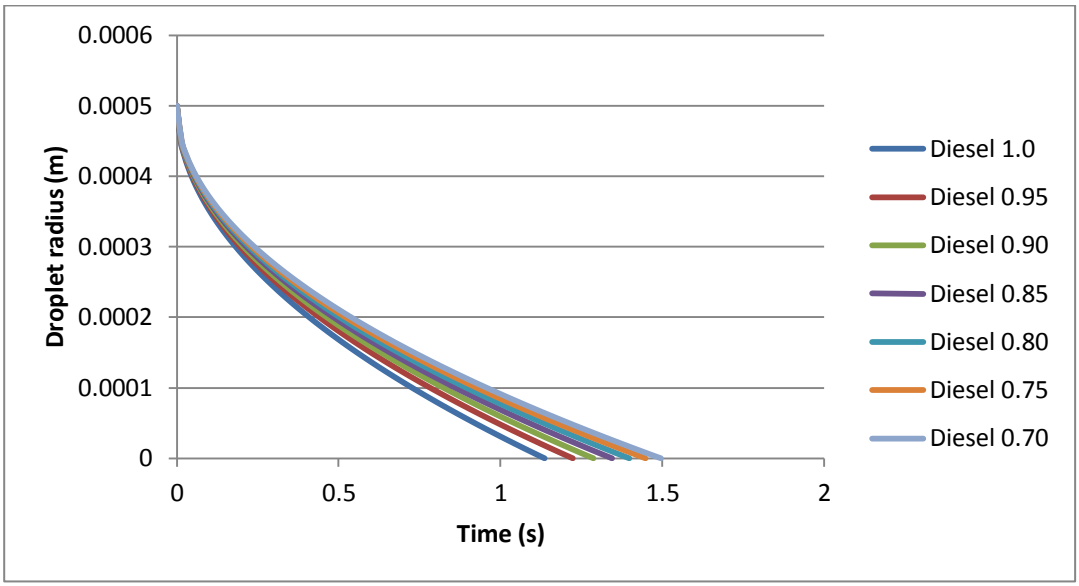

Figure 89: Diesel droplet size throughout combustion life at a furnace temperature of 813 K. Each data set represents a different emulsion concentration, with the number shown being the fuel oil concentration and the water concentration being the remainder.

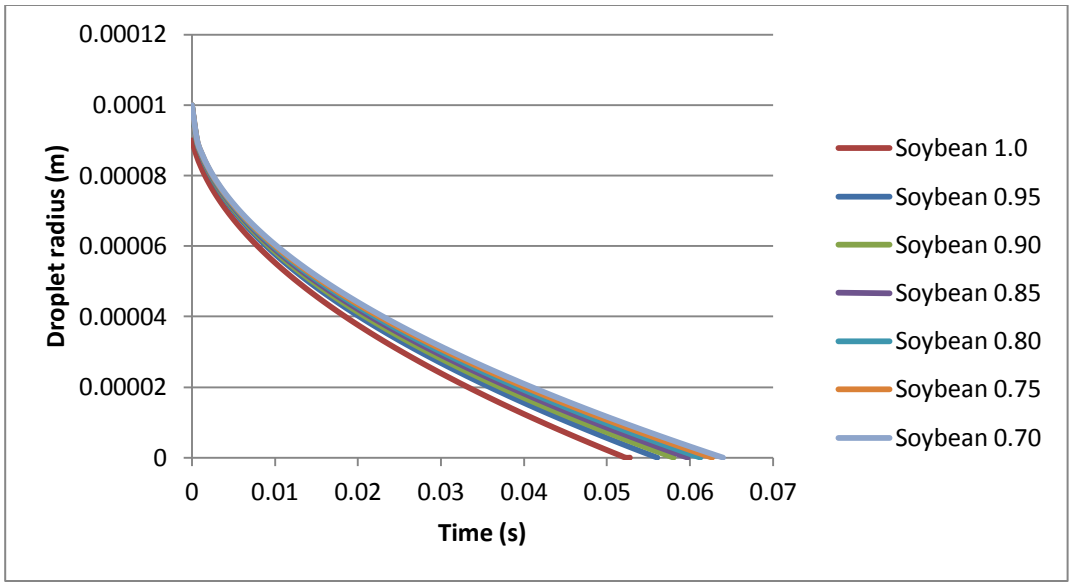

Figure 90: Soybean droplet size throughout combustion life at a furnace temperature of 933 K. Each data set represents a different emulsion concentration, with the number shown being the fuel oil concentration and the water concentration being the remainder.

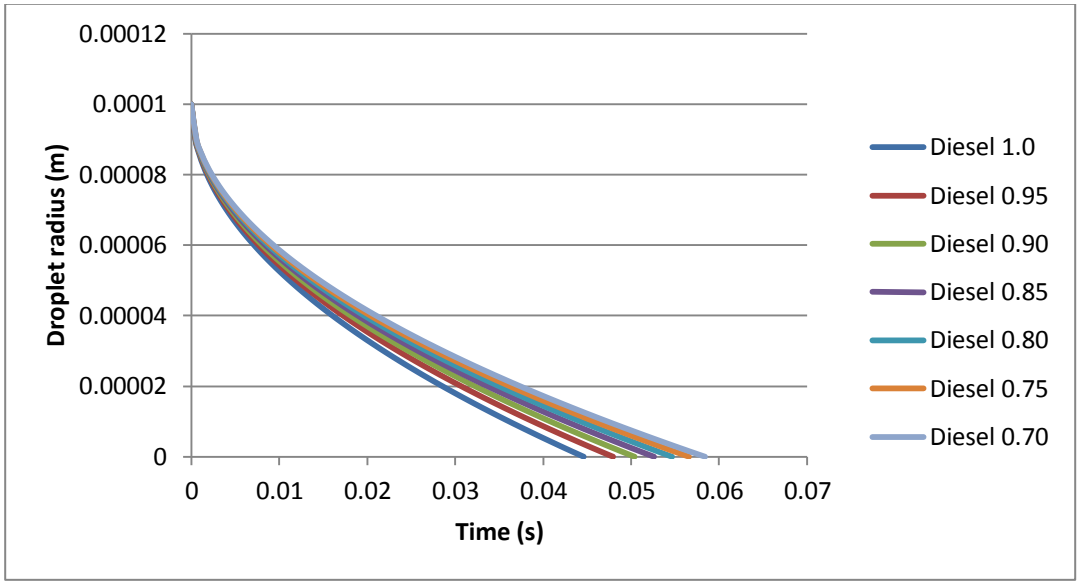

Figure 91: Diesel droplet size throughout combustion life at a furnace temperature of 933 K. Each data set represents a different emulsion concentration, with the number shown being the fuel oil concentration and the water concentration being the remainder.

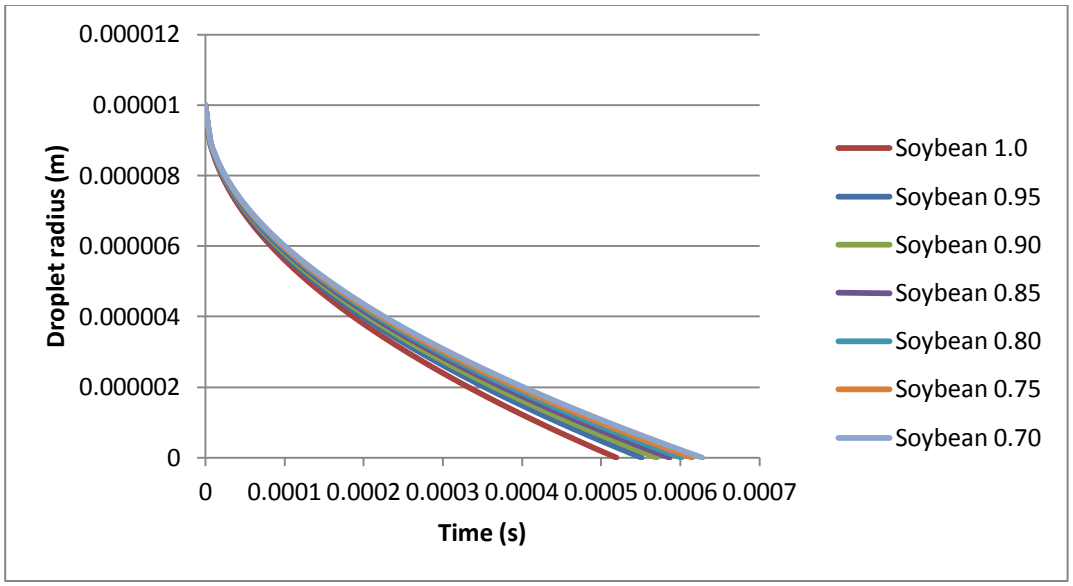

Figure 92: Soybean droplet size throughout combustion life at a furnace temperature of 1033 K. Each data set represents a different emulsion concentration, with the number shown being the fuel oil concentration and the water concentration being the remainder.

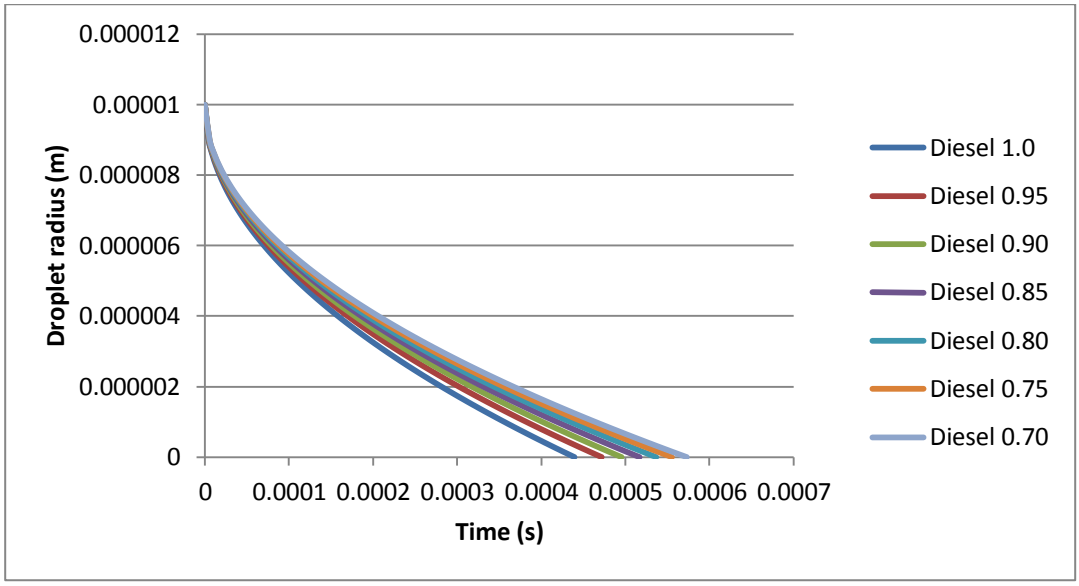

Figure 93: Diesel droplet size throughout combustion life at a furnace temperature of 1033 K. Each data set represents a different emulsion concentration, with the number shown being the fuel oil concentration and the water concentration being the remainder.

8.6 Discussion

The results will be discussed as far as they pertain to the differences created by the emulsion. The differences between soybean oil and diesel combustion have been discussed and will therefore not be repeated. Adding water decreased the flame temperature, surface temperature , and droplet burning rate. This is because water does not have a heat of combustion and therefore does not contribute as a fuel source towards combustion. Not only this, but the vaporization of the water still requires heat creating an overall negative energy transaction. When the emulsion is compared to a pure fuel, a lower flame temperature and slower droplet burning rate is therefore seen. Also water has a lower boiling temperature than diesel and soybean oil, so the surface temperature will therefore be lower for an emulsion than a pure fuel droplet. These changes result in a larger total droplet combustion time as well as a larger droplet size at any given time. These affects are then compounded as more water is added and fuel is removed.

8.7 Conclusions

Water, when added to liquid fuels to create an emulsion, has noticeable effects on all aspects of combustion. The most worrisome of these aspects is the combustion process and total combustion time. It can be concluded from the results that though fuel-water emulsion droplets are markedly slower than pure fuel droplets the overall combustion time for the emulsions droplets is still fast enough for combustion purposes. As will be seen in the next section, it is the solid fuel combustion times that are the rate limiting step in the combustion of a composite fuel.

8.8 Nomenclature

A	Clausius-Clapeyron constant (m^2)

B	Clausius-Clapeyron constant (K)
$B_{o,q}$	Spalding Number
c_p	Specific heat $(kJ/kg * K)$
D	diameter of fuel droplet (m)
h_c	heat of combustion (kJ/kg)
h_{fg}	Latent heat of vaporization (kJ/kg)
k	Thermal conductivity $(kW/m * k)$
K	Combustion rate constant (m^2/s)
$\dot{m}_F$	Mass burning rate of the fuel (kg/s)
MW	Molecular weight
P	Pressure (Pa)
r	Radius (m)
R_u	Universal gas constant $(kJ/kmol * K)$
t_d	Total droplet combustion time (s)
T	Temperature (K)
Y	Mass fraction
ρ	density (kg/m^3)
v	Oxidizer to fuel stoichiometric ratio

Subscripts

bp	boiling point
d	droplet

e	emulsion
f	flame
F	Fuel
g	Gas
l	Liquid
Pr	Products
s	Surface
∞	Far removed from the surface
0	initial

8.9 References

[1] Law, C. K. "A model for the combustion of oil/water emulsion droplets." *Combustion Science and Technology* 18.1-2 (1977): 29-38.

[2] Law, C. K., C. H. Lee, and N. Srinivasan. "Combustion characteristics of water-in-oil emulsion droplets." *Combustion and flame* 37 (1980): 125-143.

[3] Turns, Stephen R. *An introduction to combustion*. Vol. 499. New York: McGraw-Hill, 1996.

[4] Law, C.K., and Williams, F.A., "Kinetics and Convection in the Combustion of Alkane Droplets," Combustion and Flame, 19(3): 393-406 (1972).

[5] Gunstone, Frank, ed. *Vegetable oils in food technology: composition, properties and uses*. Wiley. com, 2011.

[6] Sazhin, Sergei S. "Advanced models of fuel droplet heating and evaporation." *Progress in energy and combustion science* 32.2 (2006): 162-214.

[7] Hammond, Earl G., et al. "Soybean oil." *Bailey's Industrial Oil and Fat Products* (2005): 577-672.

[8] "Triglyceride Molecular Weight Calculator » Biodiesel Fuel Education Program." *Biodiesel Fuel Education Program*. N.p., 2013. Web. 17 June 2013.

[9] Godsave, G.A.E., "Studies of the Combustion of Drops in a Fuel Spray: The Burning of Single Drops of Fuel," *Fourth Symposium (International) on Combustion*, Willkiams & Wilkins, Baltimore, MD, pp 818-830, 1953.

[10] Spalding, D.B., "The Combustion of Liquid Fuels*," Fourth Symposium (International) on Combustion*, Williams & Wilkins, Baltimore, MD, pp 847-864, 1953.

[11] Ballester, Javier M., Norberto Fueyo, and Cesar Dopazo. "Combustion characteristics of heavy oil-water emulsions." *Fuel* 75.6 (1996): 695-705.

[12] Gao, Yuanping, and Kewen Li. "New models for calculating the viscosity of mixed oil." *Fuel* 95 (2012): 431-438.

CHAPTER 9 - COMPOSITE FUEL COMBUSTION MODELING

9.1 Introduction

In this chapter, the combustion of composite emulsions will be examined and modeled. In the previous chapters, liquid fuel combustion, solid fuel combustion and emulsion combustion were examined and modeled. Based on success of the previous chapters, a model for composite emulsions will be attempted here. The end goal is to see how the addition of water and solid fuel to liquid fuel affect the combustion properties of the fuel.

9.2 Physical model description

To begin will be a general description of the model. A given composite mixture will have a mass percentage of solid fuel particles, a mass percentage of liquid fuel and a mass percentage of water. While these percentages will change depending on the application, the model will be represented by a composite mixture with mass ratios that are close to those used in the settling chapter experiments. When injected into the furnace, there will be two major phases of fuel. One phase will be liquid only droplets consisting of liquid fuel and water, while the other phase will be solid particles surrounded by a layer of liquid fuel and water. The liquid only phase will undergo the entire combustion process much faster the solid-liquid-water phase, due to the lack of a char combustion step. While this is the most likely scenario in reality, the composite model will be assumed to consist only of a spray of the solid particles surrounded by an emulsion shell. There will be no free floating emulsion droplets.

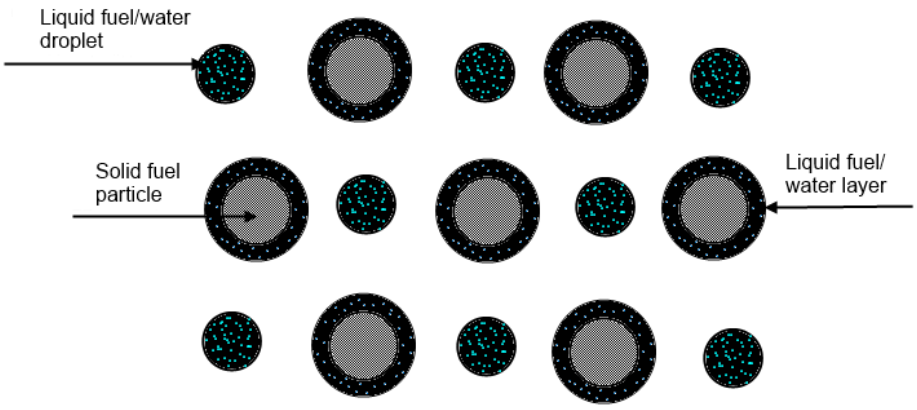

Figure 94: Solid/emulsion composite fuel spray

The following assumptions will be made considering the combustion of the solid-liquid-water phase:

22.) The burning particle/emulsion is surrounded by a spherically symmetric flame and exists in a quiescent, infinite medium

23.) The emulsion layer is a two component liquid with zero solubility for gases

24.) Pressure is constant at 1 atmosphere

25.) The gas phase consists of 4 species: Fuel vapor, oxidizer, water vapor and combustion products

26.) Fuel and oxidizer are assumed to react in stoichiometric proportions to the flame, while the chemical kinetics are so fast the flame is idealized as an infinitesimally thin sheet

27.) The Lewis number is assumed to be 1

28.) The gas phase thermal conductivity, specific heat and density are all constants. (k_g, C_{pg}, ρ)

29.) The liquid emulsion layer is the only condensed phase

30.) The water and fuel emulsion is well mixed

31.) Vaporization occurs at the surface of the layer

32.) The fractional vaporization rate of water and fuel will assumed to be equal to the initial liquid mass fraction of each component, and therefore constant or $\varepsilon_i = Y_{il}$

33.) Drying of the solid will begin after the liquid layer has combusted and when the temperature of the particle reaches that of the boiling temperature water

34.) Moisture content of the solid consists mostly of free water, therefore drying of bound water will be neglected

35.) The solid fuel particles are so small that the concentration of water within the particle is constant throughout

36.) Drying of free water will be modeled at a constant rate

37.) The majority of the drying process will end at the time heavy devolatilization begins

38.) All heat transfer due to air flow will be assumed to be natural convection, low Reynolds number

39.) Char combustion rate is diffusion limited

40.) Model results are a per colloid particle basis

As can be seen, the assumptions made are a combination of the assumptions from the emulsion model combined with the assumptions from the solid combustion model. The model equations for solid-emulsion combustion will also be a combination of both the emulsion combustion model and the solid combustion model. The two

processes will be combined in a way such that a linear model is formed. A linear model provides the simplest model, while still achieving accurate results.

The steps of this linear model as follows

1.) Furnace is operating at around 933 K

2.) Feed composite mixture is injected into the heater begins to increase in temperature

3.) Oil/water emulsion shell vaporizes and forms a combustible gas

4.) Gas combusts

5.) Solid particle releases water as it heats up (drying)

6.) Solid particle beings to undergoes devolatilization and combustion while simultaneously undergoing char formation

7.) Volatile gases completely combust completing char formation

8.) Char combustion

With these steps in mind a simple branch model will be shown to represent the combustion process.

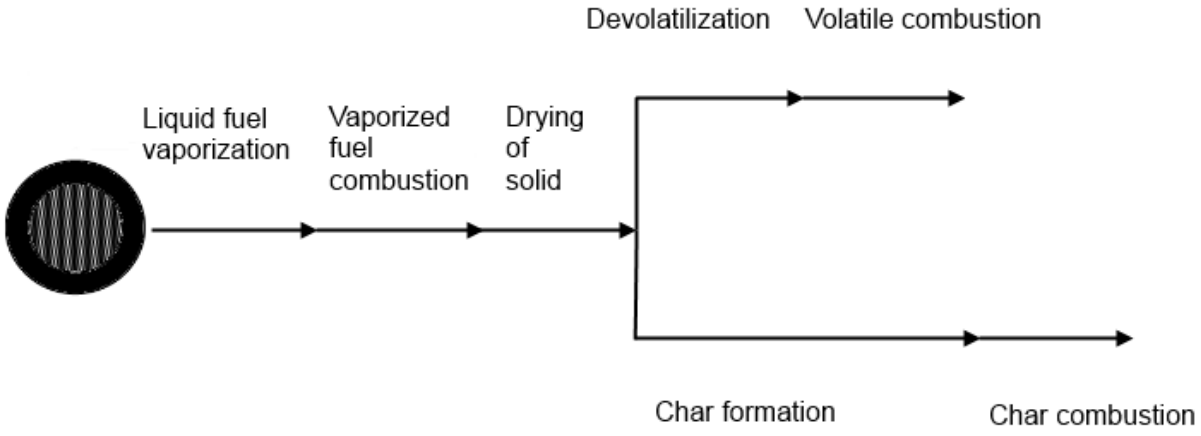

Figure 95: Linear model of solid/emulsion fuel combustion

The solid combustion model will therefore be the emulsion droplet combustion model, followed by the solid combustion model for the remaining solid particle. Because of this, this chapter will have very little new concepts and equations.

9.3 Model Equations and Parameters

The equations being used in this modeling section are the same that were used for emulsion combustion and solid combustion. There will be some minor differences that are as follows:

Solid model portion: Once the emulsion combusts, all that will remain is the solid particle. Because of this, the only difference that needs to be accounted for is a higher initial particle temperature. As the emulsion shell combusted the solid particle absorbs some of that heat. This will end up speeding up the heating up process, which is already so fast due to small particle size, the affect is hardly noticeable.

Emulsion portion: The emulsion shell combustion will still use the same equations. What needs to be accounted for is the difference in the shape being used in the model equations. Before the shell volume, radius and combustion time was to be found for a sphere, now it is for a spherical shell. The shell dimension will not be guessed, as it is not a controllable variable. Due to the assumption all liquid mass will be surrounding the solid particle, the initial mass ratio of emulsion to solid is known and controllable, therefore the volume and radius of the emulsion shell can be found:

$$\boldsymbol{m_l = \frac{Y_l m_S}{Y_S}} \quad \textbf{(9.1)}$$

$$\boldsymbol{V_l = \frac{m_l}{\rho_l}} \quad \textbf{(9.2)}$$

Where Y_s is solid mass percent of the particle/emulsion shell. Y_l is the liquid mass percent of the particle/shell. m_s and m_l are the masses of the solid and liquid portion of the particle/emulsion shell and V_l is the volume of the emulsion shell. Now the radius of the emulsion shell can be found:

$$\boldsymbol{V_l = \frac{4}{3}\pi R^3 - \frac{4}{3}\pi r_S^3} \quad \textbf{(9.3)}$$

Where R^3 is the radius of the colloid particle, consisting of both the solid particle and the emulsion shell, and r_S^3 is the radius of just the inner particle which is a controllable variable. R can be solved for as follows:

$$\boldsymbol{R = \left(\frac{3V_l}{4\pi} + r_S^3\right)^{\frac{1}{3}}} \quad \textbf{(9.4)}$$

With R and r now being known, the thickness of the shell can be found:

$$\boldsymbol{R - r_S = r_{shell}} \quad \textbf{(9.5)}$$

Now that the radius of the shell is known the spherical emulsion combustion equations need to be altered for a shell. Because a shell and a sphere of the same size have the same shape and surface area the transition will be easy. The first of the equations effected by the shell versus sphere is the r_f equation:

$$\boldsymbol{r_f = r_s \frac{\ln(1+B_{o,q})}{\ln\left(\frac{1+v}{v}\right)}} \quad \textbf{(9.6)}$$

Here r_s will be substituted with R. This is because the flame is a direct function of the sphere it is surrounding. The flame does not know the emulsion is a shell v.s. a droplet and will still act the same as long as the emulsion exists.

The next change is for the total droplet combustion time. This process will begin with the equation for $\dot{m}_F$

$$\dot{m}_F = \frac{4\pi k_g r_s}{c_{pg}} \ln(1 + B_{o,q}) \quad \textbf{(9.7)}$$

Again r_s will be substituted with R, because the shell will have a surface area that is equivalent to the particle/emulsion shell so all that needs to be accounted for is the different radius. Next the combustion constant equation needs to be addressed:

$$K = \frac{8k_g}{\rho_l c_{pg}} \ln(1 + B_{o,q}) \quad \textbf{(9.8)}$$

This equation is specifically for spherical drops. K directly leads to the total combustion time by the following equation:

$$D^2(t) = D_0^2 - Kt \quad \textbf{(9.9)}$$

While the K for a shell could be solved for, a simpler solution was to use the following method. By finding the time an emulsion droplet of radius r to combust and subtracting it from the time it takes an emulsion droplet of radius R, the shell combustion time was effectively solved:

$$t(shell) = t(R) - t(r_S) = \frac{(2R)^2}{K} - \frac{(2r_S)^2}{K} \quad \textbf{(9.10)}$$

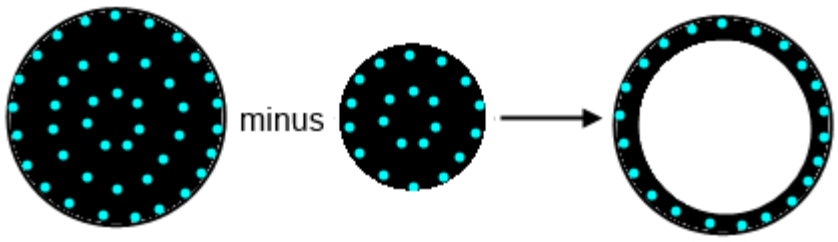

Figure 96: Visual of equation 10.10

9.4 Model Results

There are many different combinations of composite mixture due to what liquid fuels are used, what solid fuels are used, the composition of the emulsion, and the composition of the composite mixture. Because of this a very large amount of results can be produced. For this section, results being presented will be for an emulsion type of 80-20% diesel-water mixed with either coal or wood. The liquid to solid mass ratio will range from 70-30 to 50-50. These numbers are chosen because the experimentation done previously had similar a similar emulsion make up, and these numbers are the most likely to be seen in the industry. Droplet sizes are optimum size range taken from the literature that have historically provided good flow and combustion properties.

The first set of figures will compare a pure diesel shell surrounding coal versus the 80-20% diesel-water emulsion shell surrounding coal. Figure 97 shows the total combustion time increasing with increasing initial solid particle radius. There is no noticeable difference in combustion time with varying mass solid-liquid ratio.

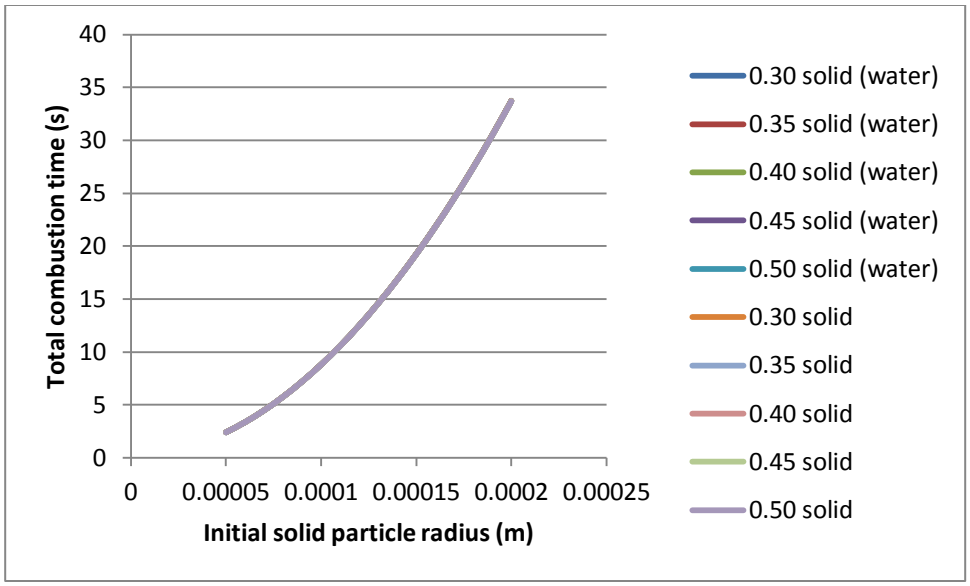

Figure 97: Total combustion time varying initial coal particle size of the colloid particle at a furnace temperature of 933 K. The data sets represent a different colloid particle composition. Each set contains 20% water, shown percentage of coal, and remainder liquid fuel. All data sets are present on figure, they are difficult to see values being similar.

Figure 98 shows the radius of the liquid shell increasing as the initial solid particle size increases. As the initial solid particle radius increases so does the emulsion shell radius. At lower solid mass percentages in the composite mixture, the radius of the liquid shell per particle increases. Pure fuel shell radiuses are shown to be larger than emulsion shell radiuses when the solid fuel particle they surround is the same size.

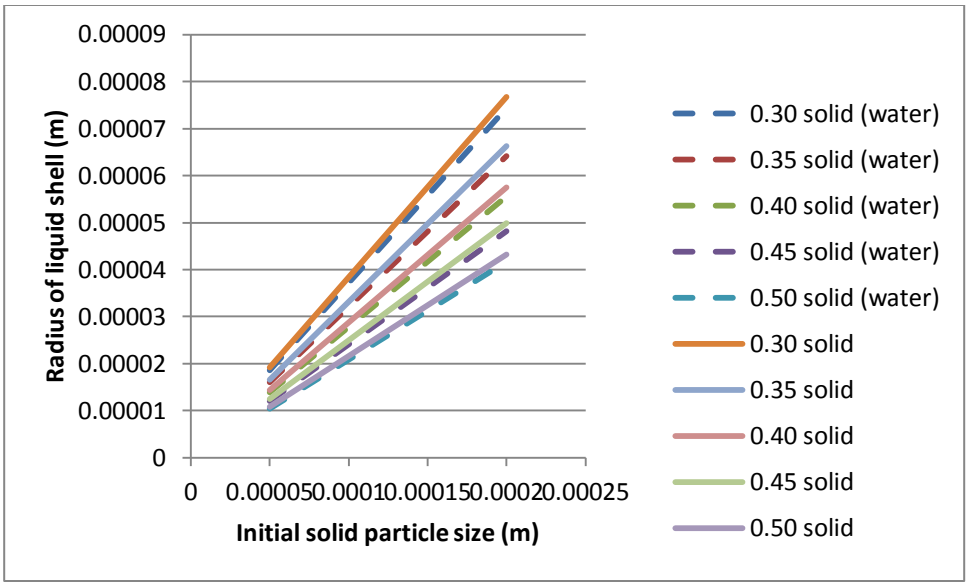

Figure 98: Radius of the liquid shell, varying initial coal particle size of the colloid-emulsion particle as well as colloid-non-emulsion particle at a furnace temperature of 933 K. The data set represent a different colloid particle composition. Each set contains 20% water, shown percentage of coal, and remainder liquid fuel.

The next set of figures will make comparisons between 80-20% diesel-water emulsion shell surrounding a coal particle versus the same emulsion surrounding a wood particle. Figure 99 is very similar to the coal versus wood combustion version of the figure, in that the wood colloid takes less time to combust especially at larger particle sizes.

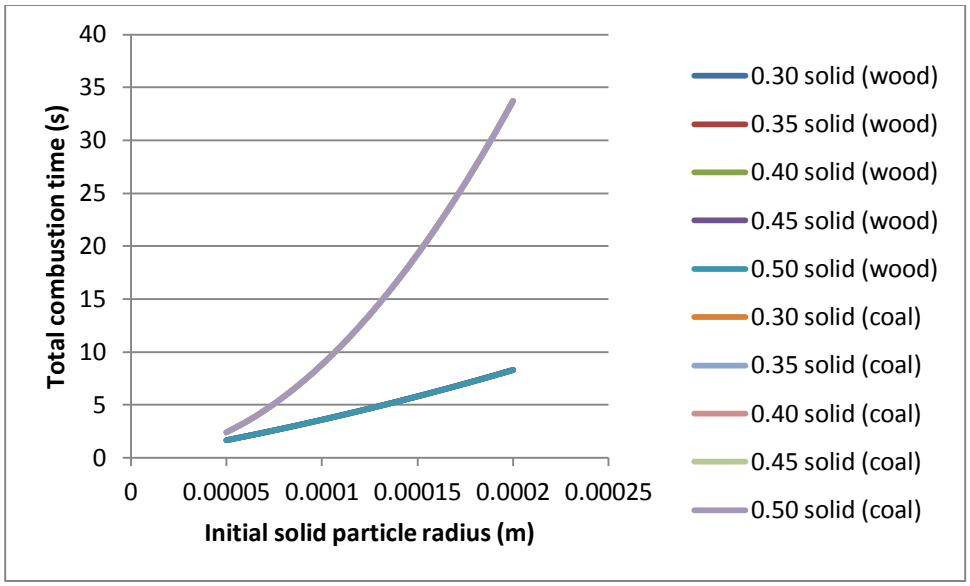

Figure 99: Total combustion time, varying initial solid particle size of the colloid-emulsion particle at a furnace temperature of 933 K. The data sets represent a different colloid particle composition. Each set contains 20% water, shown percentage of solid fuel, and remainder liquid fuel. All data sets are present on figure, they are difficult to see values being similar.

Figure 100 shows that increasing the initial particle radius and decreasing the mass percent solid in the composite mixture both increase the radius of the emulsion shell. In all cases wood has a thicker emulsion shell than coal.

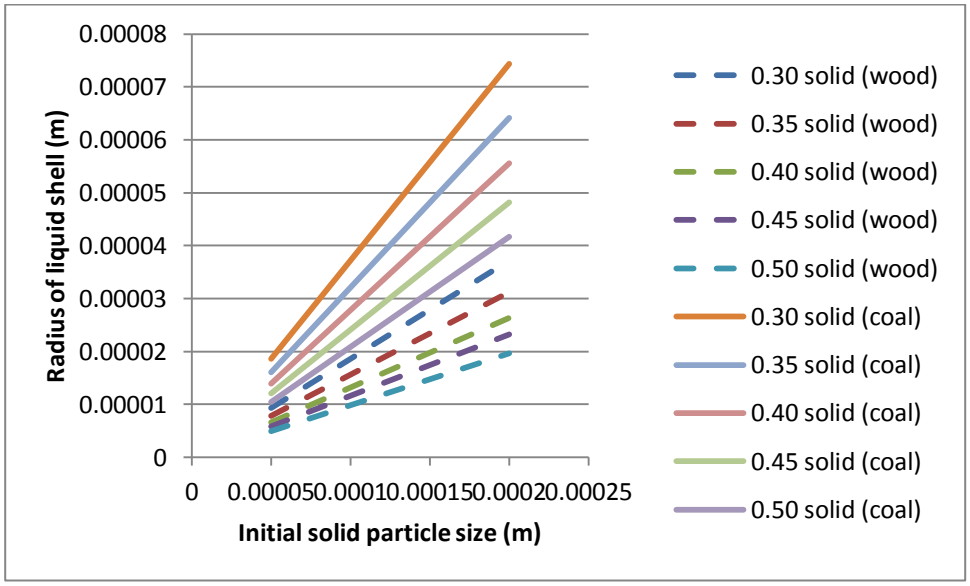

Figure 100: Radius of the emulsion fuel shell varying initial solid particle size of the colloid-emulsion particle at a furnace temperature of 933 K. The data set represent a different colloid particle composition. Each set contains 20% water, shown percentage of solid fuel, and remainder liquid fuel.

The last set of graphs will show the how the total combustion time varies with mass percent for each particle size. Again the composite mixture being modeled is an 80-20% diesel water emulsion shell surrounding coal or wood. Figure 101, the coal colloid, shows that as the percent mass increases the total combustion time slightly decreases for a given initial particle size.

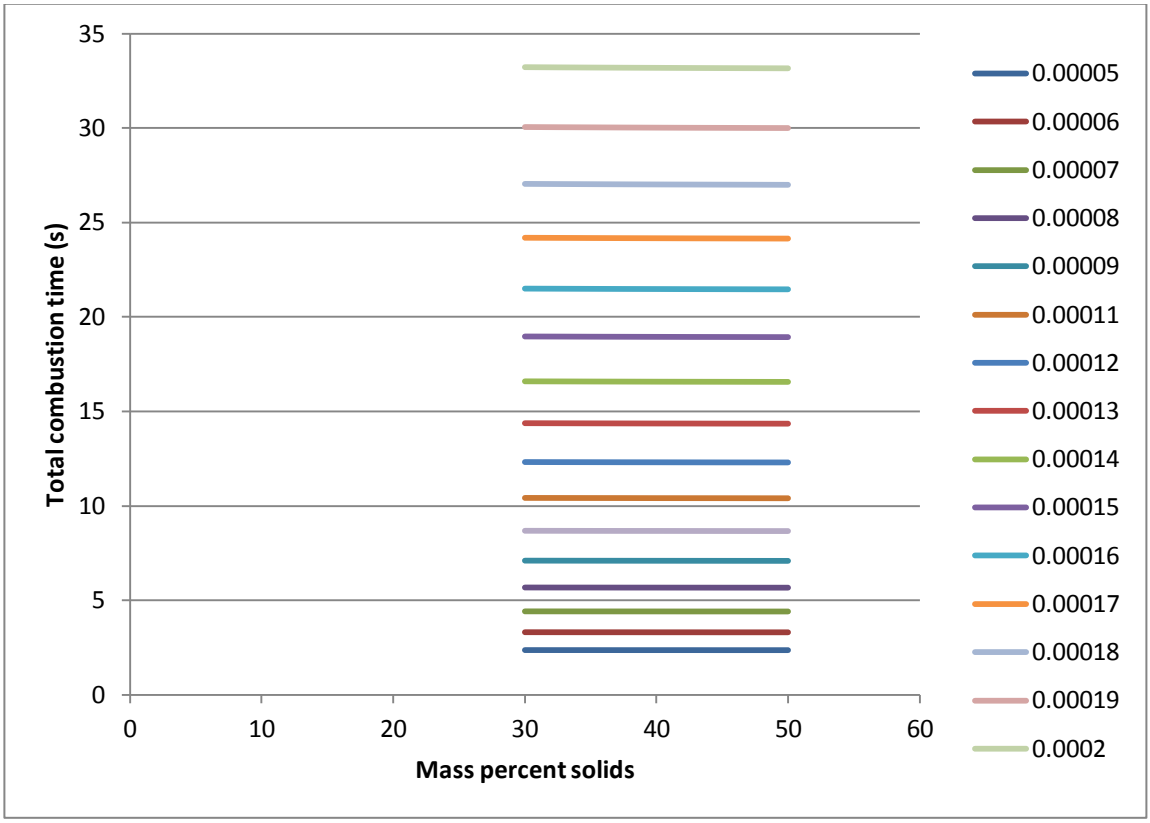

Figure 101: Total combustion time varying initial coal particle size of the colloid-emulsion particle at a furnace temperature of 933 K. The data set represent a different colloid particle composition. Each set contains 20% water, shown percentage of coal, and remainder liquid fuel.

Figure 102 shows the same comparison except with wood as the solid particle. The same general trend to the results is seen. The only difference is that at the higher initial solid particle sizes, the differences between total combustion times are not as pronounced as with coal particles. This was seen in the solid combustion chapter results.

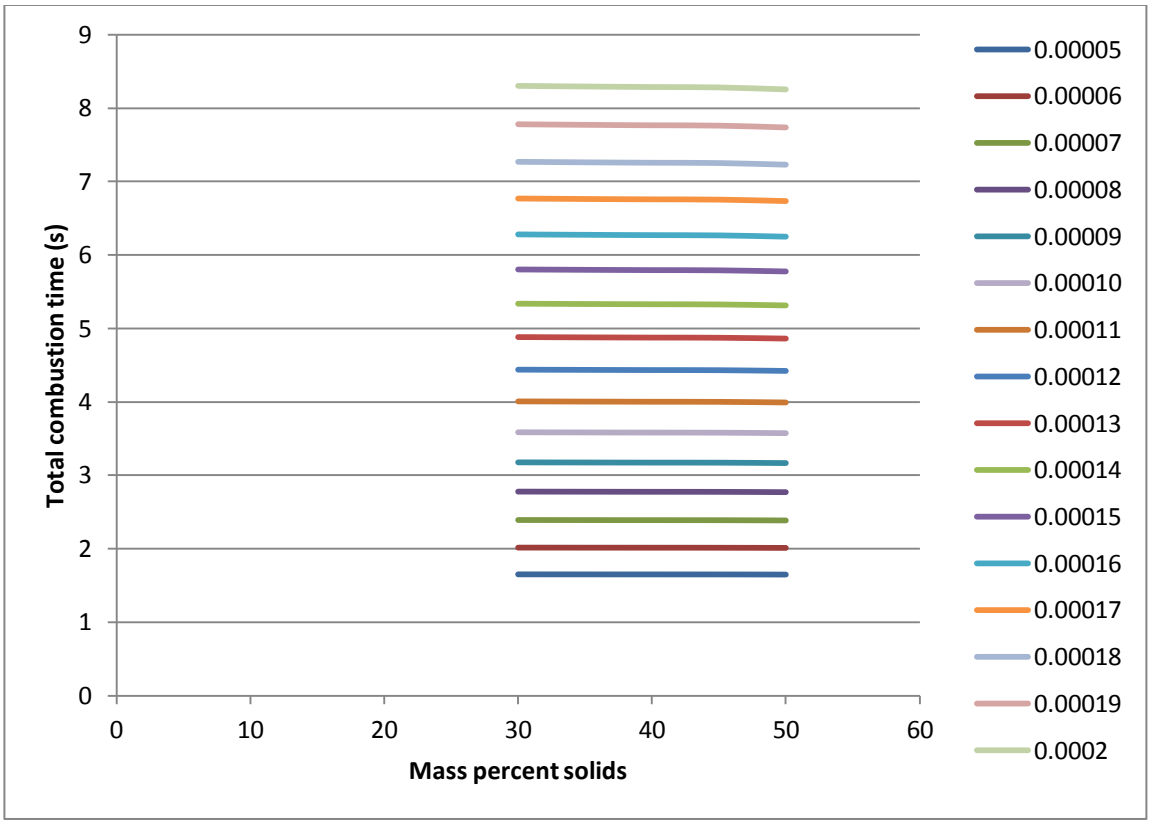

Figure 102: Total combustion time varying initial wood particle size of the colloid-emulsion particle at a furnace temperature of 933 K. The data set represent a different colloid particle composition. Each set contains 20% water, shown percentage of wood, and remainder liquid fuel.

The next figure will show how the heat of combustion varies with differing composite fuel composition. Each mixture has 20% water.

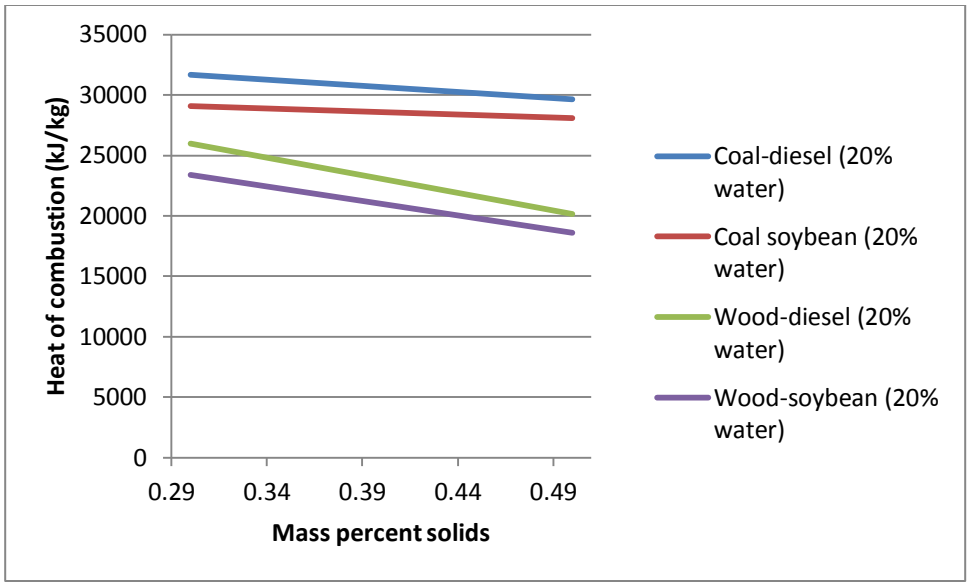

Figure 103: Heat of combustion variance with only liquid-solid fuel mass ratio changing, water ratio kept at 20 mass percent

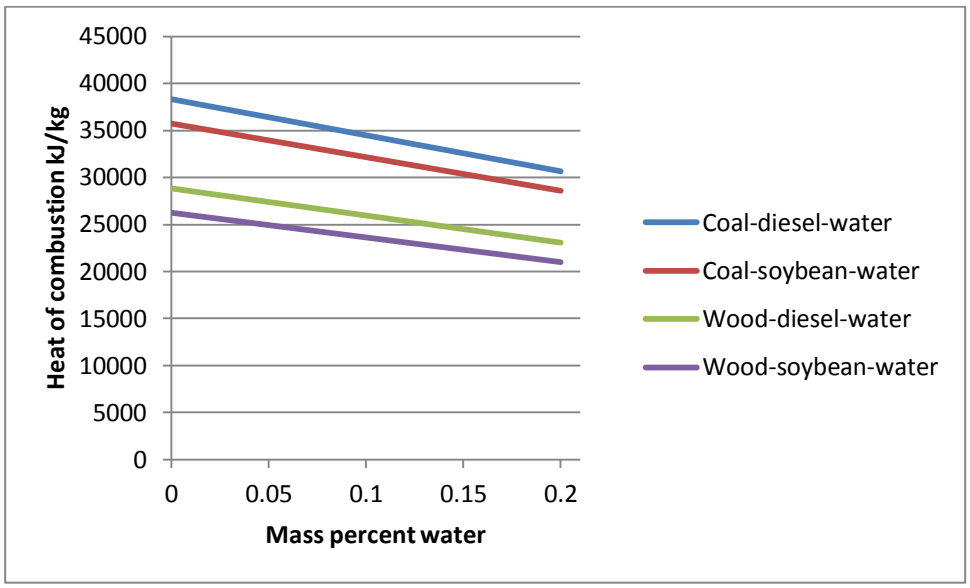

Figure 104: Heat of combustion variance with composite fuel water composition change. Liquid to solid fuel mass ratio is always 50-50 and its total mass percent is always the remainder after the water mass percent is taken into account

Last will be linear models with average temperatures and combustion times of all modeled composite fuel particles. In regards to the linear combustion models showing average combustion times, the models are not drawn in a manner that necessary represent combustion time step lengths.

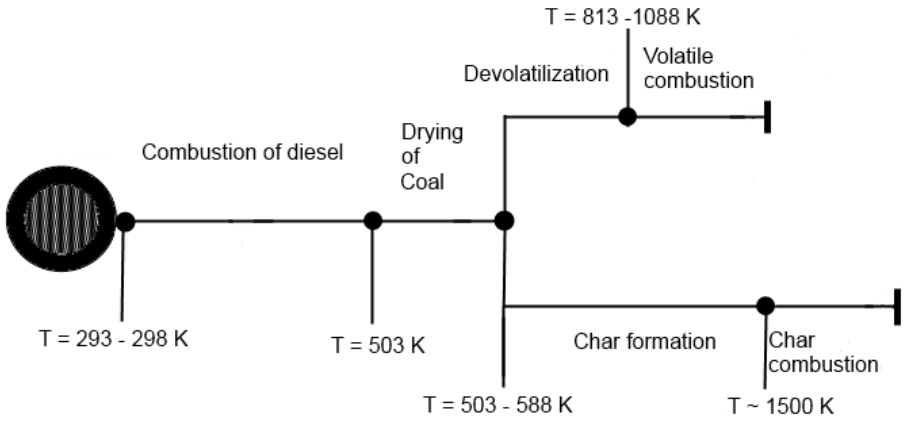

Figure 105: Linear combustion model for coal-diesel-water composite droplet with average temperatures. Solid particle radius range of 0.00001 m to 0.0005 m.

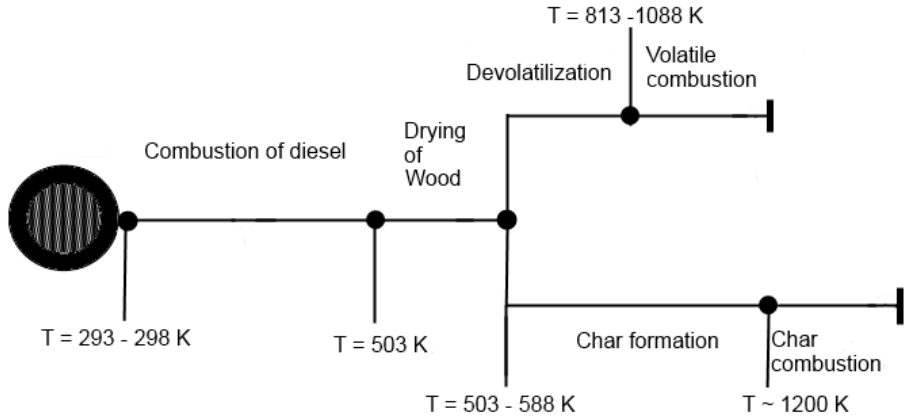

Figure 106: Linear combustion model for wood-diesel-water composite droplet with average temperatures. Solid particle radius range of 0.00001 m to 0.0005 m.

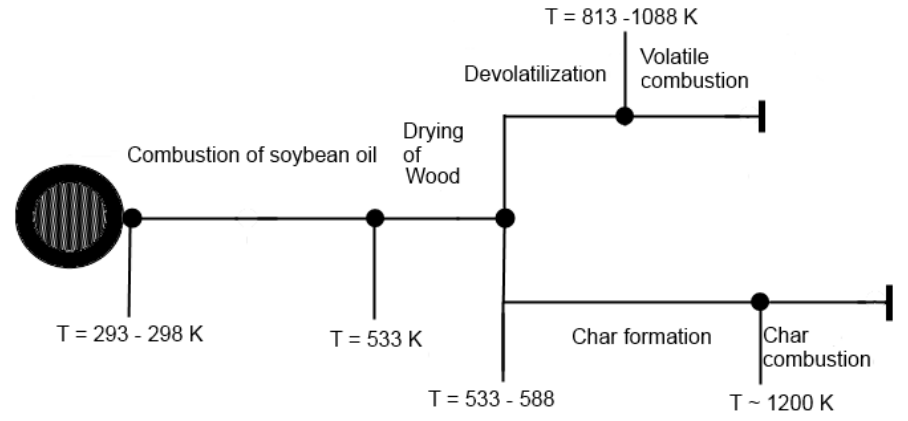

Figure 107: Linear combustion model for coal-soybean-water composite droplet with average temperatures. Solid particle radius range of 0.00001 m to 0.0005 m.

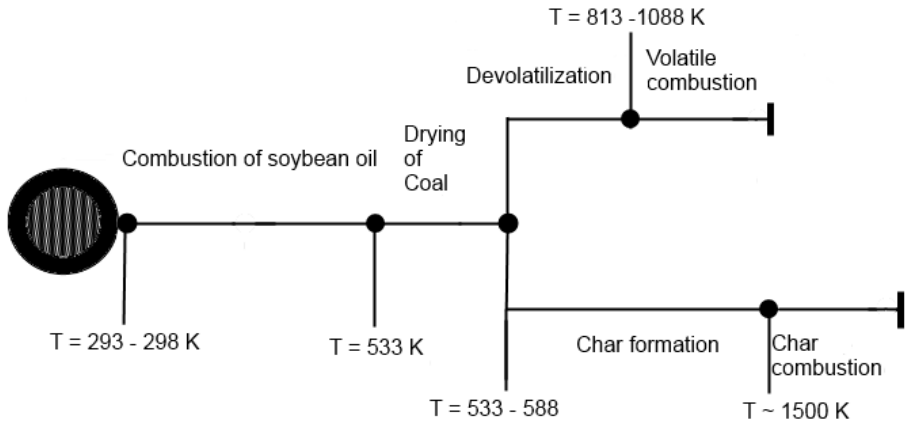

Figure 108: Linear combustion model for wood-soybean-water composite droplet with average temperatures. Solid particle radius range of 0.00001 m to 0.0005 m.

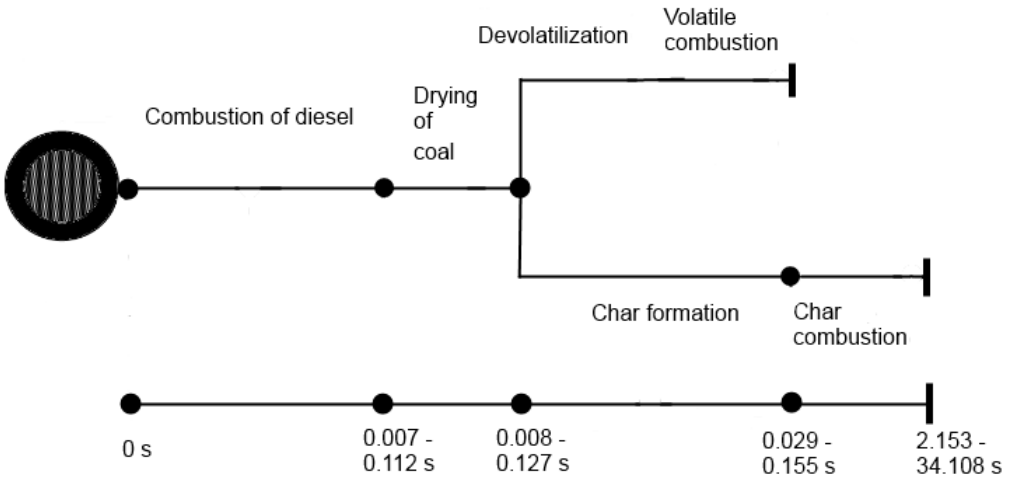

Figure 109: Linear combustion model for coal-diesel-water composite fuel droplet with average combustion times. Solid particle radius range of 0.00001 m to 0.0005 m.

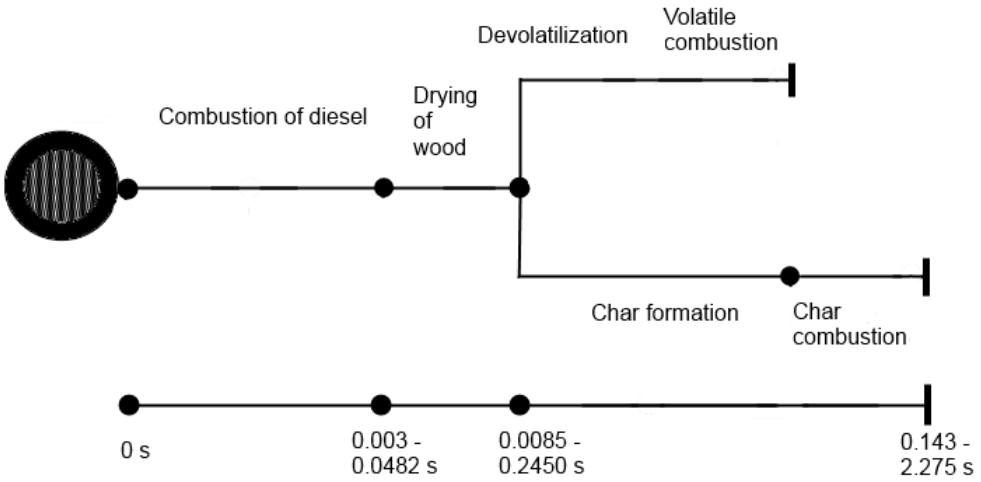

Figure 110: Linear combustion model for wood-diesel-water composite fuel droplet with average combustion times. Solid particle radius range of 0.00001 m to 0.0005 m. Wood volatilization time is very small.

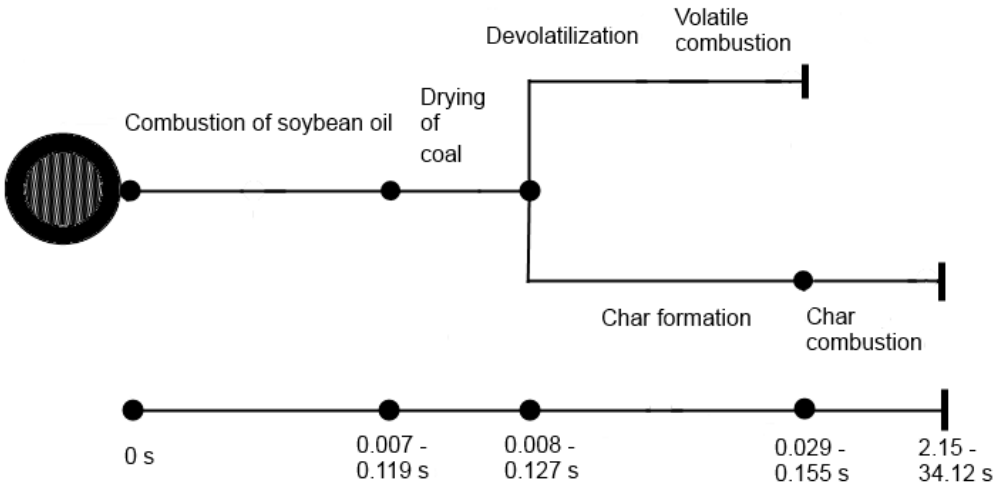

Figure 111: Linear combustion model for coal-soybean-water composite fuel droplet with average combustion times. Solid particle radius range of 0.00001 m to 0.0005 m.

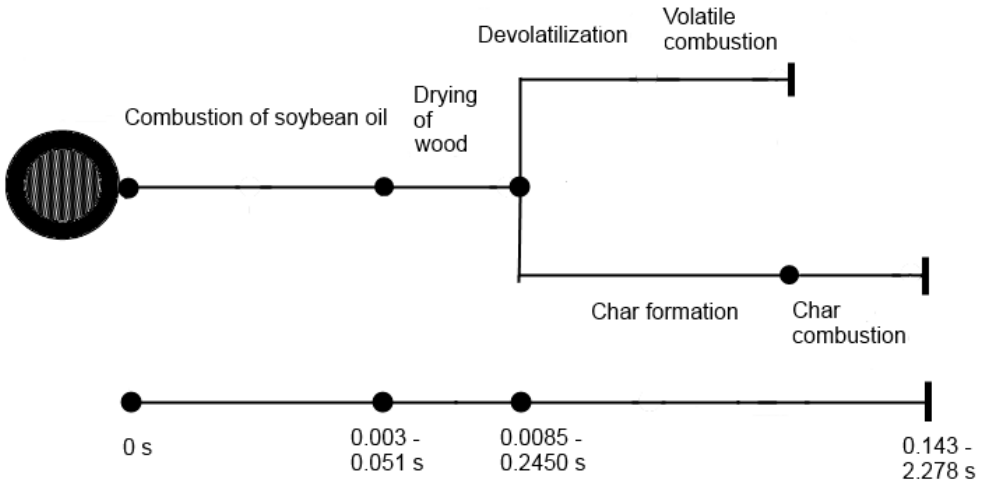

Figure 112: Linear combustion model for wood-soybean-water composite fuel droplet with average combustion times. Solid particle radius range of 0.00001 m to 0.0005 m. Wood volatilization time is very small.

9.5 Discussion

Figure 97 follows the general trend that has been seen throughout the modeling process; that a larger particle will take longer to combust. However this figure should have multiple curves visible. In reality all the curves are over lapping one another due to how the model functions. Normally as a composite mixture is increasing its liquid mass and decreasing its solid mass, the overall mixture combustion time will be shortened. But with a per-particle basis model, where the liquid shell thickness is variable and based on the controlled and constant initial solid particle size, increasing the liquid mass and decreasing the solid mass percent only results in a thicker liquid shell. Then, because the shell combustion time is a very small percent of the total combustion time due to how much longer the coal takes to combust, the difference cannot be seen. This is represented below in figure 110.

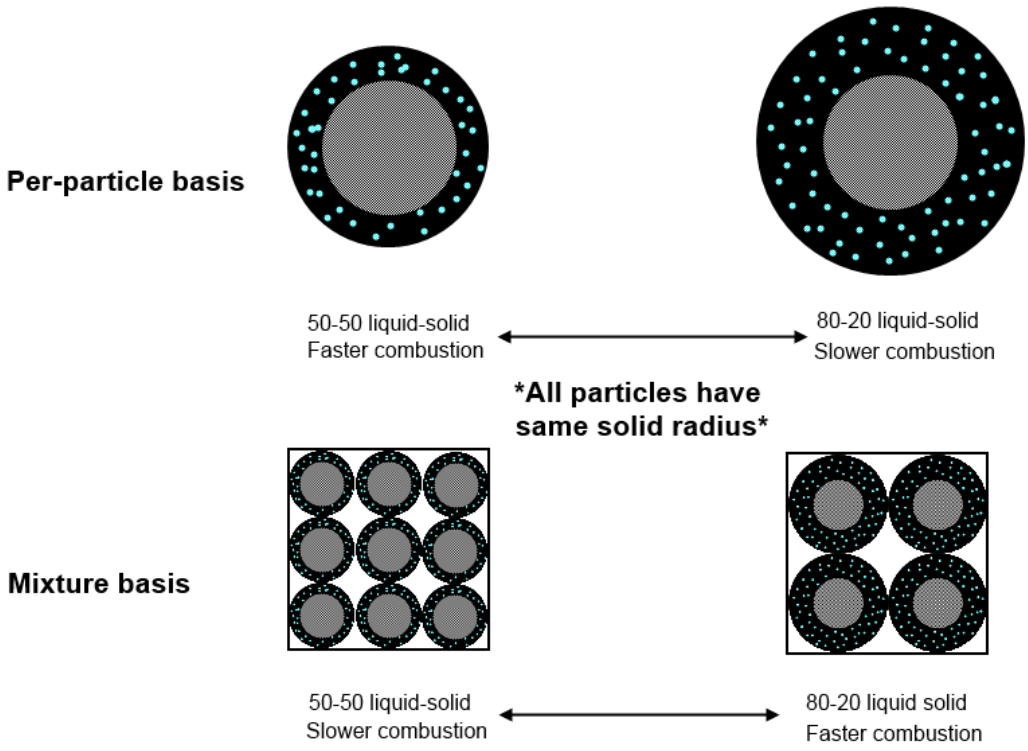

Figure 113: Explanation of per particle model effect on results

But as was seen in previous chapters there *is* a difference between the emulsion and non-emulsion fuel combustion times. With that in mind the results found are expected. Explanations of figures 101 and 102 address the issue of the what is happening as solid mass percent is increased and will be explained later.

Figure 98 shows the liquid fuel shell increasing depending on three variables. The first variable is initial solid particle size. The larger each individual solid particle is, the more emulsion it will take to surround it, which is what the model predicts. The second variable is composition of the colloid particle. If there is less mass solid percent, there has to be more liquid mass, and according to the model assumption there is no free floating liquid, so the radius of the shell must increase to account for

more liquid, so it the model is correct in predicting that as the solid mass percent decreases the liquid fuel shell radius increases. The last variable is whether the liquid fuel shell is pure fuel or a fuel/water emulsion. It is predicted that between the emulsion and the non-emulsion shells, non-emulsion shells are thicker. This is because the model calculates shell thickness depending on the mass ratio of solid to liquid. Since the emulsion is denser than the pure fuel, it will require less volume to achieve the same total mass.

In figure 99 the shell composition for both composite mixtures is the same, so the only variable between the two models is the type of solid. It should be noted that the wood colloid has a thicker emulsion shell than an equivalent coal colloid particle in these models. This will be explained in the next paragraph. As it turns out because the solid takes so much longer than the emulsion shell to combust, this variance in shell thickness does not distort the expected results.

In figure 100 these results occur again because the model calculates shell thickness depending on the mass ratios of solid to liquid in the composite mixture. Since wood is less dense than coal, a wood colloid particle requires more liquid shell to equal the same total mass as an equivalently sized coal colloid particle.

Figures 101 and 102 show what was very difficult to see in figures 97 and 99, that as the solid mass percent of a composite mixture increases the shell radius per particle decreases. In these figures a slight decrease in shell radius is noticeable in each curve as solid mass percent increases. It is this slight decrease that is indiscernible in figures

Figure 103 shows that composite fuels will have lower heats of combustion than their pure liquid fuel counterpart. This is expected since the liquid fuels which are more energy dense are being removed and replaced with less energy dense fuels and water which has no energy density. When coal is the solid being added with 20% water, a loss of between a 25% energy loss is predicted. When wood is the solid being added with 20% water a loss of around 45% is predicted. Because of these energy losses, the smallest amount of water that creates a successful composite fuel should be used. This is because however much water is used, directly relates to how much of an decrease in energy will be seen because water has no heat of combustion. For example, if water is cut to 10% instead of 20%, the previous energy loss for coal-water of 25% will become 15%, a more acceptable loss. In regards to how the solid-liquid fuel mass ratio, that is dependent on the user. If higher heats of combustion are desired more liquid should be used. If the application does not call for such large energy requirements more solid fuel could be used.

9.6 Conclusions

This chapter predicted the combustion times and heats of combustion for composite fuels. It was found that a composite fuel will burn as fast as the solid fuel within it would burn on it's own. The liquid fuel does add to the overall combustion time, but by a very small margin when compared to the solid fuel combustion time. This is an important conclusion for eventually determining residence times for composite fuels in combustion chambers. It was also predicted that composite fuels will not be as energy dense as pure fuel oils, though this is expected as the solid fuels used have lower heats of combustion and water has no heat of combustion. Even

though the energy values are lower, they are still higher than standard solid fuels and therefore still a feasible substitute for fuel oil.

9.7 Nomenclature

A	Clausius-Clapeyron integration constant (m^2)
B	Clausius-Clapeyron integration constant (K)
$B_{o,q}$	Spalding Number
c_p	Specific heat $(kJ/kg * K)$
D	diameter of fuel droplet (m)
h_c	heat of combustion (kJ/kg)
h_{fg}	Latent heat of vaporization (kJ/kg)
k	Thermal conductivity $(kW/m * k)$
K	Combustion rate constant (m^2/s)
$\dot{m}_F$	Mass burning rate of the fuel (kg/s)
MW	Molecular weight
P	Pressure (Pa)
r	Radius (m)
R	Radius colloid particle (m)
R_u	Universal gas constant $(kJ/kmol * K)$
T	Temperature (K)
Y	Mass fraction
ρ	density (kg/m^3)
v	Oxidizer to fuel stoichiometric ratio

Subscripts

d	droplet
f	flame
F	Fuel
g	Gas
l	Liquid
Pr	Products
s	Surface
S	Solid
∞	Far removed from the surface
0	initial

CHAPTER 10 - CONCLUSION

Through experimentation, literature review and modeling, many conclusions have been made about the feasibility of emulsion fuel mixtures and more importantly, composite fuel mixtures. The majority of these conclusions will be summarized in this chapter.

10.1 Settling

The settling experiments showed that if a composite fuel mixture was emulsified with water, the time to settle increased dramatically. Emulsions lengthen settling due to the increase in liquid mixture density and decrease in viscosity in accordance with Stokes Law for settling. This can be seen in the following two figures showing non-emulsion versus emulsion settling fronts.

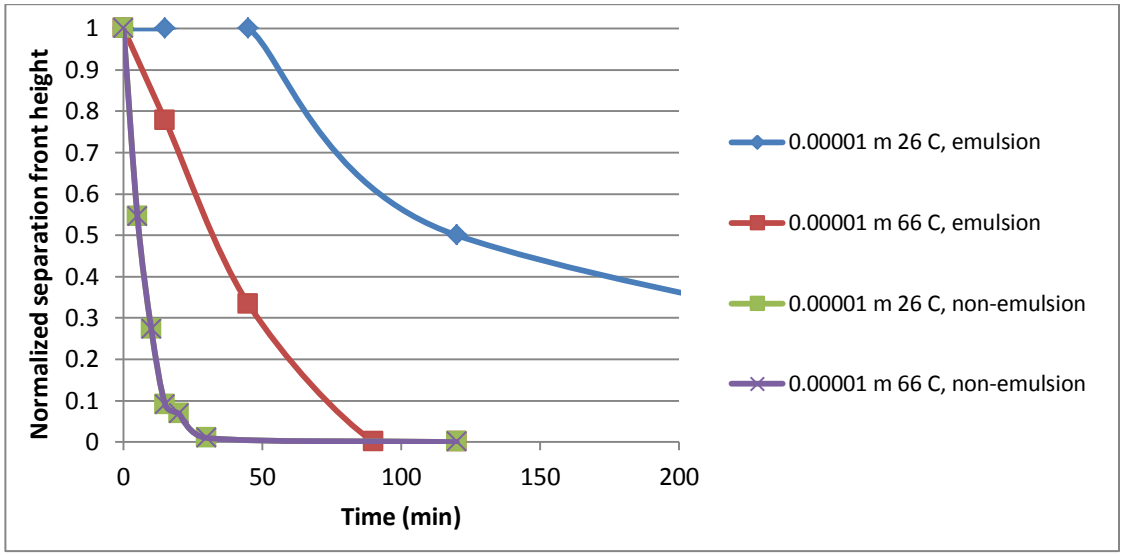

Figure 114: Experimental comparison of wood soybean oil emulsions and wood soybean oil systems

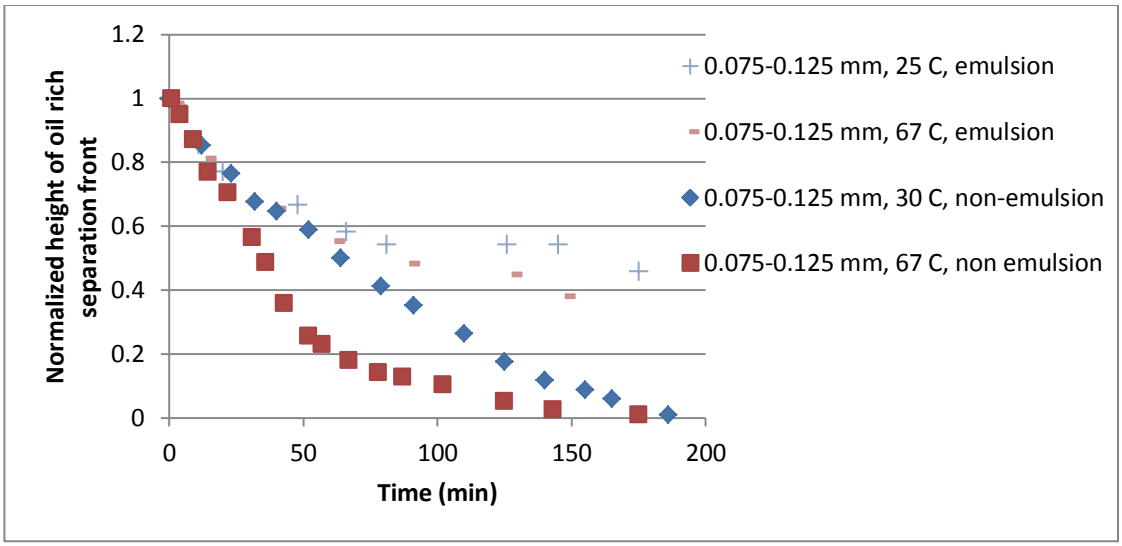

Figure 115: Experimental comparison of coal soybean oil emulsions and wood soybean oil systems

Even though settling was still observed, it must be kept in mind that these experiments did not use surfactants, which further increase mixture stability as well as the fact that the bare minimum energy requirement to create the emulsions was used. If more energy was put in to creating an emulsion, again a more stable mixture would be observed. The fact that the experimental composite emulsions showed such stability over their non-emulsion counter parts is a credit to how well emulsifying a composite should work if a surfactant is used and appropriate energy is spent in creation of the emulsion. Even without surfactant treatment or large energy input 50% settling wasn't seen until at least 50 minutes in the worst case. In a plant setting, it is highly unlikely that any composite fuel will be in transfer between its storage tank and combustion chamber for longer than 50 minutes. It was also learned that when keeping temperature constant in a given composite mixture, the smaller the solid particle size, the more stable the mixture. When particle size is kept constant, it is seen that increasing temperature decreases stability. This can be seen in the figure below

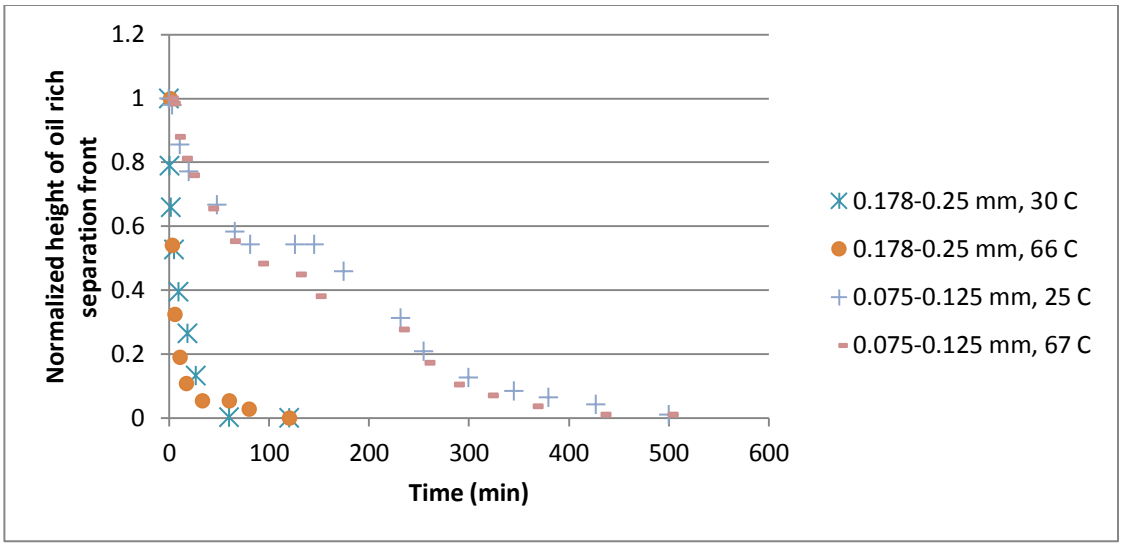

Figure 116: Experimental comparison of coal soybean oil emulsions

Coal was observed to create more stable composite mixtures than wood. Equations were found for specific mixture compositions and temperatures that would predict the separation front at various times. It would seem that the problem of non-emulsion composite mixture settling can be averted through application of an emulsion.

10.2 Viscosity

By examining experiments available in the literature, it was found that composite fuel mixture viscosity is affected by mixture concentration and temperature. Specifically, the more solids a mixture contains the more viscous it will be and the more liquid it contains the less viscous. This is shown in the next figure.

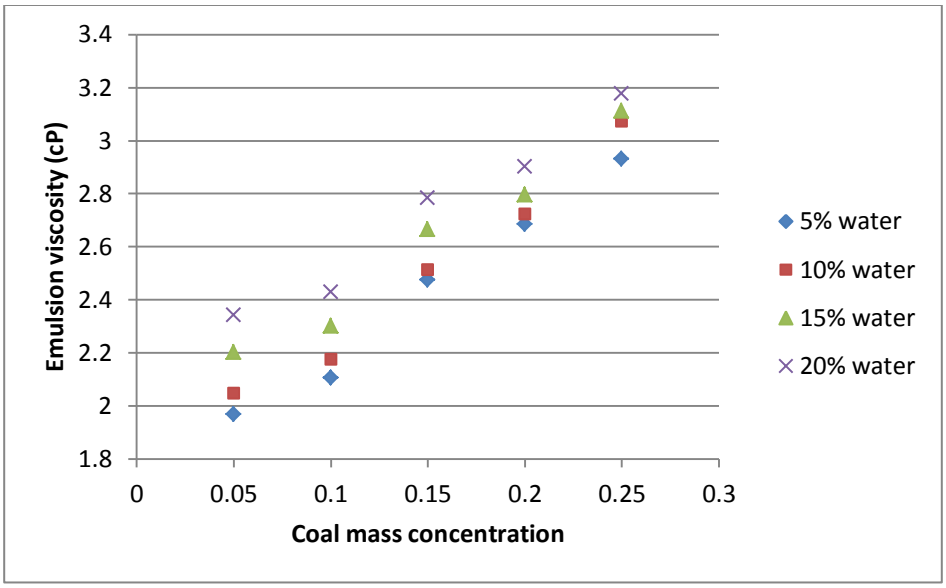

Figure 117: Viscosity of coal-diesel emulsion varying coal mass concentration [1]

In figure 115 it is shown that emulsified slurry mixtures have much smaller viscosities when compared to non emulsified slurry mixtures in figure 114. When comparing emulsions of differing water content, it is seen that more water will slightly increase the mixture viscosity, but not an amount to cause concern. [1].

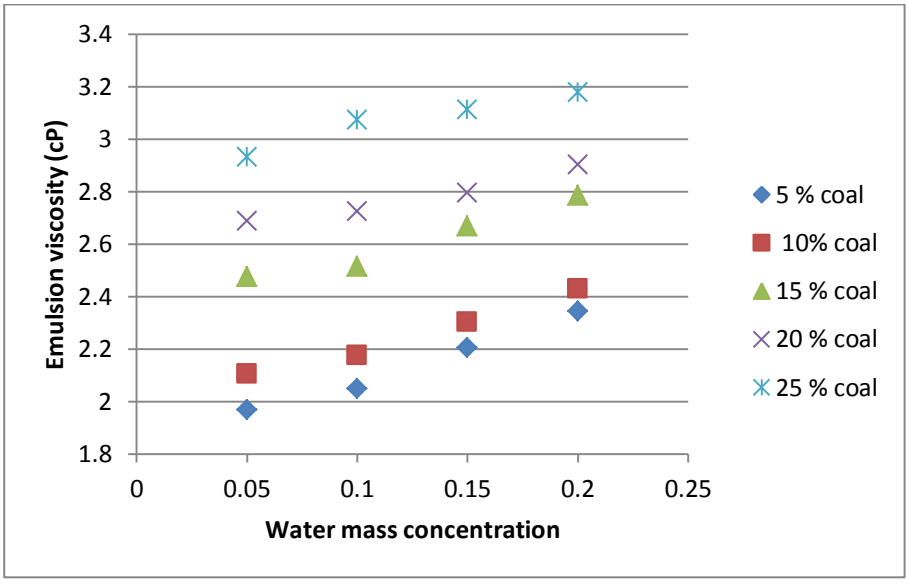

Figure 118: Viscosity of coal-diesel emulsion varying water mass concentration [1]

Water's effect on vegetable oil viscosity is simply due to its much lower viscosity. This chapter also lead to an equation that could predict the viscosity of composite mixtures, both emulsion and non-emulsion.

$$\mu_{sL} = kC_w^m C_c^n \rightarrow 4.855 C_c^{0.225} C_w^{0.0829} \quad \textbf{(88)}$$

Through experimentation and modeling it was concluded that two major problems regarding the use of composite fuel mixtures, settling and viscosity, can be averted through the application of an emulsion.

10.3 Combustion Models

Models were developed that combustion times, heating values, combustion temperatures and burning rates properties of solid, pure liquid, emulsion. Then combining the models from these three processes, a model for composite combustion was designed. The important combustion conclusions were as follows:

1. Liquid fuel combustion is very fast.
2. Higher furnace temperatures equate to better combustion related properties in all types of combustion. This is already common knowledge, but it is good to see the models in this thesis confirm this.
3. Smaller droplets, solid particles and solid particles with emulsion fuel shells will lead to a faster overall mixture combustion rate. This was also seen experimentally in other literature sources, so it was good to see the model predicting the same effect.

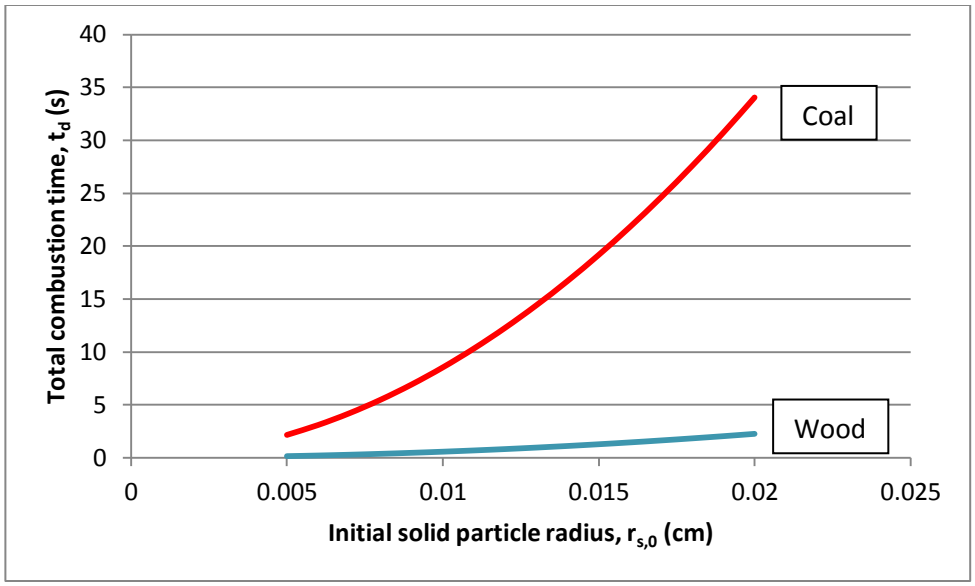

Figure 119: Total combustion time comparison between 50% wood-50% soybean oil/water colloid particle and 50% coal-50% soybean oil/water emulsion colloid particle at various particle sizes at a fixed furnace temperature of 933 K

4. The drying rate of a solid is a strong function of how much water it contains
5. The shortest stage of solid combustion is devolatilization, the longest and rate limiting step is char combustion
6. Solid fuel combustion is orders of magnitude slower than liquid fuel combustion. The merits of this conclusion will be discussed later.
7. Coal takes longer to combust than wood. The difference is increased at larger particles sizes and decreased at smaller particle sizes.

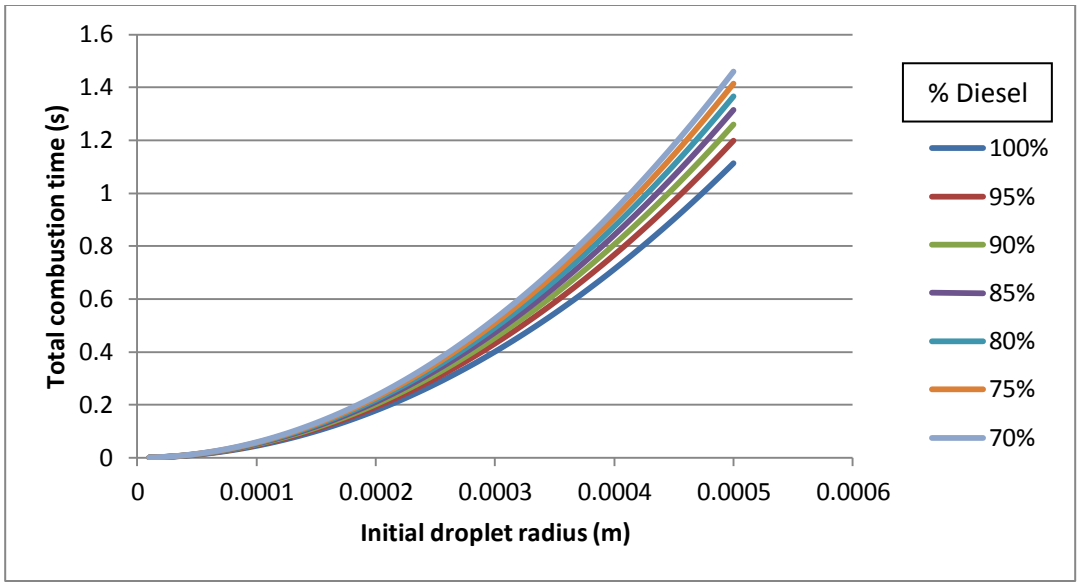

Figure 120: Total combustion time of diesel emulsion droplets for a furnace temperature of 933 K. Data sets represent the composition of diesel and water in each emulsion drop.

8. When water is added to a fuel to create an emulsion, concentration dependent properties are negatively affected, eg: (combustion time is increased, heat of combustion decreased)

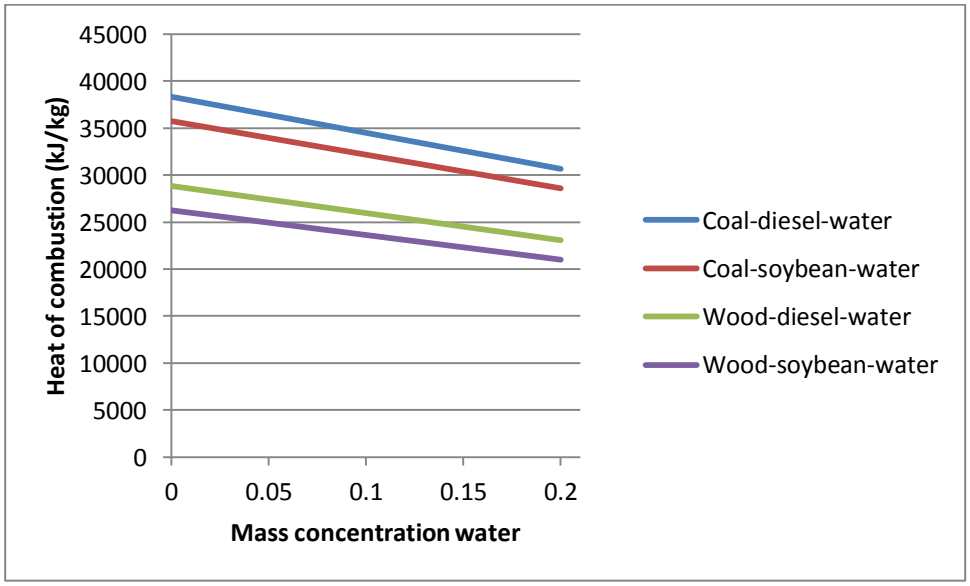

Figure 121: Mixture heat of combustion for equal mass fractions of solid and liquid fuel

9. Water does not have a very large effect on combustion time. This is an important conclusion because water's effects on fuel combustion time might have been a major concern. To see that the model predicts a very slight increase in combustion time should successfully negates one of the major issues with using water in composite fuel combustion.

10. The rate limiting step of composite combustion is solid combustion, by orders of magnitude, regardless of emulsion or non-emulsion liquid fuel. Because of this fact, solid particles should be kept at the smallest size possible. Not only will a smaller particle size help with composite mixture flow properties, but it will dramatically cut down on combustion time.

10.4 Economics

Economically, composite fuels will be cheaper to produce than equivalent pure fuel oil. This is because the composite fuel oils will only be a fraction of the more expensive pure liquid fuel oils. The remainder of the mixture will be cheaper or in some cases free fuels. The following tables highlight some major fuel prices.

Table 69: Approximate fuel prices for various common fuels, 2013

Fuel	Market Price ($/kg)	Heat of Combustion (million kJ/kg)	Energy Price ($/million kJ)
Coal [3]	0.08	0.033	2.27
Wood [3]	0.12	0.014	8.41
Heating Oil (#2) [3]	0.91	0.458	19.93
Gasoline [3]	1.06	0.045	23.50
Diesel [3]	0.97	0.434	22.29
Residual Oil (#6) [3]	0.71	0.046	15.55
Soybean [4]	1.05	0.038	27.45
Canola oil [4]	1.14	0.039	29.60
Palm oil [4]	0.79	0.040	19.75

Table 70: Predicted composite fuel prices, 2013. Composite fuel compositions are 0.50-0.30-0.20

Fuel	Predicted Market Price ($/kg)	Heat of Combustion (million kJ/kg)	Energy Price ($/million kJ)
Coal-Palm Oil-Water	0.27	0.0286	9.60
Coal-Soybean Oil-Water	0.35	0.0280	12.55
Coal-Canola Oil-Water	0.38	0.0282	13.48
Wood-Residual Oil-Water	0.27	0.0209	13.11
Wood-Palm Oil-Water	0.30	0.0191	15.52
Wood-Soybean Oil-Water	0.37	0.0186	20.14
Wood-Canola Oil-Water	0.40	0.0187	21.51

As can be seen, coal, wood and palm oil are all cheaper than the more commonly used gasoline, diesel, heating oil and residual oil. Composite fuels allow coal, wood and palm oil to not only extend oil reserve life, but also, depending on the markets, allow a for a cheaper fuel to be created. This will save companies money because even though these fuels are less energy dense, their price/energy value is much better than the commonly used fuel oils. As can be seen, some vegetable oils are more expensive than all fuel oils, while others are less expensive. Because there are so many viable vegetable oils that could be used in composite fuel mixtures, all a company would have to do is follow the futures market and use the current cheapest available vegetable oil. It is also important that coal, wood and vegetable oils are not industries controlled by organizations, such as OPEC, so they are much safer fuels to rely on. In addition coal and oil combined with vegetable can reduce sulfur emissions versus using straight coal. It should be noted that this is not a full scale economic study. The previous economic numbers are predicted based on the assumption of only slight modifications on existing combustion plants being required. If new combustion plants must be made to implement the composite fuel, the capitol costs would have to be factored in.

From the conclusions gathered, it would seem as though composite mixtures can have a future as long as they are emulsified with water to obtain certain properties essential to their use and the solid fuel particle size are kept relatively small.

10.5 Future Work

One major aspect of emulsifying fuel mixtures with water that was not examined was the phenomenon referred to as 'microexplosions'. This is when the mixture fuel droplets, after being atomized, undergo the usual heating that occurs in a combustion chamber. After a brief moment of heating, the water dispersed within the oil reaches its boiling point before the surrounding oil, causing the volume of the dispersion phase (the water) to suddenly increase by several orders of magnitude. This change induces shattering of the already atomized droplet, into even smaller droplets. The shattering, or further atomization, leads to a higher surface to volume ratio. This promotes combustion by reducing carbon loss, reducing the required amount of air and increasing overall combustion efficiency. [2] This is one of the two main reasons that emulsions are being considered a requirement when creating composite fuels, the other being settling effects discussed earlier. It should be noted that some of the latent heat produced by the combustion of both the solid and liquid fuels that otherwise would have contributed to the heating value of the fuel will be lost to the heating and vaporizing of the water. This is seen as a necessary loss due to the other positive effects of a composite fuel.

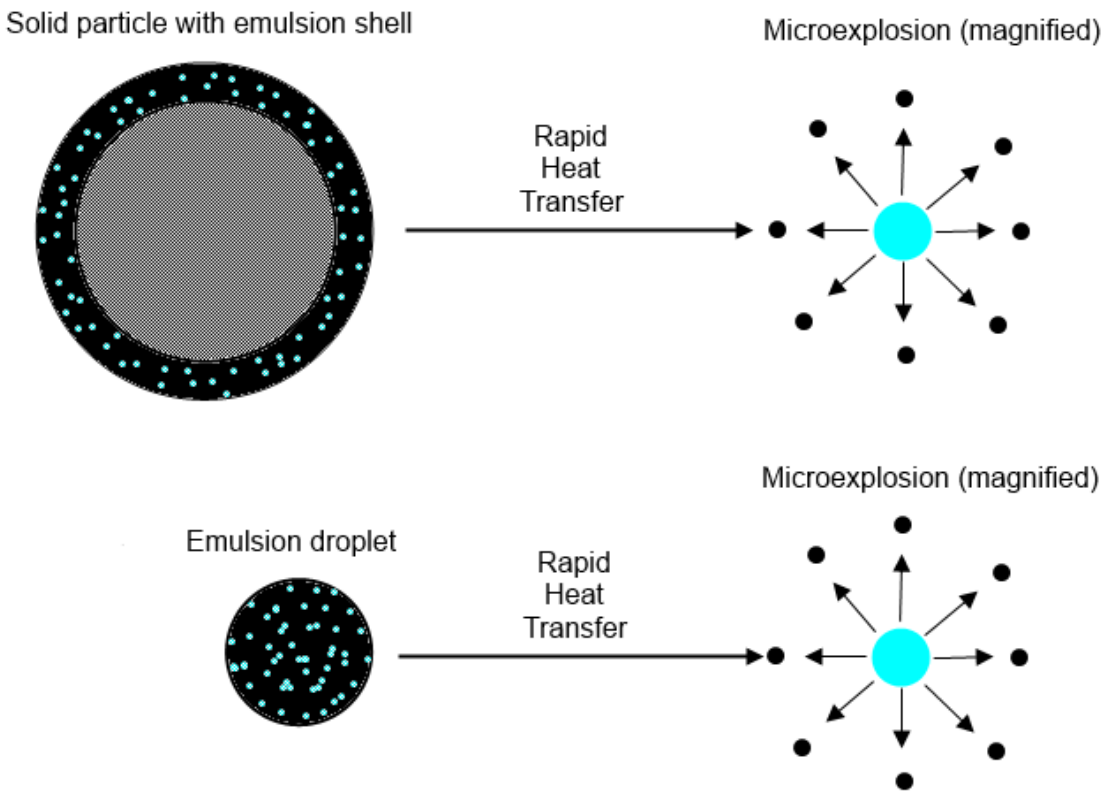

Figure 122: Microexplosion, occurs within fractions of a second

A linear combustion model for composite fuels would look like the following:

1.) Furnace is operating at around 933 K

2.) Feed composite mixture is heated

3.) Micro-explosions of any liquid fuel/water phases take place

4.) Smaller separate droplets of liquid fuel and water are created

5.) Liquid fuel vaporizes and forms combustible gases

6.) Vaporized fuel combusts

7.) Water droplets vaporize

8.) Oil/water emulsion phase vaporizes and forms a combustible gas

9.) Gas combusts

10.) Solid particle releases water as it heats up (drying)

11.) Solid particle undergoes devolatilization while simultaneous undergoing char formation

12.) Volatile gases combust

13.) Char formation continues to completion

The fact that the microexplosion phenomenon was ignored should not be a cause for concern, as it would only support the combustion process and as it stands, combustion model results were still acceptable. Future results would be more accurate if the effects of the phenomenon were included.

Another topic that will need to be expanded on in the future is the economics of using composite fuel technology. It is clear that composite fuel technology will create cheaper comparable fuels to the fuels used commonly today, but a more exact cost analysis should be done. This cost analysis also has to factor in expenses to create the composite fuel as well as expenses to retrofit current combustion equipment if upgrades are necessary. It is assumed that the extra cost to create the composite fuel will be small due to the fact that creating a composite fuel is rather simple and that retrofitting of current combustion appliances will be kept to a minimum if the composite fuel has similar rheological properties to the fuel oil it would be replacing. The cost of potential retrofitting, which is a one-time cost, and the extra cost to make a composite fuel should not outweigh the money saved by not having to use pure fuel oil.

10.6 References

[1] Kumar Majumder, Subrata, et al. "Studies on flow characteristics of coal–oil–water slurry system." *International Journal of Mineral Processing* 79.4 (2006): 217-224.

[2] Nag, P. K. *Power plant engineering*. Tata McGraw-Hill Education, 2002.

[3] U.S. Energy Information Administration. "Short term energy outlook – October 2013" Oct. 2013.

[4] United States Department of Agriculture. "Oildseeds: World Markets and Trades" *Circular Series.* Sep 2013.

BIBLIOGRAPHY

[1] "ChemicalBook---Chemical Search Engine." *ChemicalBook---Chemical Search Engine*. N.p., n.d. Web. 12 Feb. 2013.

[2] "Triglyceride Molecular Weight Calculator » Biodiesel Fuel Education Program." *Biodiesel Fuel Education Program*. N.p., 2013. Web. 17 June 2013.

[3] Agarwal, Pradeep K., and Ian Pedler. "Drying, devolatilization and volatile combustion for single coal particles: a pseudo steady state approach." *Fuel* 65.5 (1986): 640-643.

[4] Allen J. Johnson & George H. Auth, *Fuels and Combustion Handbook*, First ed., McGraw-Hill, New York, 1951

[5] Ballester, Javier M., Norberto Fueyo, and Cesar Dopazo. "Combustion characteristics of heavy oil-water emulsions." *Fuel* 75.6 (1996): 695-705.

[6] Bartle, K. D., et al. "The combustion of droplets of liquid fuels and biomass particles." *Fuel* 90.3 (2011): 1113-1119.

[7] Baum, M. M., and P. J. Street. "Predicting the combustion behavior of coal particles." *Combustion science and technology* 3.5 (1971): 231-243.

[8] Bryden, Kenneth M., and Mathew J. Hagge. "Modeling the combined impact of moisture and char shrinkage on the pyrolysis of a biomass particle< sup>☆</sup>." *Fuel* 82.13 (2003): 1633-1644.

[9] Chan, Wai-Chun R., Marcia Kelbon, and Barbara B. Krieger. "Modelling and experimental verification of physical and chemical processes during pyrolysis of a large biomass particle." *Fuel* 64.11 (1985): 1505-1513.

[10] Coupland, John N., and D. Julian McClements. "Physical properties of liquid edible oils." *Journal of the American Oil Chemists' Society* 74.12 (1997): 1559-1564.

[11] *Diesel Fuel, All Types*; MSDS No. 9909 [Online]; Hess Corporation: Woodbridge, NJ, August 13, 2012, <http://www.hess.com/ehs/msds/9909dieselfuelalltypes.pdf> (accessed December 12 2011)

[12] Gao, Yuanping, and Kewen Li. "New models for calculating the viscosity of mixed oil." *Fuel* 95 (2012): 431-437.

[13] Gao, Yuanping, and Kewen Li. "New models for calculating the viscosity of mixed oil." *Fuel* 95 (2012): 431-437.

[14] Geankoplis, Christie J. *Solutions Manual to Accompany Transport Processes and Separation Process Principles:(includes Unit Operations)*. Prentice Hall Professional Technical Reference, 2003.

[15] Ghannam, Mamdouh T., et al. "Rheological properties of heavy & light crude oil mixtures for improving flowability." *Journal of Petroleum Science and Engineering* 81 (2012): 122-128.

[16] Ghassemzadeh, M. R., and S. Carmi. "Rheological studies of coal-oil mixtures." *Rheologica Acta* 20.2 (1981): 198-202.

[17] Godsave, G.A.E., "Studies of the Combustion of Drops in a Fuel Spray: The Burning of Single Drops of Fuel," *Fourth Symposium (International) on Combustion*, Willkiams & Wilkins, Baltimore, MD, pp 818-830, 1953.

[18] Gunstone, Frank, ed. *Vegetable oils in food technology: composition, properties and uses*. Wiley. com, 2011.

[19] Guth, Eugene, and R. Simha. "Untersuchungen über die viskosität von suspensionen und lösungen. 3. über die viskosität von kugelsuspensionen." *Colloid & Polymer Science* 74.3 (1936): 266-275.

[20] Hammond, Earl G., et al. "Soybean oil." *Bailey's Industrial Oil and Fat Products* (2005): 577-672.

[21] Innovative Hydrocavitation Technology Knickle

[22] John Dean, *Lange's Handbook of Chemistry (11th edition)*. McGraw-Hill, New York, U.S.A, 1973

[23] Kumar Majumder, Subrata, et al. "Studies on flow characteristics of coal–oil–water slurry system." *International Journal of Mineral Processing* 79.4 (2006): 217-224.

[24] Kumar Majumder, Subrata, et al. "Studies on flow characteristics of coal–oil–water slurry system." *International Journal of Mineral Processing* 79.4 (2006): 217-224.

[25] Law, C. K. "A model for the combustion of oil/water emulsion droplets." *Combustion Science and Technology* 17.1-2 (1977): 29-38.

[26] Law, C. K., C. H. Lee, and N. Srinivasan. "Combustion characteristics of water-in-oil emulsion droplets." *Combustion and flame* 37 (1980): 125-143.

[27] Law, C.K., and Williams, F.A., "Kinetics and Convection in the Combustion of Alkane Droplets," *Combustion and Flame*, 19(3): 393-406 (1972).

[28] Lechtenberg, Dirk. "Tyres as an Alternative Fuel." *CemFuels.com*. MVW Lechtenberg & Partner, 03 Mar. 2011. Web. 14 Dec. 2011. <http://www.cemfuels.com/articles/318-tyres-as-an-alternative-fuel>.

[29] Lishtvan, I. I., et al. "Fuel suspensions based on fuel oil, peat, waste wood, and charcoal." *Solid Fuel Chemistry* 43.1 (2009): 1-4.

[30] Lu, Hong, et al. "Effects of particle shape and size on devolatilization of biomass particle." *Fuel* 89.5 (2010): 1156-1168.

[31] Maloney, James O. *Perry's chemical engineers' handbook*. Vol. 7. New York: McGraw-Hill, 1999.

[32] Manfred, R. K., et al. "Current progress in coal-water slurry burner development." *Prepr. Pap.-Am. Chem. Soc., Div. Fuel Chem.;(United States)* 28.CONF-830303- (1983).

[33] Miller, K. S., R. P. Singh, and B. E. Farkas. "Viscosity and heat transfer coefficients for canola, corn, palm, and soybean oil." *Journal of Food Processing and preservation* 18.6 (1994): 461-472.

[34] Momeni, Maryam, et al. "Comprehensive Study of Ignition and Combustion of Single Wooden Particles." *Energy & Fuels* 27.2 (2013): 1061-1072.

[35] Moroianu, Corneliu, and Gheorghe Samoilescu. "numerical modeling for the vaporization and combustion of water-heavy fuel oil emulsion droplet."

[36] Nag, P. K. *Power plant engineering*. Tata McGraw-Hill Education, 2002.

[37] Ndiaye, Papa M., et al. "Vapor pressure data of soybean oil, castor oil, and their fatty acid ethyl ester derivatives." *Journal of Chemical & Engineering Data* 50.2 (2005): 330-333.

[38] Papachristodoulou, G., and O. Trass. "Coal slurry fuel technology." *The Canadian Journal of Chemical Engineering* 65.2 (1987): 177-201.

[39] Peters, Bernhard, and Christian Bruch. "Drying and pyrolysis of wood particles: experiments and simulation." *Journal of analytical and applied pyrolysis* 70.2 (2003): 233-250.

[40] Pettersen, Roger C. "The chemical composition of wood." *The chemistry of solid wood* 207 (1984): 57.

[41] Porteiro, J., et al. "Mathematical modelling of the combustion of a single wood particle." *Fuel processing technology* 87.2 (2006): 169-175.

[42] Ragland, K. W., D. J. Aerts, and A. J. Baker. "Properties of wood for combustion analysis." *Bioresource technology* 37.2 (1991): 161-168.

[43] Red'kina, N. I., G. S. Khodakov, and E. G. Gorlov. "Rheology of coal-water slurries." *Solid Fuel Chemistry* 43.6 (2009): 341-350.
[44] Rossberg, Manfred, et al. "Chlorinated hydrocarbons. Ullmann's encyclopedia of industrial chemistry." (2003).
[45] Sazhin, Sergei S. "Advanced models of fuel droplet heating and evaporation." *Progress in energy and combustion science* 32.2 (2006): 162-214.

[46] Schmidt, Paul Frank. *Fuel oil manual*. Vol. 10. Industrial Press Inc., 1985.

[47] Shukla, Satish Chandra, et al. "Coal–oil–water multiphase fuel: Rheological behavior and prediction of optimum particle size." *Fuel* 87.15 (2008): 3428-3432.
[48] Singer, Stanley. "Pulverized coal combustion-recent developments." (1984).
[49] Smith, Marion L. *Fuels and combustion*. McGraw-Hill, 1952.

[50] Smoot, Leon Douglas. *Fundamentals of coal combustion: for clean and efficient use*. Vol. 20. Elsevier Science Ltd, 1993.
[51] Soybean chapter Pharos

[52] Spalding, D.B., "The Combustion of Liquid Fuels*," Fourth Symposium (International) on Combustion*, Williams & Wilkins, Baltimore, MD, 1953: 847-864.

[53] Steenari, B-M, and O. Lindqvist. Fly ash characteristics in co-combustion of wood with coal, oil or peat. Fuel, 78; 1999, 479-488, Print.

[54] Su, Yaxin, Benson B. Gathitu, and Wei-Yin Chen. "Efficient and cost effective reburning using common wastes as fuel and additives." *Fuel* 89.9 (2010): 2569-2582.

[55] Thomas, David G. "Transport characteristics of suspension: VIII. A note on the viscosity of Newtonian suspensions of uniform spherical particles." *Journal of Colloid Science* 20.3 (1965): 267-277.

[56] Tillman, David A. *Wood Combustion: Principle, Processes, and Economics*. Academic Press, 1981.

[57] Timbalia, Avanti. "Solvent Refined Coal and Coal-Oil Mixtures." Master's Thesis, Ohio University 1981

[58] Turns, Stephen R. *An introduction to combustion*. Vol. 499. New York: McGraw-Hill, 1996.

[59] U.S. Energy Information Administration. "Short term energy outlook – October 2013" Oct. 2013.

[60] United States Department of Agriculture. “Oildseeds: World Markets and Trades” Circular Series. Sep 2013.

[61] Versteeg, Henk Kaarle. *An introduction to computational fluid dynamics the finite volume method, 2/E*. Pearson Education India, 1995.

[62] Vinh, Vu Quang, and S. C. Bhattacharya. "A study on the combustibility of torrefied wood oil/water mixture droplets." *International journal of energy research* 20.3 (1996): 215-236.

[63] Watanabe, Hirotatsu, et al. "Numerical simulation of emulsified fuel spray combustion with puffing and micro-explosion." *Combustion and flame* 157.5 (2010): 839-852.

[64] Wen, C. Y. "Noncatalytic heterogeneous solid-fluid reaction models." *Industrial & Engineering Chemistry* 60.9 (1968): 34-54.

[65] White, Robert H. "Effect of lignin content and extractives on the higher heating value of wood." *Wood and fiber science* 19.4 (1987): 446-452.

[66] Wildegger-Gaissmaier, A. E., and P. K. Agarwal. "Drying and devolatilization of large coal particles under combustion conditions." *Fuel* 69.1 (1990): 44-52.

[67] Xu, Jian, and Li Qiao. "Mathematical Modeling of Coal Gasification Processes in a Well-Stirred Reactor: Effects of Devolatilization and Moisture Content." *Energy & Fuels* 26.9 (2012): 5759-5768.

[68] Yang, Yao B., et al. "Combustion of a single particle of biomass." *Energy & Fuels* 22.1 (2007): 306-316.

[69] Jared, John Marano, and Ronald Munson. Carbon Capture and Storage. Chemical Engineering Process.; Aug 2011. 33-54, Print.

[70] "Educations Fact Sheets." *Aie.org.au*. N.p., n.d. Web. 30 Nov. 2011. <http://www.aie.org.au/AIE/Energy_Info/Educational_Fact_sheets/AIE/Energy_Info/Educations_Fact_sheets.aspx?hkey=06810f4b-06be-4647-af90-c7a9dafbfa4f>.

[71] <http://dailycaller.com/2011/03/10/new-report-says-u-s-has-largest-fossil-fuel-reserves-in-world/>June 12 2012

[72] "9. ENERGY USE OFPEAT." *Fao.org*. N.p., n.d. Web. 29 Dec. 2011. <http://www.fao.org/docrep/x5872e/x5872e0b.htm>

[73] "Tire Chips." *Europeanrecycle.com*. N.p., n.d. Web. 28 Dec. 2012. <http://www.europeanrecycle.com/subpagine.asp?id=71>

[74] "Engineering ToolBox." *Engineering ToolBox*. N.p., n.d. Web. 5 Apr. 2013.